THE APPLICATION OF MICRO DOPPLER FEATURES IN TARGET CLASSIFICATION

A THESIS SUBMITTED TO
THE GRADUATE SCHOOL OF NATURAL AND APPLIED SCIENCES
OF
MIDDLE EAST TECHNICAL UNIVERSITY

BY

ÖZGE TOPUZ ALEMDAROĞLU

IN PARTIAL FULLFILLMENT OF THE REQUIREMENTS
FOR
THE DEGREE OF MASTER OF SCIENCE
IN
ELECTRICAL AND ELECTRONICS ENGINEERING

JANUARY 2014

Approval of the thesis:

THE APPLICATION OF MICRO DOPPLER FEATURES IN TARGET CLASSIFICATION

submitted by **ÖZGE TOPUZ ALEMDAROĞLU** in partial fulfillment of the requirements for the degree of **Master of Science in Electrical and Electronics Engineering Department, Middle East Technical University** by,

Prof. Dr. Canan ÖZGEN
Dean, Graduate School of **Natural and Applied Sciences** _____

Prof. Dr. Gönül TURHAN SAYAN
Head of Department, **Electrical and Electronics Engineering** _____

Assoc. Prof. Dr. Çağatay CANDAN
Supervisor, **Electrical and Electronics Engineering Dept., METU** _____

Prof. Dr. Sencer KOÇ
Co-Supervisor, **Electrical and Electronics Engineering Dept., METU** _____

Examining Committee Members:

Prof. Dr. Mete SEVERCAN
Electrical and Electronics Engineering Dept., METU _____

Assoc. Prof. Dr. Çağatay CANDAN
Electrical and Electronics Engineering Dept., METU _____

Prof. Dr. Sencer KOÇ
Electrical and Electronics Engineering Dept., METU _____

Prof. Dr. Şimşek DEMİR
Electrical and Electronics Engineering Dept., METU _____

Dr. Erdem ERTAN
Aselsan Inc., REHİS _____

Date: **24.01.2014**

I hereby declare that all information in this document has been obtained and presented in accordance with academic rules and ethical conduct. I also declare that, as required by these rules and conduct, I have fully cited and referenced all material and results that are not original to this work.

Name, Last name	:	Özge TOPUZ ALEMDAROĞLU
Signature	:	

ABSTRACT

THE APPLICATION OF MICRO DOPPLER FEATURES IN TARGET CLASSIFICATION

TOPUZ ALEMDAROĞLU, Özge

M. Sc., Department of Electrical and Electronics Engineering
Supervisor: Assoc. Prof. Dr. Çağatay CANDAN
Co-Supervisor: Prof. Dr. Sencer KOÇ

January 2014, 158 pages

This study aims to experimentally investigate the feasibility of discriminating human motions with the help of micro Doppler features by using radar. In this work, the human walking simulator by V. Chen is examined and is modified according to requirements of the study. Then, the time-frequency distributions to obtain the spectrograms of human motions are examined and the Wigner Ville Distribution and Short Time Fourier Transform (STFT) are chosen for the application. After the simulation studies, experimental data is collected by using a ground surveillance radar. The first part of the experimental data consists of walking data with 7 realizations for the ranges of 150 meters and 1000 meters. The second part of the experimental data consists of 3 human subjects with 7 realizations for different human motions as walking, running, crawling, creeping and for different walking azimuth angles of 0°, 30°, 60°. After the collection of the experimental data, the sequence of signal processing steps, which are matched filtering, MTI filtering, windowing, FFT and CFAR are applied to the data to obtain the target range information. After that the micro Doppler feature extraction process is started. A high pass filter is designed and applied to the matched filtered matrix.

After windowing on the high pass filtered output, the ranges with target are extracted. Then, STFT is applied to the range columns of the target to get the spectrogram. Some feature extraction methods are discussed and a set of features is chosen. Six features, which are torso frequency, bandwidth of the signal, offset of the signal, bandwidth without micro Dopplers, the standard deviation of the signal strength, the period of the arms or legs motions are extracted from the spectrograms of running, crawling, creeping and walking with azimuth angles of 0°, 30°, 60°. Lastly, a simple neural network based classifier is constructed. The classification performances of different human motions by neural network classification are examined.

Keywords: Micro Doppler, Human Motion Classification, Feature Extraction, Neural Network Classification

ÖZ

MİKRO DOPPLER ÖZELLİKLERİN HEDEF SINIFLANDIRMASINDAKİ UYGULAMASI

TOPUZ ALEMDAROĞLU, Özge

Yüksek Lisans, Elektrik Elektronik Mühendisliği Bölümü
Tez Yöneticisi: Doç. Dr. Çağatay CANDAN
Ortak Tez Yöneticisi: Prof. Dr. Sencer KOÇ

Ocak 2014, 158 sayfa

Bu yüksek lisans tezinde, radar sistemlerinde mikro Doppler özelliklerin kullanımının insan hareketlerinin sınıflandırılmasına uygunluğu deneysel olarak araştırılmıştır. Bu çalışmada, V. Chen'e ait insan yürüme simülatörü incelenmiş ve simulatör bu tezin gereksinimleri doğrultusunda geliştirilmiştir. Ardından, insanın hareket spektrogramlarını oluşturmak için kullanılan zaman frekans dönüşümleri incelenmiştir ve insan yürüme simülatörü üzerine STFT (Short Time Fourier Transform) ve WVD (Wigner Ville Distribution) yöntemleri uygulanmıştır. Simülasyon çalışmalarından sonra, bir kara gözetleme radarı kullanılarak deneysel veri toplanmıştır. Deneysel verilerin ilk kısmı 150 metre ve 1000 metre mesafelerden 7'şer tekrar olacak şekilde yürüme verilerinden oluşmaktadır. Deneysel verilerin ikinci kısmı ise 3 farklı insana ait 7'şer tekrara sahip yürüme, koşma, emekleme, sürünme hareketlerinin verilerini ve 0, 30 ve 60 derece yanca açılarındaki yürüme verilerini içermektedir. Deneysel veri toplama işlemi tamamlandıktan sonra, uyumlu filtreden geçirme, hareketli algılama filtresinden geçirme, pencereleme yapma, FFT ve CFAR tekniklerini uygulama gibi sinyal

işleme adımları uygulanarak hedefin menzili bulunmuştur. Daha sonra mikro Doppler özellik çıkarma işlemlerine geçilmiştir. Bir yüksek geçirgen filtre tasarlanmış ve eşleştirilmiş filtre sonrasındaki matrise uygulanmıştır. Pencereleme yapıldıktan sonra da hedef menzillerinin bulunduğu sütunlar matrislerden çekilip birleştirilmiştir. Hedef menzillerinden oluşturulmuş matrisin üzerine STFT yöntemi uygulanarak spektrogram elde edilmiştir. Bazı özellik çıkartma yöntemleri incelenmiş ve bir kısım özellikler seçilmiştir. Altı adet özellik spektrogramlardan çıkartılmıştır; insan gövdesi frekansı, sinyalin bant genişliği, sinyalin ofseti, mikro etkiler olmayan sinyalin bant genişliği, sinyal gücünün standart sapması ve uzuvlara ait periyot değeri bu altı özelliği oluşturmaktadır. Bu özellikler koşma, emekleme, sürünme, 0°, 30°, 60° yanca açılarıyla ile yürüme spektrogramlarından çıkartılmıştır. Son olarak, sinir ağına dayalı basit bir sınıflandırıcı oluşturulmuştur. Sinir ağı sınıflandırmasının insan hareketlerini sınıflandırma başarımları incelenmiştir.

Anahtar Kelimeler: Mikro Doppler, İnsan Hareketi Sınıflandırması, Özellik Çıkarımı, Sinir Ağı Sınıflandırması

...to my husband, our beloved families and valuable friends who support me enormously

ACKNOWLEDGEMENTS

I would like to express my gratitude to Assoc. Prof. Dr. Çağatay Candan, Prof. Dr. Sencer Koç for their crucial guidance, advice, elegant criticism, valuable encouragement, and insight throughout the completion of the thesis.

I would like to thank to ASELSAN Inc. for the facilities and important equipments which are provided me to collect very valuable experimental data.

I am indebted to my friends and colleagues, Ayşe Dinçer, Meryem Altınsoy, Selçuk Öksüz for their support, patience and work stations which I needed to process my data for days.

I am thankful to my unique brother Özgün Ali Topuz and my husband Cengiz Alemdaroğlu for their crucial effort while crawling and creeping for me.

Finally, I am grateful to our precious families for their continuous support and encouragements.

TABLE OF CONTENTS

LIST OF TABLES

TABLES

LIST OF FIGURES

FIGURES

LIST OF ABBREVIATIONS

BW	Bandwidth
FAM	Free Arm Motion
FFT	Fast Fourier Transform
KNN	K-Nearest Neighbor
LOS	Line of Sight
NAM	No Arm Motion
PAM	Partial Arm Motion
PW	Pulse Width
SNR	Signal-to-Noise Ratio
STFT	Short Time Fourier Transform
SVM	Support Vector Machine
WVD	Wigner Ville Distribution

CHAPTER 1

INTRODUCTION

1.1 Statement of the Problem

Radar has some important advantages over other sensors for detecting human motion. First of all, radar can work in both daytime and nighttime with full performance, because it does not depend on additional external light sources for its operation. Furthermore, radar is affected only slightly by weather conditions such as smoke, dust and fog, and radar can operate behind walls or at very long distances from the targets. These features make the radar usage superior for security and surveillance in many applications.

Classifying human motions by using radars has become an important emerging research field for both civilian and military applications. Although it is a quite new research area, the developments on this field are remarkably fast. It can be noted that the first studies on this issue are published in 2005, and until today, literature has expanded significantly.

Classifying human activities by using radar sensors have a broad scope of applications such as physical security, urban military operations and law enforcement. Human intention can be anticipated from the motions, therefore, the classification of human motions can be important in several security applications. Discriminating the human motions and detecting abnormal activities by radar can be potentially useful for many applications.

1.2 Scope of Thesis

The primary purpose of the thesis is classifying different human motions from the radar echos. The thesis work has developed in a number of phases.

Initially, the human walking simulator of V. Chen is examined. Moreover, time-frequency transformations are examined and Short Time Fourier Transform (STFT) and Wigner Ville Distribution (WVD) are applied to the human walking simulator and the efficiencies of these transformations in terms of distinguishing features and clearness of the spectrograms are compared. In addition, the feature extraction methods are examined and applied to the spectrogram of the human walking simulator.

The real radar data is collected by field experiments. The collected data is processed through the radar signal processing steps of matched filtering, moving target indicator filtering, windowing, Fast Fourier Transform and Constant False Alarm Rate.

The micro Doppler feature extraction process is implemented. A high pass filter is designed and applied to suppress the clutter. After that windowing is applied, and the range columns of the Range-Doppler matrix containing target are selected. By applying the STFT on the range columns of the target, the spectrogram is obtained. Finally, the feature extraction methods are applied to the spectrograms to obtain the features for different types of motions.

A simple neural network is implemented to examine the success of human motion classification.

1.3 Organization of Thesis

In the introduction part of the thesis, the aim of the study and the importance of the task (classification of human motions by radar) is discussed.

In Chapter 2, some basic information of Doppler effects of radars is presented. In addition, the studies based on micro Doppler features in radar literature are examined. The connections with the time-frequency transformations, feature extraction methods, classification types and literature survey results for micro Doppler studies are presented.

In Chapter 3, the human walking simulator is examined and feature extraction methods on the simulator are explained. In addition, the theoretical aspects of experimental human data collection, signal processing, feature extraction and classification subjects are presented in this chapter.

In Chapter 4, the experimental results and discussions about the results are given. Comparison of the simulator to the experimental results, analysis of spectrograms and extracted features of each motion, the comparison between them, the classification results of motion types are presented.

The last chapter presents the conclusions on the human motion classification by using radar. In addition, outlines of further research directions that can be explored are given.

CHAPTER 2

BACKGROUND

In this chapter, background information on Doppler effects of radars is presented. In addition, several topics, such as time-frequency transformations, feature extraction methods and classification types, related to the micro Doppler features are examined.

2.1 Background on Doppler Effect in Radar

Radar (Radio Detection and Ranging) is an electromagnetic device, which transmits electromagnetic signal to the environment and calculates range and velocity of object from the returned signal. Range calculation is made by using the time delay of the signal. The velocity of the target is obtained by using Doppler effect. It is known that for the stationary objects, the phase difference of the transmitted signal and the returned signal does not change in time; however, the phase difference changes for the moving objects. The change of the phase depends on the radial velocity of the target because of the physical phenomenon of Doppler effect. The Doppler frequency shift formulation is given as following:

$$f_d = f_t \frac{2v_r}{c} \tag{2-1}$$

where

f_d *: Doppler frequency shift*

f_t *: Transmitted frequency*

v_r *: Radial speed of the target*

c *: Speed of the light*

While the target is approaching to the radar, the radial velocity and the Doppler shift of the target are positive. The situation is the opposite for moving away targets.

It is seen from Equation (2-1) that Doppler frequency shift depends on the radial velocity of the target. In addition, it should be noted that some targets can have several moving parts with different velocities such as helicopters with rotating propellers or a walking man with swinging arms and legs. Each moving component of the target produces a different Doppler shift because of their different velocities. Different motion characteristics are obtained with the help of various Doppler shifts from the different parts of the target and classification of the targets can be made by using these characteristics.

2.2 Background on Micro Doppler Classification for Radar

The repetitive motions of different parts of an object besides the motion of the entire object such as rotating blades of an helicopter, flapping wings of a bird, swinging arms and legs of a human walking is named as micro motion [1]. Human motions, which consist of micro motions of limbs, are studied with the time-frequency transformations to obtain the spectrogram of the motion, and efficiently distinguish and classify them from noisy input.

2.2.1 Time-Frequency Distributions

The main purpose of time-frequency analysis is to examine the distribution of energy in both time and frequency domains [2]. One of the most well-known transformation is the Fourier Transform, which basically decomposes a signal into basic sinusoid functions with different frequencies [3]. The analysis equation of the Fourier Transform for time signal, s(t), can be given as (2-2):

$$S(\omega) = \int_{-\infty}^{\infty} s(t)\exp\{-j\omega t\}dt \qquad (2\text{-}2)$$

Although the Fourier Transform is a very efficient transformation for stationary signals, it is not appropriate for the signals with varying frequency

components in time. Therefore, for the time varying signals, use of joint time-frequency transformations is more convenient than the Fourier Transform. One of the most widely used joint time-frequency transformations is Short-Time Fourier Transform (STFT) which is the windowed version of the Fourier Transform [3]. STFT formulation is derivated from the Fourier Transform formulation by applying windowing with w(t), and the STFT of the time signal s(t) can be expressed as:

$$\mathrm{STFT}(t,\omega) = \int_{-\infty}^{\infty} s(t')w(t'-t)\exp\{-j\omega t'\}dt' \quad (2\text{-}3)$$

The Wigner Ville Distribution (WVD) is a quadratic time-frequency transformation that can also be used to obtain human motion spectrograms. WVD is an effective indicator to view the energy of the signal as a function of time and frequency, because it both satisfies the time and frequency marginal conditions. In addition, WVD provides a high resolution among all time-frequency transformations. On the other hand, it can cause cross term interferences for multicomponent signals [3]. WVD is defined as follows:

$$\mathrm{WVD}(t,\omega) = \int_{-\infty}^{\infty} s\left(t+\frac{t'}{2}\right)s^*\left(t-\frac{t'}{2}\right)\exp\{-j\omega t'\}dt' \quad (2\text{-}4)$$

Furthermore, the Cohen's Class of time-frequency distributions is general form of bilinear time frequency transformation with different alternatives by changing defining kernels [3]. The general form of Cohen's Class is written as:

$$C(t,\omega) = \iint_{-\infty}^{\infty} s\left(u+\frac{t'}{2}\right)s^*\left(u-\frac{t'}{2}\right)\phi(t-u,t')\exp\{-j\omega t'\}dudt' \quad (2\text{-}5)$$

In addition to the well known joint time-frequency transformations, some other time-frequency transformations which are especially important in the micro Doppler analysis are proposed. Hilbert Huang Transform (HHT) is a time-frequency transform which decomposes signal into intrinsic mode functions (IMFs). It is indicated that Cohen's Class transforms use kernels like a smoothing function to attenuate cross terms; however, these kernels reduce the time-frequency resolution; on the other hand, HHT does not use kernels and the resolution of HHT is high enough for the time-frequency demonstrations. In addition, it is pointed out

that the Cohen's Class Transforms have limitations on window lengths because of predefined kernel; however, Hilbert transform does not have such limitations. Moreover, it is stated that the Hilbert transform with EMD beforehand extracts micro Doppler signature from the contaminated signals easier than the Cohen's Class transforms with the help of the reduction of the noise and backscattering interference. Furthermore, it is emphasized that the small frequencies of a vibrating object causes lack of the resolution by the Cohen's Class transform; however, the sinusoidal frequency modulation for small frequency deviations could be plot by using the Hilbert Huang Transform. In brief, it is deduced that HHT is more effective than Cohen's Class transforms [4].

Another time-frequency procedure, which is named as Hermite-S method (multi-window S-method), is also suggested to classify the human motions. S-Method can be formulated as Equation 2-6, where STFT is the short time Fourier transform and P(θ) represents the frequency domain window [5]:

$$\mathrm{SM}(t,\omega) = \int_{-\infty}^{\infty} P(\theta)\mathrm{STFT}(t,\omega+\theta)\mathrm{STFT}^{*}(t,\omega-\theta)d\theta \qquad (2\text{-}6)$$

Hermite-S method is the convolution of Hermite based STFT. Hermite S-Method can be formulated as Equation (2-7), where STFT_k is the STFT of k^{th} order Hermite function [5]:

$$\mathrm{MSM}(t,\omega) = \sum_{k=0}^{K-1} P(\theta)\mathrm{STFT}_k(t,\omega+\theta)\mathrm{STFT}_k^{*}(t,\omega-\theta)d\theta \qquad (2\text{-}7)$$

It is claimed that this method provides more noise reduction and has a better representation with higher resolution than S-Method [5].

Finally, it is noted that some arrangements on the STFT are required to get spectrogram. One of the arrangements is to take the square of the STFT. Squared STFT can be formulated as Equation 2-8, where h(t) is the frequency smoothing window [6]:

$$SP_x(t,f) = \left|\int_{-\infty}^{\infty} x(u)h^{*}(u-t)e^{-j2\pi fu}du\right|^{2} \qquad (2\text{-}8)$$

It is stated that this method always provides positive values and the cross terms are not occurred for this method [6].

2.2.2 Feature Extraction

Feature extraction is one of the most important aspect of classification, because classification success depends on the selection of the features. For this reason, different features are suitable for different applications.

In [7], Youngwook et al. propose methods to classify seven different human motions. These human activities are sitting, boxing, crawling, walking, running, boxing while walking, walking without moving arms. In order to differentiate these human activities, six features are selected as the torso frequency, the bandwidth of the signal, the offset of the signal, the bandwidth without micro Dopplers, the standard deviation of the signal strength, the period of the arms and legs. These features are extracted from the spectrograms. The spectrograms of human motions are given in Figure 2.1. The strongest radar return comes from torso; therefore, the average of peak signals over time bins gives the first feature as the torso frequency. Bandwidth is calculated as the difference between the largest point of the high envelope and the smallest point of the low envelope. Offset is calculated as taking the average value of the mean frequency value of the high envelope and the mean frequency value of low envelope. Bandwidth without micro Dopplers is calculated as the difference between the smallest point of the high envelope and the largest point of the low envelope. Standard deviation is the standard deviation of the signal strength over noise divided to mean of the signal to normalize it. Lastly, the period represents the period of limb motions and is calculated as the time difference between peaks.

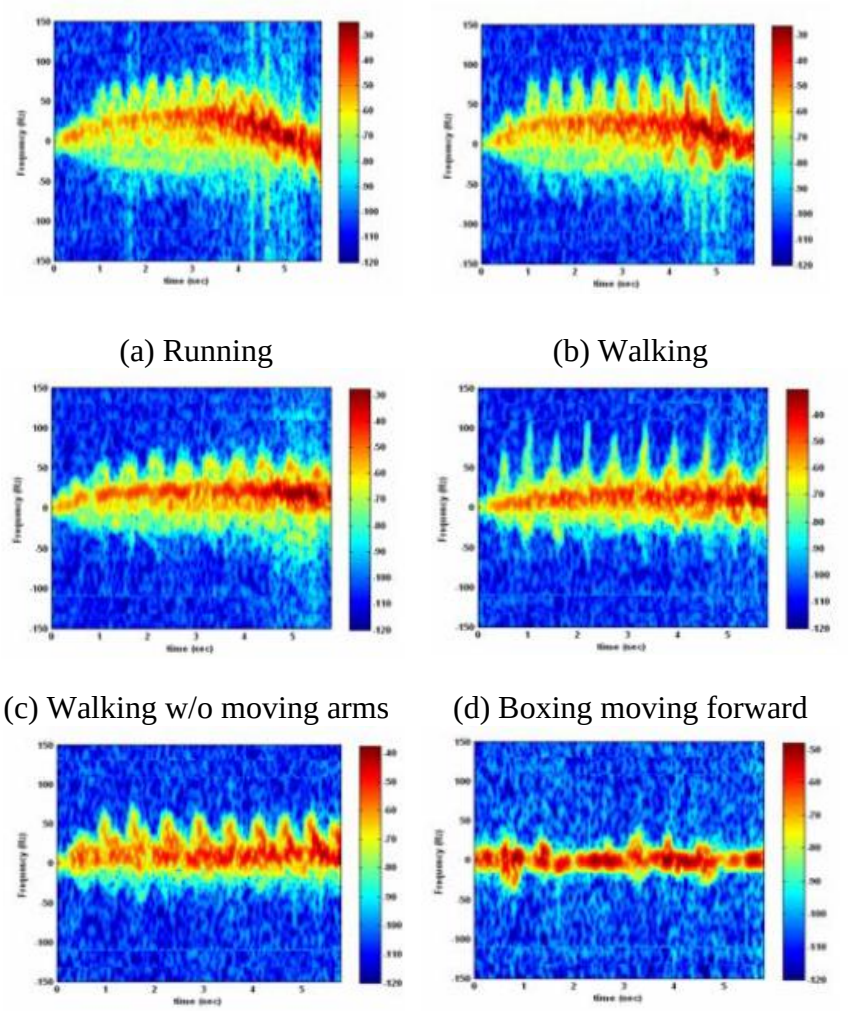

(a) Running (b) Walking

(c) Walking w/o moving arms (d) Boxing moving forward

(e) Crawling (f) Sitting with slight motion

Figure 2.1 Spectrograms of different human motions [7]

In [8], Kim et al. examine feature extraction methods in detail with an experimental data obtained from 12 human subjects for the activities such as walking, boxing, running, crawling, walking with a stick, boxing while walking forward and sitting. The data is obtained by a Doppler radar. STFT is applied to obtain spectrograms, and noise is eliminated by setting a threshold and setting everything to zero that are under that threshold. The six discussed features, which are the torso frequency, the BW of the signal, the offset of the signal, the BW

without micro Dopplers, the standard deviation of the signal strength, the period of the arms and legs, are then extracted. The classification performance of the features is listed from the least important one to the most important one as the torso frequency, BW without micro Dopplers, the BW of the signal, the offset of the signal, the standard deviation of the signal strength and the period. In addition, it is stated that torso frequency alone is successful 70%, while the standard deviation and period achieve only 30%.

In [9], Tahmoush et al. propose other feature extraction methods from the micro Doppler signatures for a human at long ranges. Initially, the returned signals from the head, knees, hands, shoulder, etc. are simulated. After that, the real radar signals which are returned from the torso, the legs, the arms are collected and Short-Time Fourier Transform is applied to get the spectrograms. The stride rate, which is used as biometric, is extracted as feature from the spectrograms. The torso is extracted from the spectrogram with the isolation of the maximum signals at each time. In order to reduce the noise effect, a median filter is used. Data from two people are examined and when only the stride rate is used as the feature of classification, its performance is poor. Then, data from eight people is studied and a signature database is created. By using this database, the correlation matrix of range, Doppler and time is calculated. With the help of the distance function and by using nearest neighbor classification, 80% success is achieved for the test. It is also noted that the change of the azimuth angle of the target reduced the accuracy of the classification; on the other hand the elevation angle does not significantly affect the accuracy like azimuth angle.

In [10], Otero proposes several features to obtain the information of the presence of a human target. The experimental human data is collected by using a CW radar which operates at 10.525 GHz. On the spectrograms, FFT is applied for every Doppler bins on the vertical axis. By this way, cadence frequency is estimated on the horizontal axis. The x-axis of the spectrograms demonstrates the frequency of the moving parts, the velocities is showed on the y-axis, the RCS values are on the z-axis. The first feature is accepted as stride which is the division of velocity to

the cadence frequency. Second feature is defined as appendage/torso ratio is which is the division of the summation of the RCS of the arms and legs to the RCS of the torso. By using these features, the classification is applied to decide whether there exists a person or not. The classification performance with the stride-velocity feature and appendage/torso ratio-velocity feature is 88%.

In [5], Orovic et al. propose features for classification of arm movements. These extraction methods from the envelopes of the arms are used for the classification of a human as two (free) arm motion (FAM), partial (one) arm motion (PAM), no arm motion (NAM). Experiments are done with a radar which has center frequency of 2.4 GHz, transmitter power of 5 dBm, the BW of 70 kHz and the sampling frequency of 1 kHz, and NAM, PAM and FAM data with angles of 0 degree and 30 degree to the line of sight (LOS) of the radar are collected. The first feature is accepted as mean square error, which is assumed as the total variations of the swinging arms with respect to the main motion, and the decision rule is the comparison of the mean square error with a predefined threshold. This feature is applied to the collected data and with the help of this feature, classification of NAM or PAM/FAM is made with 3.54% probability of error. The second feature is defined as time differences of the local minimum and maximum of the envelope functions, the motion is classified as PAM or FAM with only 0.22% probability of error by using this feature.

In [11], Ram et al. investigate the other specifications of human motions which can be seen from the simulated and experimental data. The simulation method is proposed to obtain micro Doppler signatures from the computer animation data for the human motions like walking, crawling and running. Initially, three dimensional positions of each bones are formed by using the computer animation data. Then, the radar returns of the human body parts for each time instant are calculated by considering radar cross section (RCS) of these parts, STFT is applied to get the spectrograms and interpolations are performed to get sufficient Doppler BW. By using these techniques, the simulated radar returns are obtained for the walking, running and crawling human. It is observed that the feet and lower

legs have the highest frequencies, forward/backward swing is visible for running model, Doppler signatures for torso and legs are higher for running than walking model, and the torso has nearly zero Doppler for crawling. After that, an experiment is conducted by using a 2.4 GHz radar in a laboratory and data for walking, running and crawling human is collected. It is observed that experimental results has good correspondence with the simulated results for all walking, running and crawling motions. Moreover, simulated data for 12 GHz radar is also generated and it is demonstrated that higher frequency provided a more detailed spectrogram. Lastly, the position of the radar is changed on the simulator and it is observed that different view angles give different results.

In [12], Tahmoush et al. proposed optimal radar characteristics which provide estimation of human walking parameters. The outdoor experimental data of a walking human is obtained by using a radar with the operating frequency of 17 GHz, the range resolution of 2 m and the Doppler ambiguity of 10.45 m/s. When high PRF (about 2400 Hz) is used, the limbs of the human are observed clearly. When the PRF is decreased, it is observed that decrease in the PRF makes the discrimination of the limbs worse, and for the values less than 400 Hz, the spectrogram loses clearness. In addition, when data is taken by changing the azimuth angle of the human as 0°, 45°, 90°, it is observed that the micro Doppler effects become imperceptible for the values approaching perpendicular to the radar. The effect of azimuth angle on the spectrogram can be seen in Figure 2.2. Moreover, the elevation effect is also investigated on the micro Doppler signatures with data for elevation angles of 15°, 30°, 60°. It is observed that the elevation does not affect the micro Doppler spectrograms significantly. Lastly, an experiment is conducted by illuminating the parts of the body such as legs instead of illuminating the whole body, and it is concluded that it is useful to distinct the micro Doppler signatures of the human parts separately, because the interference of the other parts are suppressed with this method.

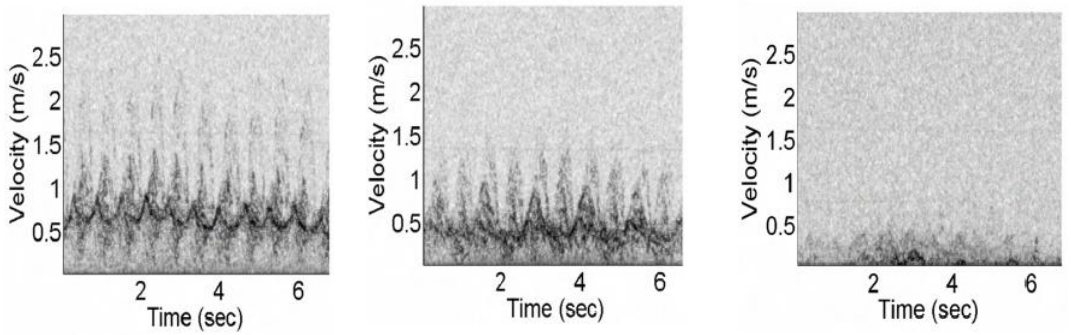

(a) Azimuth Angle of 0° (b) Azimuth Angle of 45° (c) Azimuth Angle of 90°

Figure 2.2 Doppler signatures with different azimuth angles [12]

In [13], Van Drop et al. propose a feature based method for estimation of the global Boulic parameters for walking human. The walking model is constructed by extracting average velocity of the human, torso and legs velocity and the personalization parameters such as frequency, amplitude, phase of the torso and leg. It is assumed that the torso and legs had sinusoidal characteristic and the torso and leg parameters are calculated from the upper, center, lower velocities of the spectrograms. The velocity lines are used to get the repetition frequency. The spectrogram and radial velocity lines are shown in Figure 2.3. By using these features, a realistic walking model is obtained. The experimental data of walking, jogging, running person in the terrain is collected by using a FMCW radar with 9.68 GHz of operating frequency. The detection, percentiles and correlation methods are applied on the experimental data for the feature based model and it is observed that all methods give similar results; however, the percentile method is more efficient. Lastly, the feature-based and the model-based approaches are compared and it is concluded that although the feature based model has deviations from the estimation values for some parameters, their accuracies are equivalent and also the feature-based model is a faster approach.

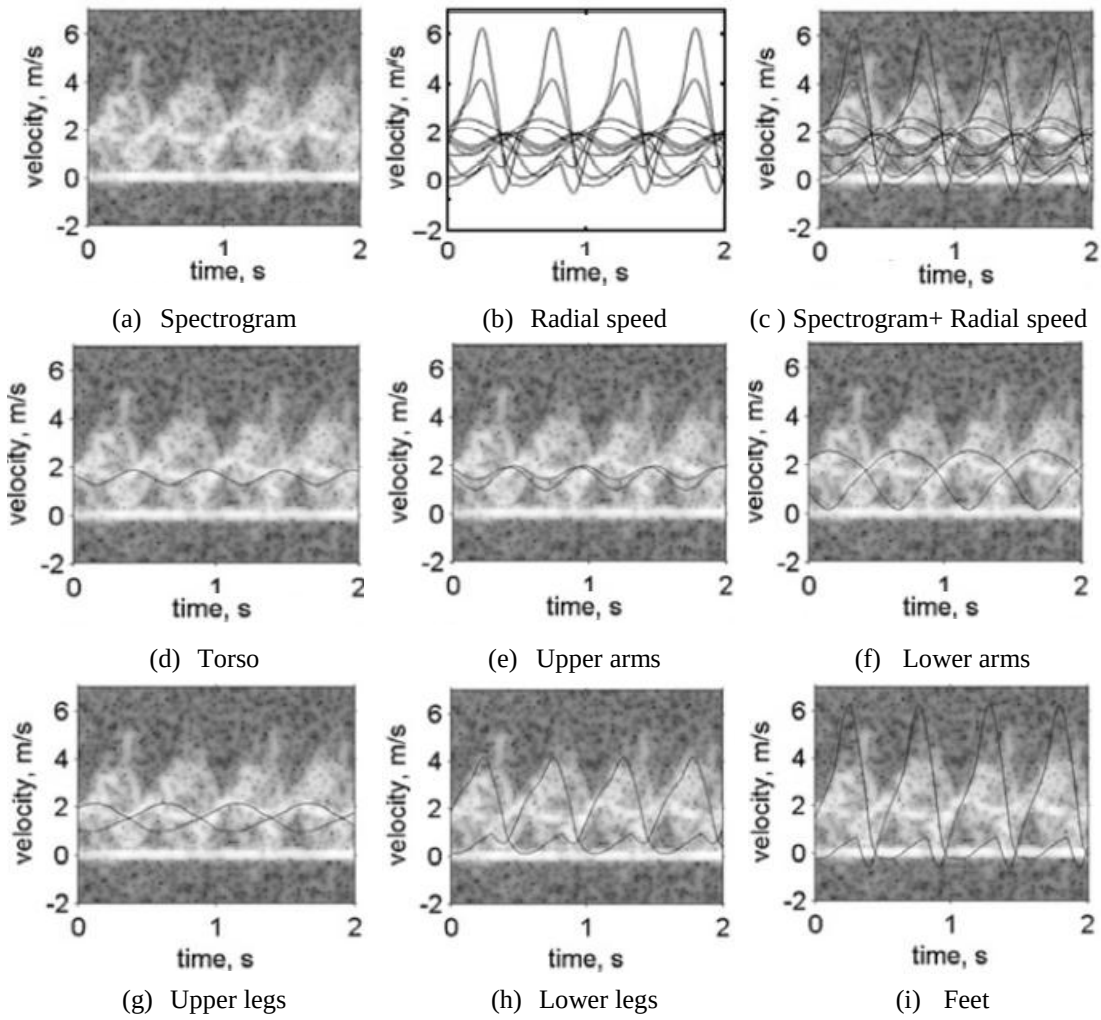

Figure 2.3 Walking spectrogram with radial velocities of Boulic model [13]

In [14], the micro Doppler characteristics of human walking are examined to find out the distinctive signatures. Data from 20 men and 20 women are collected by using motion capture program and animations are made from the collected data and micro Doppler signatures are extracted from the animation. Simulated spectrograms are made for all parts of the body, which can be seen in Figure 2.4. When the measured and the simulated spectrograms of body parts are compared, it is seen that there are some mismatch between them. In addition, when the aspect angle is changed, the Doppler signatures become invisible after 45°. Moreover,

variations are made on the simulations by changing the gender and the effects of sway, bounce, hop, and draw spectrograms are examined to understand the differences between spectrograms. In addition, it is seen that the gender type could not be easily distinguished from radar data.

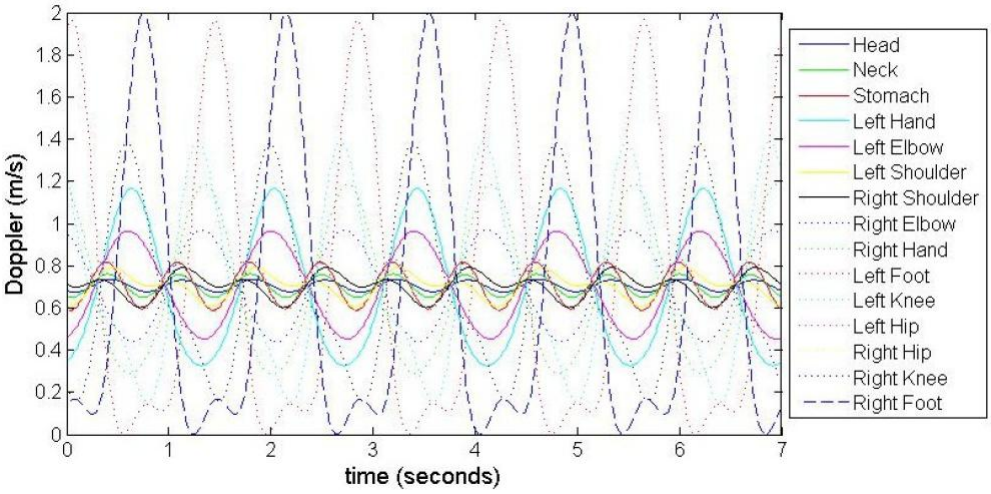

Figure 2.4 Doppler signature of each part of a walking man [14]

In [15], the issue of distinguishing genders is examined in detail. Data from 20 men and 20 women are collected by using motion capture program and animations are made from the collected data and extracted micro Doppler signatures from the animation. It is stated that there are small differences in the footfall, the shapes of torso line and hands on the spectrograms; in other words, spectrograms of men and women seem very similar but have slight differences, which can be distinguished with modern measurement methods.

In [16], Tan et al. propose the usage of a Ka-band radar for the detection of the individuals and groups of people. Firstly, data from a walking man and a running man is collected to investigate the characteristic of walking and running human motion and observed that there was not an important difference between

them when using FFT. In addition, the orientation of the target is focused on, and data is collected for depression angles of 15°, 30°, 60° and azimuth angles of 0°, 45°, 90°. It is also observed that high depression angle made lower RCS value. Moreover, the effect of the number of people on the Doppler spectrum is investigated and data is collected from 2 men and 5 men. From this data, it is deduced that the micro-Doppler signature for 5 men is more distorted than 2 men but has greater SCR for the group data. Lastly, distinguishing a man with a rocket propelled grenade launcher (RPG) from one without is examined, and data is collected for walking and running man with RPG. The paper emphasizes that the distinction of person with RPG is difficult by using FFT spectrogram [16]. In order to obtain a successful feature extraction process, the time-frequency representation is important. The usage of inappropriate time-frequency transforms causes the spectrogram to be blurred and the feature extraction results on blurred spectrograms are not good enough. For example in [16], Tan et al. use FFT, which is not appropriate for human walking because of time-varying nature of the motion, to get the spectrograms; therefore, while their results are being examined, this fact should be taken into consideration.

In [17], feature extraction methods for vibrating, coning, tumbling are examined. A new feature extraction method is proposed for micro Doppler classification of the simulated radar data. For the simulation of tumbling, coning, rotating and vibrating models, Chen's models are used and simulated data is created for point scatters. Pattern recognition is defined for the classification, as first, extracting features from the time-frequency distributions, then creating different patterns for each micro-Doppler signatures, and finally matching the unknown signal with one of the patterns. The time-frequency distributions of 4 dynamics are examined and it is observed that there is no middle line for vibration; there is a middle line for rotation and also the other scatterers of rotating object make symmetric sinusoids around the middle line; there is a middle line for coning however the other scatterers of coning object are not symmetric; the middle line and the symmetry exist for tumbling however the middle line has a slope. With the help

of these features, the patterns are extracted such as the existence of middle line, symmetry and the slope and it is seen that these patterns are efficient for classification. It is concluded that the success of the classification depends on the good description of the feature vectors and the small size of the feature set.

In [18], it is stated that micro Doppler signatures of vibrating and rotating structures are time varying; therefore, the time-frequency transformations of these structures give frequency changes according to time and this feature is used for classification. For the vibrating objects, vibrating is seen from time samples. Swinging arms are distinctive for human walking on the time-frequency signature. For the rotating objects, an helicopter with rotors is modeled and when the time-frequency transform are applied to the signals, the returns from the helicopter body and the blades become distinctive.

In [19], features are extracted from human gait, by using time-frequency analysis and high range resolution. Initially, 2D imaging space is made with the combination of the time frequency analysis and the high range resolution analysis. Data of a pedestrian while walking or running, with or without the motions of arms, with the angles of 0°, 45° and 90° to the LOS of the radar is collected by using a high resolution radar. For the simulation data, a motion capture program which provides data files with 3-dimensional coordinates for the markers on a walking/running human model is used. STFT is applied as the time-frequency transform, and movie analysis is used to get the positions of reflectors relatively. First, the time-frequency analysis and range-Doppler analysis are applied on the simulation of walking data and on the experimental data. Second, this procedure is repeated for the running data. It is concluded that the experimental results are consistent with the simulation results. With the help of high range resolution, the parts of the body are distinctive on the range-Doppler graphs and for the walking/running examples, the stance and the swing phases of feet are different.

In [20], human detection and identification is also analyzed with the synthetic aperture radar (SAR). Human targets are discriminated from other targets

with slow motion by examining the features on the spectrograms. By applying SAR techniques such as pulse compression, range migration correction, quadratic phase error correction and Doppler compression, the Range-Doppler map is obtained, and after that, by taking slice of the range of the target and applying STFT, the spectrogram is obtained. On the spectrogram, Otero [10]'s cadence frequency is taken as the first feature. It is stated that peak of zero cadency gives torso frequency, which is directly related with walking speed. In addition, the next peak gives the fundamental frequency which gives the stride length. Moreover, subsequent peaks give the arms and legs motion and by using amplitudes of these peaks, the RCS value of appendages is calculated. By dividing RCS value of appendages to RCS of the torso gives the appendage torso ratio (AppTorR) which is the third feature. As the fourth feature, height of thigh (HT) is computed by parameters of Thalmann's kinetic model. It is emphasized that the target velocity and AppTorR can be useful for the discrimination of human from animals. Finally, it is concluded that estimates of these features from cadence frequency becomes unreliable if data length is not sufficient for FFT.

In [21], different classification methods are applied to same data and their efficiency is compared to each other. Firstly, statistical classification methods are studied on simulated data which are point scatter model and RCS model. The target is modeled as a cylinder with 1 m length and 0.125 m radius and the radar is modeled as a X-Band pulsed radar. The spectrograms of coning, tumbling, rotating and vibrating for both simulations are obtained. One of the differences between RCS model and scatter model is that for rotation and tumbling, there are vertical lines which occur because of the strong reflections for certain aspect angles at RCS model. For vibration and coning, there are no such vertical lines. In addition, the performance of Principal Component Analysis (PCA) and Independent Component Analysis (ICA) is the same for the point scatter model; however, for the RCS model, PCA works better than ICA because the length is an important parameter for the cylindrical target.

In [22], Gabor feature extraction methods is used to discriminate vibration, rotation, coning and tumbling,. Eight Gabor functions are derived as the feature extraction methods and only the scale factor is chosen to use as the classification feature because of computational efficiency.

In [23], a new algorithm named as empirical mode decomposition (EMD) which provides an efficient way of extracting micro Doppler signatures is proposed in addition to the known feature algorithms. EMD is described as the decomposition of the signal into its intrinsic oscillatory components according to the local characteristics of time scale. The simulated data with vibration frequency of 20 Hz is obtained to test the EMD method. Seven intrinsic mode functions (IMFs) and residue are extracted from the data. When the frequency representation for each IMFs and the residue are obtained, it is observed that the micro Doppler signature can be obtained from IMF2; hence, the other components are redundant. A truck with vibrating engine is used as the experimental data. EMD method is applied on the truck engine data and extracted one IMF and residue from the data are extracted and after STFT is applied. It is observed that the micro Doppler signatures of IMF1 are at ±30 Hz. When the mean value is subtracted from the spectrogram of the original data, the micro Doppler effect could not be discriminated sufficiently; on the other hand, the result of the EMD demonstrates the micro Doppler signatures clearly.

Extraction of micro Doppler features from vehicles is investigated in [24]. Initially, a homodyne radar which provides in-phase and quadrature components of Doppler signatures is designed and an experiment is conducted with a truck. A vibrating reflector on the top of the truck is placed and data is collected while the truck is moving towards the radar. Short-Time Fourier Transformation (STFT) is applied to get spectrograms. The spectrogram of reflector at 5 Hz on stationary truck and the spectrograms of moving truck with 5 Hz and 20 Hz oscillating reflector and Gabor filtered applied spectrograms of moving truck with 5 Hz are obtained and the Doppler signatures are investigated from the spectrograms. Two straight lines are seen for stationary truck and reflector; two concave lines are seen

for moving truck with reflector at 20 Hz; two nested concave lines for reflector at 5 Hz; however, it should be emphasized that they are not very clear spectrograms.

In [6], different kinds of time-frequency transforms are studied to classify animate or inanimate urban objects. For the first experiment, a fan whose blade is covered with aluminum foil is used as a target and a Doppler radar which operates at 906 MHz is used. The second experiment is conducted with a metallic sphere with the diameter of 12'' by accelerating the sphere from the radar, and then decelerated to the sphere. As the third experiment, the radar is placed 4 ft from a thick wall and at the other side of the wall, a person with a corner reflector is walked through the wall and turned back within 20 feet of range. STFT is applied for the data of the fan, WVD is applied for the data of the linear positioner, B-distribution is used for the data of the walking person and it is emphasized that the choice of time-frequency transformation is important for the urban sensing applications. It is concluded that the inanimate objects rotate, vibrate or oscillate but do not translate; therefore, inanimate objects have only zero Doppler component at the time-frequency graphs. On the other hand, because the animate objects translate, they both have the zero Doppler and micro Doppler parts.

2.2.3 Classification Methods

There are many different methods for classification. In this section, some of them are examined to evaluate their efficiency.

Neural network is one of the classification methods for micro motions. In [7], seven human activities which are sitting, boxing, crawling, walking, running, boxing while walking, walking without moving arms are differentiated by using an artifical neural network (ANN) method using the micro Doppler signatures. For the experimental data, a Doppler radar which operates at 2.4 GHz is used. Data from twelve people is collected in a laboratory. Short time Fourier transform (STFT) which has 0.25 seconds time-window is applied on to the experimental data. After the feature extraction, ANN is applied for classification. In the ANN, 8 subjects are

used for training, 4 subjects are used for testing set. The results of the validation test demonstrated that the classification accuracy is 87.8%. It is stressed that walking and walking without arms classes have the most misclassification.

In [8], the support vector machine (SVM) is proposed as the classification method. The experimental data from 12 human subjects for the activities such as walking, boxing, running, crawling, walking with a stick, boxing while walking forward and sitting for 12 realizations is collected by using a Doppler radar. For the classification, a decision tree classifier which consists of support vector machines (SVMs) is applied to the data. The classification error for SVM is about 8% and the accuracy is 92%. The classification of the combination of the activities is also studied and it is observed that there are misclassifications on the transition parts. Moreover, the effect of the aspect angle on the classification is investigated with experimental data for angle of 30°, and it is observed that the classification accuracy is not affected much for the small angles. Finally, a through wall experiment is conducted and it is observed that micro Doppler effects are hardly identified because of the reduction of the SNR because of the wall.

In [25], Bayesian classification is used for micro motions. A Bayesian formulation which simply makes classification on only the number of micro Doppler signals on the returned radar signal is proposed. Experiments with a human and a vehicle are conducted by using a scanning-beam continuous wave (CW) radar which operates at the frequency of 36 GHz, has long dwell times which provides the classification of multiple targets. The experiment is repeated and it is seen that the probabilities of a human and a vehicle changed according to probabilistic formula. For the evaluation of the tests, Pd (probability of detection), accuracy, Pfa (probability of false alarm) are calculated according to the value of N (the number of event). When N is less than 8, Pfa is still applicable; however, Pd value changes between 0.54-0.67 which is too low for the classification. When N is equal to 10, Pd changes between 0.79-0.92 and Pfa is between 0.01-0.15 for the all values of probability of threshold, and these parameters can be the optimal solutions for the Bayesian applications.

In [26], there are different approaches to increase the efficiency of the known classification methods for micro Doppler signatures of human motion. In this work, Short-Time Fourier Transform (STFT) is used as a time-frequency transformation to get spectrogram from the signal. In order to extract features for micro Doppler classification, two-directional two dimensional Principal Component Analysis (2D2-PCA) and two directional two dimensional Linear Discriminant Analysis (2D2-LCA), which is the novel part of their approach, are applied to the spectrograms. The last part of their approach is to use the support vector machine (SVM) to classify the feature vectors. Their new approach is applied to differentiate two arm motion, one arm motion and no arm motion. In order to understand the efficiency of the new approach, it is compared with one-directional Principal Component Analysis (1D-PCA) and combination of Discrete Fourier Transform (DFT) and PCA. The classification accuracy rates are 91.9% for 2D2-PCA, 75.2% for 2D2-LDA, 92.1% for 1D PCA, 65.4% for DFT+PCA. Although it is seen that classification accuracy is higher for 1D PCA, the covariance matrix for 2D2-PCA is smaller than 1D-PCA which provides efficient computation. In brief, the new approach provides efficient classification.

In [27], there is an approach that using a speech processing technique for micro Doppler classification. Dynamic time warping (DTW) which is normally used as a speech processing technique is used with radar signal for the micro Doppler classification. The speech signals are varying in time and the classification of these signals rely on probabilistic models. Because of the similarity between the speech signals and the radar signals, a probabilistic model was chosen as classifier. First, a reference data series which are obtained from the wheeled, tracked, personnel classes with time durations of 8, 16, 32, 48, 64 msec are generated. The duration of the series and the decorrelation time are chosen and confusion matrices for the time duration, the decorrelation and the classification type are made. The results of the tests demonstrate that DTW classifies personnel correctly with the percentage of 75% and vehicles correctly with the percentage of 98%; on the other

hand, DTW differentiates wheeled vehicles from the tracked vehicles for only the percentage of 28%.

In [28], efficiency of multiperspective data is compared with monoperspective data by using the dynamic time warping classification. The monoperspective data is obtained by Thales MSTAR which operates at Ku-band for wheeled, tracked vehicles and personnel and for different azimuth angles. The multiperspective data of wheeled vehicle, personnel and bicycle is obtained from 3 nodes on an arc by using NETRAD which operates at 2.4 GHz. Zero Doppler is removed, the range bins related with the target is selected, the signal of the bi-static path is formatted, micro Doppler signature is analyzed, the signal is separated into shorter frames and lastly data sets are created as the post processing of the multiperspective data. Because of the low transmit power, pulses are integrated to observe the micro Doppler effect. Monoperspective classification and multiperspective classification are applied. The multiperspective one is a better classification; on the other hand, working with complex pre-processing procedure and higher dimensionalities of the data are the disadvantages of it. Moreover, probability of correct classification is 0.95 for monoperspective; 0.97 for multiperspective; however, probability of generalization, which is the measure of giving the same class as output for each run, is 0.70 for monoperspective and 0.24 for multiperspective. Therefore, it is concluded that the monoperspective classification is efficient; however, it is emphasized that the multiperspective classification could be better by using extra information.

In [21], the classification methods are applied to same data and their efficiency is compared. Statistical classification methods are studied on simulated data which are point scatter model and RCS model. A cylinder with 1 m length and 0.125 m radius and a X-Band pulsed radar are modeled and radar return for coning, tumbling, rotating and vibrating are obtained for both point scatterer and RCS model. The classification types, support vector machine (SVM), Bayes, k-nearest neighbour (k-NN) or linear discrimination classifier (LDC) are applied on these models. The test results demonstrated that for the point scatter model SVM has

7.5% error which is the lowest error, and k-NN gives 2.5% error which is the best result for the RCS model.

In [22], the classification methods are compared by means of efficiency. Firstly, 20-30 point scatters are simulated and 200 micro Doppler signatures are collected for each of tumbling, vibrating, rotating and coning motions; the classification methods are applied on this simulated data. Pattern Recognition Toolbox of Matlab are used to compare different classifiers such as Bayes linear, k-nearest neighboor (k-NN) and support vector machine (SVM) to make micro Doppler classification. The results demonstrated that the success rate of the classification is between 38% and 78% for Bayes linear, 42% and 84% for k-NN, 44% and 92% for SVM classifier. It is concluded that SVM which makes maximization of the boundries of the classes has the best performance.

Finally in [17], the specifications of classifiers are investigated. Five classifiers, Bayes linear classifier (ldc) and quadratic classifier (qdc), support vector classifier (svc), k-nearest neighboor rule classifier (k-nn), neural network classifier (nnc) are applied on the simulated data for four different motion dynamics, tumbling, coning, rotating and vibrating. It is observed that nnc classifier has classification error rate of 12.31%, the others' classification errors are 0%. The evaluations of the classifiers can be summarized such that quadratic classifier makes the separation of the classes better, neural network classifier has uncertainties which can cause wrong classification, Bayes linear classifier sets boundaries only on the distribution probabilities, support vector classifier puts maximum margins, k-nn is not strictly linear which makes the boundaries zigzag shape.

CHAPTER 3

PROCESSING, FEATURE EXTRACTION AND CLASSIFICATION

This study investigates the possibility of discriminating human motions by using radar; therefore, processing of radar returned signals, generating spectrograms from signals, extracting features from spectrograms and classification are all part of this study. In the light of these requirements, a human walking simulator is initially examined and suitable feature extraction methods using this simulator data are investigated in this chapter. In addition, the collection of experimental human data, processing this signal, feature extraction and classification methods are presented in this chapter.

Signal processing, feature extraction and classification algorithms are developed by using MATLAB. In addition, signal processing toolbox, neural network toolbox and filter builder toolbox of MATLAB are also used for this study.

3.1 Data Processing and Feature Extraction on Human Walking Simulator Output

In this section, V. Chen's human walking simulator is examined and the modifications which are required for this study are explained. In addition, feature extraction methods on the spectrogram of human walking simulator are presented. Moreover, the feasibility of applying a different time-frequency transformations for obtaining the human walking spectrograms is investigated.

3.1.1 Processing Human Walking Simulator Output

Human walking is a periodic motion with determined positions of foot according to each other, periodically swinging arms and legs and bobbing motion of

human which makes body gravity up and down. Although human walking has a general form, there are different characteristics for individuals [1]. Identifying human walking is an important issue, therefore, there are studies which model human walking. One of these studies is V. Chen's and his human walking simulator is one of the widely used tools for human walking studies, because he constructs the simulator very similar to real data with the help of empirical human segmentation and an empirical walking model.

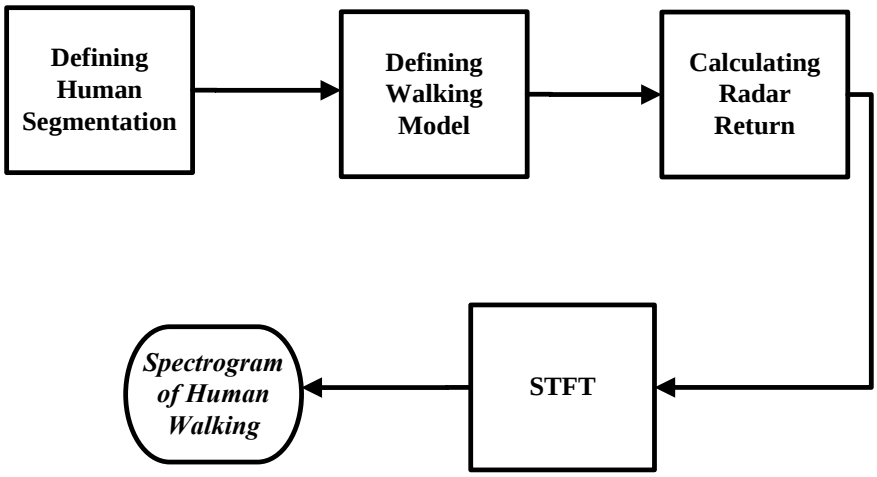

Figure 3.1 Processes of human walking simulator by Chen

In this work, the output of human walking simulator which is developed in Matlab by Chen is examined in order to visualize radar return of human walking. The processes of extracting spectrogram of human walking are explained as shown in Figure 3.1. Boulic, Thalmann, and Thalmman's empirical mathematical parameterization is used at Chen's simulator as the kinematic parameters of body segments. By this way, human segmentation of the simulator is defined. Human model segments of the simulator is given in Figure 3.2. Then, the human model is made to walk, by using human walking model of Boulic, Thalmann, and

Thalmman. Then, the radar returns from each part of human are computed. It is assumed that the radar signal is transmitted to the human and signals are returned from each body part such as head, torso, arms, legs and the returned radar signal contains all these parts. At the last stage, STFT is applied to the radar returned signal and spectrogram of human walking is obtained. The spectrogram of human walking simulator can be seen in Figure 3.3. The human walking simulator is very similar to real human walking data. The detailed information on the similarities of the simulator to the real walking data is given in Chapter 4.4.

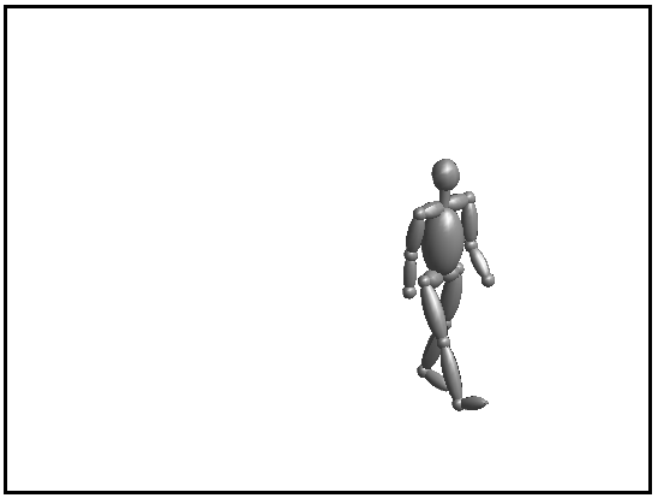

Figure 3.2 Human Walking Model of Chen [1]

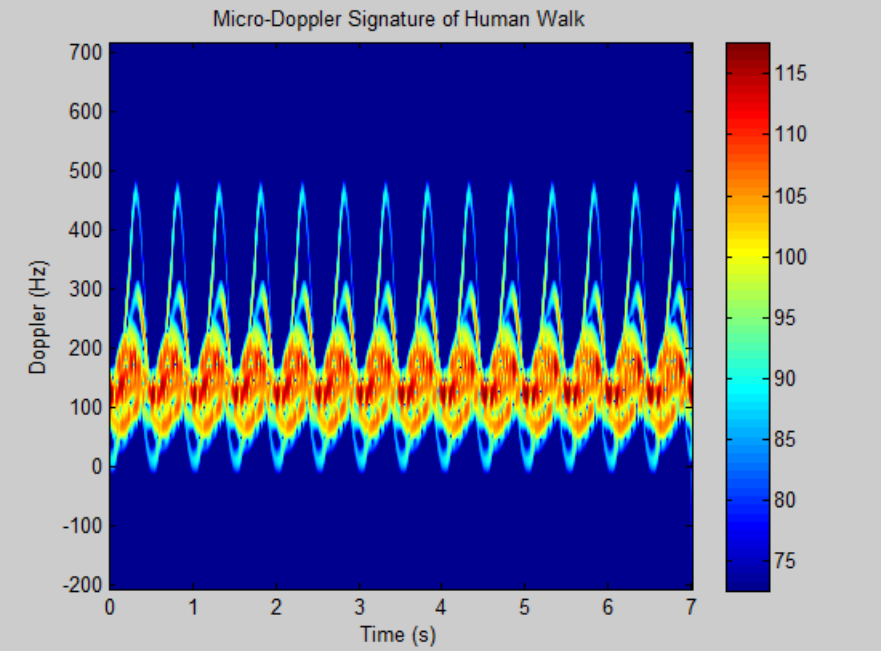

Figure 3.3 Spectrogram of human walking simulator by STFT [1]

3.1.2 Feature Extraction

In this section, feature extraction methods on the literature are examined and applicable micro Doppler features on the spectrograms are determined. At one of the articles, six Doppler features, which are the torso Doppler frequency, the total bandwidth of the Doppler signal, the offset of the total Doppler, the bandwidth without micro Doppler, the normalized standard deviation of the Doppler signal strength, and the period of the limb motions are defined to characterize the micro Doppler signatures [7]. These Doppler features seem applicable and feasible for the classification of different human motions, because the successful applications of classifying different human motions by using features are explained in only these articles. Therefore, these feature extraction method is applied on the spectrogram which is obtained from the human walking simulator. These features are presented on the spectrogram of human walking simulator in Figure 3.4.

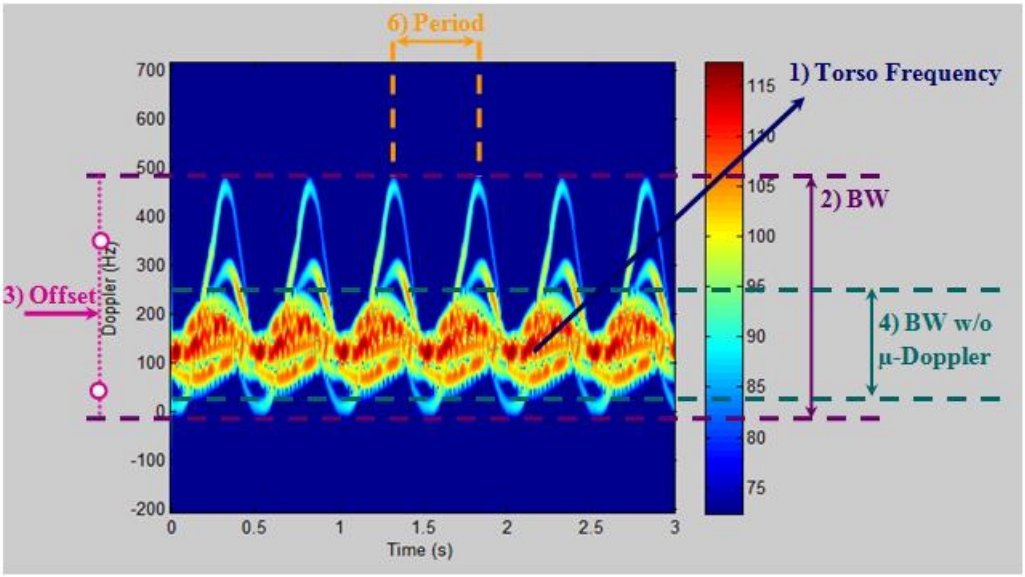

Figure 3.4 Micro Doppler features, the torso Doppler frequency, the bandwidth, the offset, the bandwidth without micro Doppler, the standard deviation, and the period, on the spectrogram of human walking simulator

Initially, discrimination of Doppler signal from noise is required; therefore, the lowest power level of the signal histogram is used as the noise threshold. In Figure 3.4, dark blue area corresponds to the noise and the minimum value of the signal histogram is found as 72.3933 dB. The signal strength values higher than this threshold is accepted as signal.

First feature is the torso Doppler frequency which can be described as the average frequency of the peak signal over the time bins. It is known that the torso produces the strongest return in the spectrogram, while arm and leg movements modulate the torso frequency with the periodic micro-Doppler modulations. Therefore, the strongest frequencies is extracted from the spectrogram. In order to determine the distribution of the strongest signals, a high signal strength threshold is assigned. An empirical threshold of torso frequency is determined as 5 dB less of the maximum signal strength, which means that the signals whose strength is higher this threshold is accepted as torso return signals. For Figure 3.4, maximum signal

strength is 117.2858 dB and the threshold for the torso frequency is calculated as 112.2858 dB. The signal strengths higher than this threshold is kept in an array; number of time bins of these signals are also counted. When the summation of these peak signal strengths is divided to the total number of time bins; the torso frequency is obtained. This value is calculated as 144.6971 Hz for Figure 3.4.

In order to extract of 2^{nd}, 3^{rd} and 6^{th} features, which are bandwidth, offset and limb period, primarily two envelopes are identified. For identification of envelopes, the signal histogram discrimination threshold, which is 72.3933 dB for Figure 3.4, is used. The method of extracting envelope is that comparing the signal strengths of each bin with the threshold and if the signal strength is greater than or equal to the threshold, this data is within low and high envelopes. The difference between high and low envelopes is the starting point and the direction of the comparison. For the high envelope, the comparison is started from the highest frequency value of the each time bin of the spectrogram and the frequency values are decreased as the signal strength becomes greater than or equal to the threshold; as a result, the calculated high envelope for Figure 3.4 is given in Figure 3.5. The low envelope is the lowest frequency in which the signal strength exceeds the noise threshold in a time bin, and the calculated low envelope is shown in Figure 3.6.

.

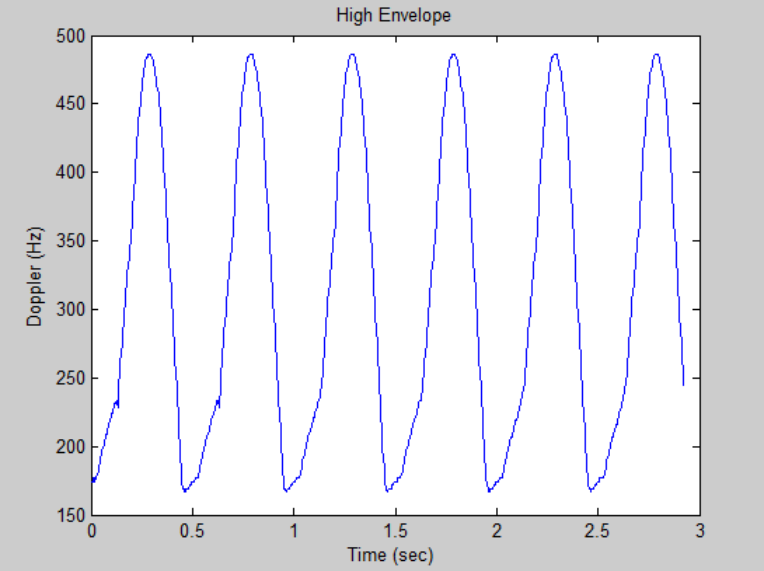

Figure 3.5 High envelope of the spectrogram

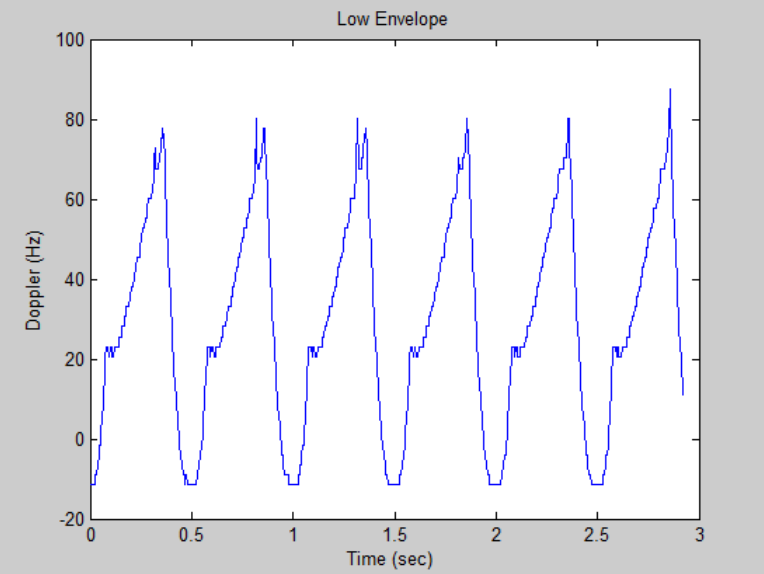

Figure 3.6 Low envelope of the spectrogram

The second feature is described as the total bandwidth of Doppler signal. In order to obtain the total bandwidth, the largest frequencies of the high envelope, and the smallest frequencies of the low envelope are calculated as shown in Figure 3.7. The difference between the largest frequencies of the high envelope and the smallest frequencies of the low envelope gives the total bandwidth. For instance, the largest frequency of the high envelope is 486.4 Hz, the smallest frequency of low envelope is -11.5613 Hz; thus, 497.9613 Hz is total bandwidth for Figure 3.7.

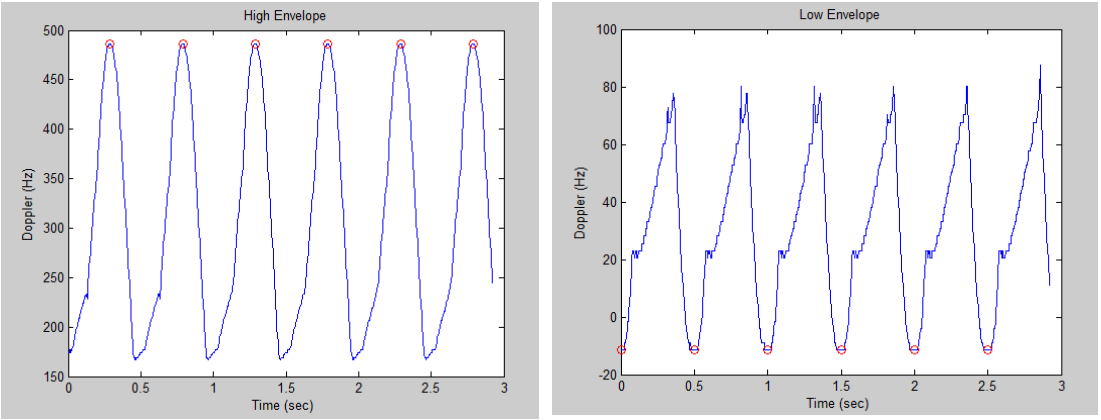

(a) High envelope (b) Low envelope

Figure 3.7 The largest points of the high envelope and the smallest points of low envelope

The third feature is described as the offset of the total Doppler signal. In order to obtain the offset, the mean frequency values of the high envelope, and the mean frequency values of the low envelope are calculated as shown in Figure 3.8. The difference between the mean frequencies of the high envelope and the mean frequencies of the low envelope gives the offset. For instance, the mean frequency of the high envelope is 310.1729 Hz, the mean frequency of low envelope is 29.3326 Hz; thus, the mean of these two means is 169.7528 Hz, which is the offset value for the human walking simulator as shown in Figure 3.8.

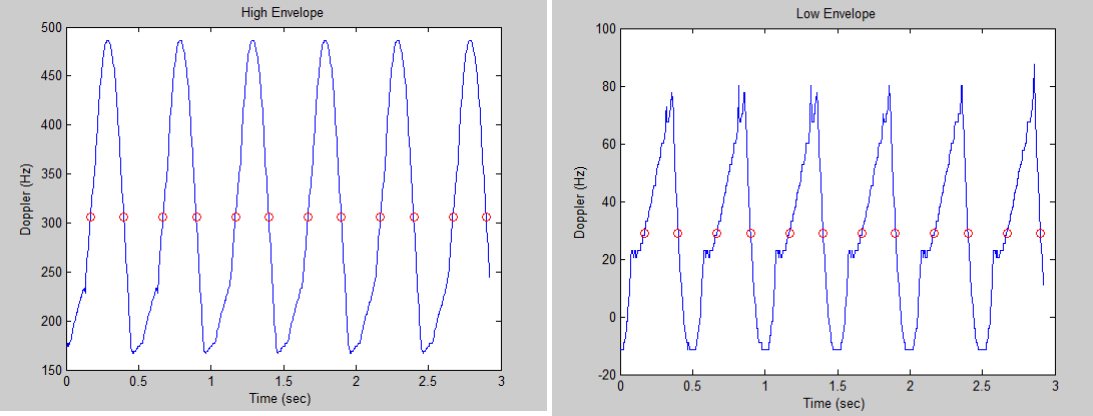

(a) High envelope (b) Low envelope

Figure 3.8 The mean points of the high envelope and the mean points of low envelope

The fourth feature for classification is the bandwidth without micro Doppler. It is known that the torso produces the strongest return in the spectrogram, the micro-Doppler modulations are limbs returns; therefore, bandwidth without micro Doppler is the bandwidth of torso only. Therefore, the high and low envelopes of the strongest Doppler frequencies from the spectrogram is extracted, by using the empirical threshold of torso frequency. After high and low envelopes of torso are extracted, the maximum frequency value for the high torso envelope and the minimum frequency value for the low torso envelope are calculated. The difference between the maximum of high torso envelope and the minimum of low torso envelope gives the bandwidth of torso, in other words bandwidth without micro Dopplers. For instance, the maximum frequency of the high torso envelope is 283.2516 Hz and the minimum frequency of low envelope is 55.3290 Hz; thus, the bandwidth without micro Doppler is 227.9226 Hz for human walking simulator.

The fifth feature is taken as the standard deviation of the total Doppler signal. In order to obtain this feature, the standard deviation of the signal strength of all the above-noise Doppler signals in the spectrogram is calculated. The standard deviation formula at (3-1) is used for this calculation; where μ represents the mean

value of the signal strength, x_i is used as the samples of the signal, N is the number of samples and σ represents the standard deviation.

$$\sigma = \sqrt{\frac{1}{N}\sum_{i=1}^{N}(x_i - \mu)^2} \quad (3\text{-}1)$$

By applying this formula to the Doppler spectrograms, the standard deviation value is calculated. For example, for the above human walking example, the standard deviation value is calculated as 7,2021.

The sixth feature is the period of the limb motions. In order to obtain the period, the time values for the maximum frequency values of the high envelope are calculated as shown in Figure 3.7. The difference between the time value of first peak and the time value for the last peak is calculated. The total peak numbers are counted and the number of time interval is 1 less than the number of peaks. By dividing the time difference between first and last peak to the number of time intervals gives the period. For instance, the time value for the first peak value is 0.29 seconds; the time for the last peak is 2.79 seconds; the time difference is 2.5 seconds. The peak values are counted as 6; therefore, the time value is divided to 5 and the period for the human walking simulator is calculated as 0.5 seconds as can be seen from Figure 3.7.

3.1.3 Applying Wigner Ville Distribution on Human Walking Simulator Output

It is explained in 2.2.1 that for time varying signals like human walking, use of joint time-frequency transformations is more convenient than Fourier Transform. STFT (Short Time Fourier Transform) is examined as explained in 3.1.1; and it is seen that STFT is an efficient TFT for micro Doppler signatures. In addition to STFT, the effectiveness of another time-frequency transformation is examined. Wigner Ville Distribution (WVD) transform is implemented in Matlab and is applied to the human walking simulator. The WVD applied human walking simulator is demonstrated at Figure 3.9.

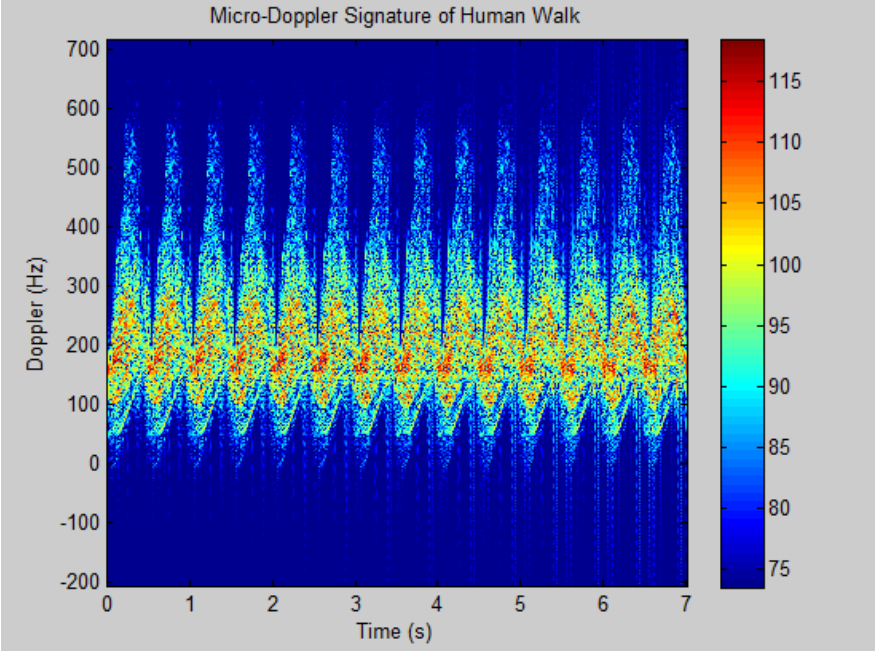

Figure 3.9 Spectrogram of human walking simulator by WVD

When Figure 3.9 is examined and it is seen that there are interferences on the signal histogram. In addition, when the spectrogram of human walking simulator by WVD in Figure 3.9 and STFT in Figure 3.3 are compared, it is seen that the envelope of the spectrogram with WVD is similar to the envelope of STFT; on the other hand, there are interferences on the spectrogram of WVD. It is an understandable result that the nature of the WVD causes cross term interferences because radar return signal of human walking is a multicomponent signal which contains torso, limb motions. Because the micro Doppler signatures of torso, and human limbs have intersections; when WVD is applied to the human walking spectrogram, cross terms make the graph complicated.

In order to compare WVD and STFT results of human walking simulator by means of micro Doppler features quantitively, the extracted feature values of WVD and STFT are listed at Table 3.1.

Table 3.1 Micro Doppler features of human walking simulator with STFT and WVD

	Comparison between STFT and WVD					
	Torso Frequency (Hz)	Bandwidth (Hz)	Offset (Hz)	Bandwidth w/o Micro Doppler (Hz)	Standard Deviation	Period (sec)
Human Walking Simulator with STFT	144,6971	497,9613	169,7528	227,9226	7,2021	0,5000
Human Walking Simulator with WVD	185,4587	552,4645	207,1810	225,4452	10,2521	0,5000

When Table 3.1 is taken into consideration, it can be seen that the results of WVD are similar to STFT. On the other hand, because of the interferences of WVD, the spectrogram is more spread and the bandwidth values are bigger than STFT.

Although the extracted features of WVD are similar to STFT, cross-term interferences of WVD smear spectrograms and it is not possible to discriminate the human limbs from the torso. Therefore, use of STFT seems more appropriate and it is used as the time frequency transform throughout this thesis.

3.2 Signal Processing, Feature Extraction and Classification on Experimental Human Data

Human motion classification from experimental human data requires the following steps shown in Figure 3.10.

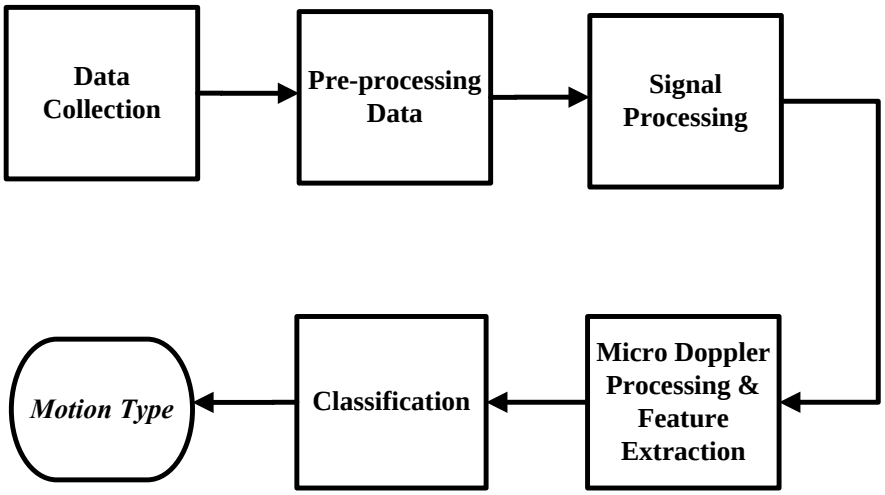

Figure 3.10 Block scheme of human motion classification

Experimental data is collected at an outdoor test facility by using a ground surveillance radar. Details about data acquisition is given in section 3.2.1.

The decimated and down converted data is pre-processed to make it suitable for signal processing. Then, each pulse repetition interval (PRI) is processed by matched filtering. After a number of PRIs are accumulated MTI filtering, windowing, and FFT is performed on the data for the same range bin. The range and velocity of the targets are obtained using CFAR algorithm. Details about these signal processing steps are presented in section 3.2.2.

The matched filtered data is passed through the high pass filter and then a window. After windowing, the columns of target range are extracted from windowed matrix and STFT is applied to obtain the spectrogram of human data. Features are extracted from these spectrograms. Details about these processes are given in section 3.2.3.

After extracting micro Doppler features, neural network classification is applied to classify the human motions by means of micro Doppler features. Details about micro Doppler classification is presented in section 3.2.4.

3.2.1 Data Collection

Experimental human data is collected in an outdoor test facility, by using a ground surveillance radar. It is a pulsed Doppler radar operating at Ku-band. For the data collection, fixed antenna position mode of radar is used, in which radar operates at selected azimuth angle without rotation. The test facility can be described as a concrete, rectangular area, whose dimensions are approximately 200 meters of length, 150 meters of width, and is surrounded by steppe.

The experimental data collection procedure at the field can be summarized as follows: Initially, radar is positioned at the middle of one of the long edges of the area, and target's exact position is determined by using a binocular which calculates the distance. The direction of the target is determined and a line which has 0° aspect angle to the line of sight of the radar is drawn on the road to guarantee the use of same path for each motion. In addition, other paths are also drawn which have 30° and 60° aspect angles to the line of sight of the radar. When the directions of the target are determined, radar is switched on and the parameters are selected. The radar antenna is then pointed to the direction of the target with the help of the optical sight of the radar. Data recording equipment is made ready. Further, related range bins are calculated and according to these range bins, recording message which is sent from radar is prepared. The target is then requested to start walking by using walkie talkies and recording is started on both the radar and the recording device at the same time. After 30 seconds walk, recording is stopped and controlled whether the recording is done successfully or not, and then, the format of the recording is converted to .txt from .dump format by using a conversion program. This procedure is repeated for all test cases for different human motions and for all test subjects.

In order to define the list of the required data, important points are taken into consideration to limit the data types. The crucial issues can be listed as what the effects of using different pulse widths could be on the spectrograms; what the micro

Doppler characteristics of human walking, running, crawling and creeping are and how various orientations of walking human affect the spectrograms.

Data collection is carried out in two steps. Initially, the use of different pulse widths are examined as the radar is capable of using different pulse widths. If there are only SNR differences between different pulse widths and not any other differences on the characteristics of the spectrograms, it would be reasonable to collect data at only a single pulse width. Therefore, as the first step of data collection, data is collected from human subjects who walk towards the radar with 0° angle using two different pulse widths. 1st data set consists of the first person walking at 150 meters towards the radar with the short PW1. 2nd data set consists of the second person walking at the range of 1000 meters towards the radar with the long radar pulse width. 1st data set and 2nd data set are processed and the results, which are explained in detail in section 4.1, are obtained. Spectrograms obtained for different pulse widths show that they have nearly same characteristics with only SNR and clutter differences. Therefore, at the end of the first part of the data collection, it is decidto use the short pulse length for collecting data for different motions and different angles.

Data of human walking towards the radar with aspect angle of 0° is collected and saved as Data Set-1. To examine the effects of various orientations of human walking, aspect angle of subject to the line of sight of the radar is arranged as 30° and 60°, data for 30° and 60° are saved as Data Set-2 and Data Set-3, respectively. In order to extract the micro Doppler characteristics of different types of human motion, running, crawling and creeping data is collected from the same person. Running data is saved as Data Set-4, crawling data is saved as Data Set-5 and creeping data is saved as Data Set-6. In order to get more accurate results and prevent dependency on one motion of the person, each motion is repeated for 7 times. If the results are different than others, the majority becomes important; therefore, data repetition number is decided to be more than 5 and so 7 is chose.

Collecting data from same person can avoid generalization for feature extraction. Therefore, data collection is repeated for two different people. 2nd person's walking data with 0° is collected and saved as Data Set-7, walking data with 30° as Data Set-8, walking data with 60° as Data Set-9, running as Data Set-10, crawling as Data Set-11, creeping as Data Set-12. Lastly, another person repeats all motions and angles; 3rd person's walking data with 0°, 30°, 60°, running, crawling and creeping data saved as Data Set-13, Data Set-14, Data Set-15, Data Set-16, Data Set-17, and Data Set-18, respectively.

The list of the collected data is given in Table 3.2. Because each motion is repeated 7 times for each data set, 140 files are obtained in total. The results of each data file are presented in Chapter 4.

Table 3.2 The list of collected data

Part Number	Number of Data Set	Target	Pulse Width	Average Range of Target (meter)	Target Motion Type	Azimuth Angles (degree)
Part-1	Data Set-1	1st man	1	150	Walking	0°
Part-1	Data Set-2	2nd man	2	1000	Walking	0°
Part-2	Data Set-1	1st man	1	150	Walking	0°
Part-2	Data Set-2	1st man	1	150	Walking	30°
Part-2	Data Set-3	1st man	1	150	Walking	60°
Part-2	Data Set-4	1st man	1	150	Running	0°
Part-2	Data Set-5	1st man	1	150	Crawling	0°
Part-2	Data Set-6	1st man	1	150	Creeping	0°
Part-2	Data Set-7	2nd man	1	150	Walking	0°
Part-2	Data Set-8	2nd man	1	150	Walking	30°
Part-2	Data Set-9	2nd man	1	150	Walking	60°
Part-2	Data Set-10	2nd man	1	150	Running	0°
Part-2	Data Set-11	2nd man	1	150	Crawling	0°
Part-2	Data Set-12	2nd man	1	150	Creeping	0°
Part-2	Data Set-13	3rd man	1	150	Walking	0°
Part-2	Data Set-14	3rd man	1	150	Walking	30°
Part-2	Data Set-15	3rd man	1	150	Walking	60°
Part-2	Data Set-16	3rd man	1	150	Running	0°
Part-2	Data Set-17	3rd man	1	150	Crawling	0°
Part-2	Data Set-18	3rd man	1	150	Creeping	0°

3.2.2 Processing of Experimental Human Data

3.2.2.1 Generation of Signals

The radar transmits the pulses, the returned signals are received through the antenna and the received analog signal in intermediate frequency (IF) is sampled with an analog-to-digital converter (ADC). The sampled signal is passed through digital down converter (DDC) which generates generating in-phase (I) and quadrature (Q) signals. These I and Q signals are passed through low pass filter, and decimated to obtain complex base band signals which are recorded in the data files mentioned in the section 3.2.1.

3.2.2.2 Signal Processing of Experimental Human Data

The recorded experimental data is processed by matched filtering, MTI filtering, windowing. After windowing, FFT is performed and by using an experimental CFAR, the range and velocity of the target are obtained as is shown in Figure 3.11.

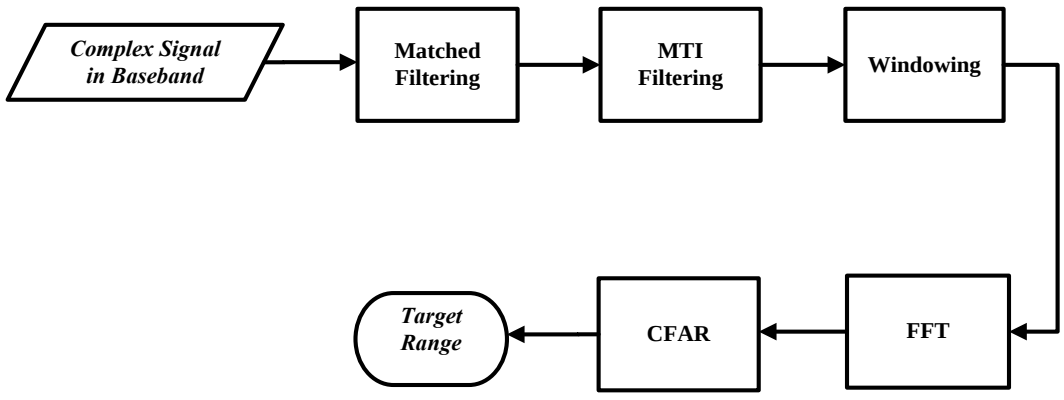

Figure 3.11 Block scheme of signal processing

3.2.2.2.1 Matched Filtering

The processing block which maximizes the output peak signal-to-noise ratio of a radar receiver to increase the detectability of a target is defined as a matched filter [29].

There are different polyphase codes of radar with different code lengths which are matched with different pulse widths; therefore, while data is being recorded at the field, the pulse width is noted. The first part of processing of the signals is pulse compression, which is done on the complex signals by convolving the signal with appropriate polyphase codes. At the end of matched filtering process, Pulse-Range Matrix which has data of range bins as its x component, pulse numbers as its y component, matched filtered output as its z component is obtained. 2nd data of single dwell from Data Set-1 is chosen as one example, and its output of the matched filtering is demonstrated in Figure 3.12.

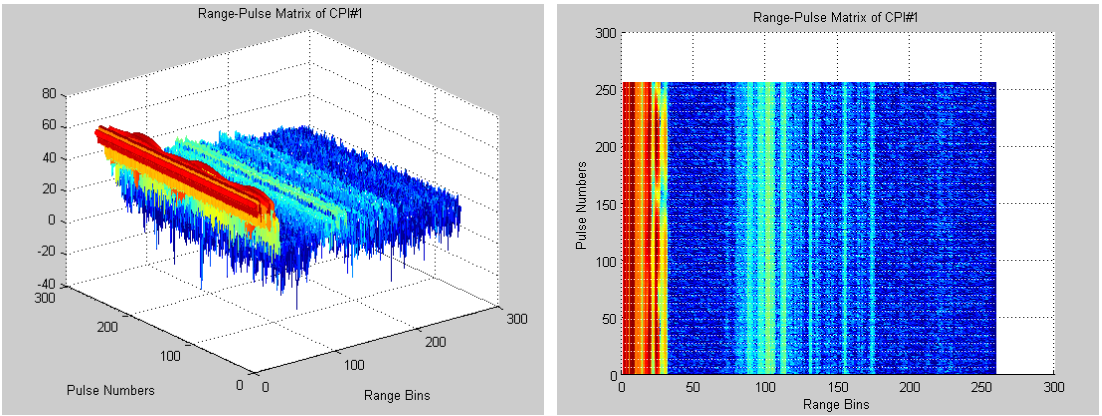

(a) View of 3 dimension (b) View of upper side

Figure 3.12 One example for the output of matched filtering

3.2.2.2.2 MTI Filtering

MTI processing is a linear filter, which is applied to the slow-time (same range-bins of successive pulses) data sequence to suppress the clutter [30]. For the experimental setup, two pulse MTI canceller is chosen. The logic behind two pulse MTI canceller is that the clutter is identical for all pulses, while the phase of moving targets change due to changing range and velocity. Therefore, subtracting successive pulses cancel the clutter components.

After matched filtering, MTI filtering is applied to the experimental data. MTI filtering after applied to the example in Section 3.2.2.2.1 is shown in Figure 3.13. It is seen that the clutters which are seen in red colour in Figure 3.12 are suppressed, and only the target remains.

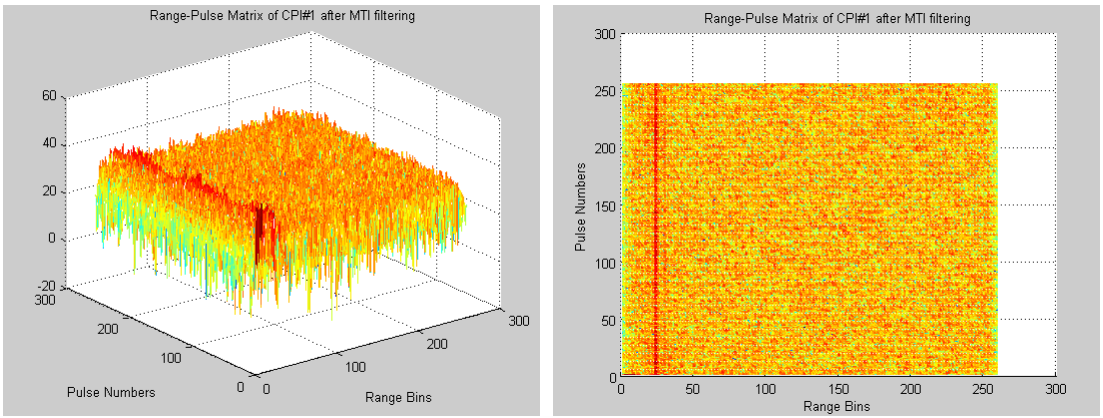

(a) View of 3 dimension (b) View of upper side

Figure 3.13 One example for the output of MTI filtering after matched filtering

3.2.2.2.3 Windowing

By taking an infinite impulse response and superimposing a rectangular frame, data captures the shape of the window. There are windowing options like Hamming, Hanning, Boxcar, Blackman and Kaiser. The Hamming window is the raised cosine function, and it is a preferred window because it consists of two parameters. The Hanning window is similar to Hamming; however, it has zero at the end points. The Blackman is the modulated version of Hanning. Kaiser is a complex window which requires arrangement of some parameters [31]. Because of the simplicity, Hamming window is preferred as the window. The formulation of Hamming window is given for k values from 0 to (N-1):

$$\omega_k = 0.54 - 0.46 \cos\left(\frac{2\pi k}{N-1}\right) \tag{3-2}$$

Hamming window applied to output of matched filter. Hamming window applied to the example in Section 3.2.2.2.2. is shown in Figure 3.14. It is seen that the matrix takes the shape of Hamming window and the edge parts are suppressed.

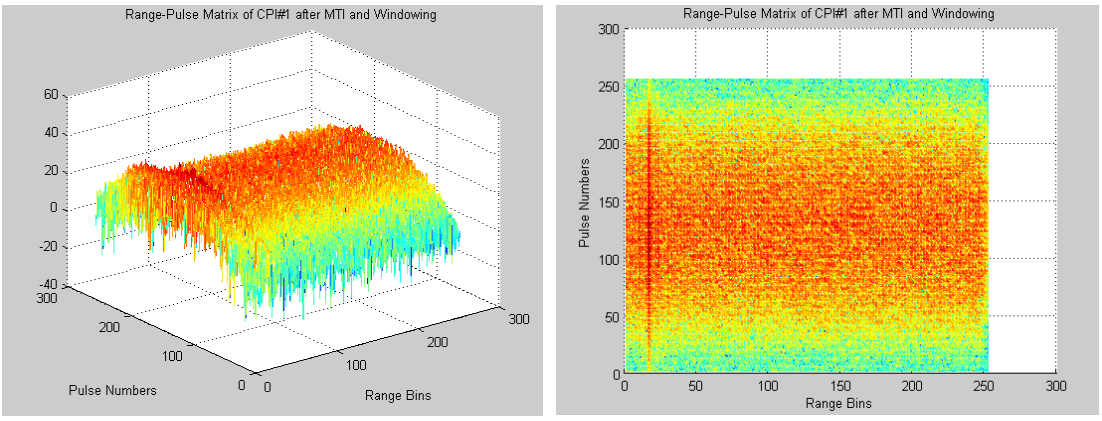

(a) View of 3 dimension

(b) View of upper side

Figure 3.14 One example for the output of windowing after matched filtering and MTI filtering

3.2.2.2.4 FFT

Detailed information about Fast Fourier Transform (FFT) is given in Section 2.2.1. It is mentioned that FFT is one of the most preferred time-frequency transformations, and basically aims to decompose any signal into orthogonal sinusoid functions with different frequencies [3].

FFT is applied to the windowed matrix to obtain the final range-Doppler matrix. FFT applied to example in Section 3.2.2.2.3. is in Figure 3.15. It is seen that the target can be identified from the range-Doppler matrix very clearly.

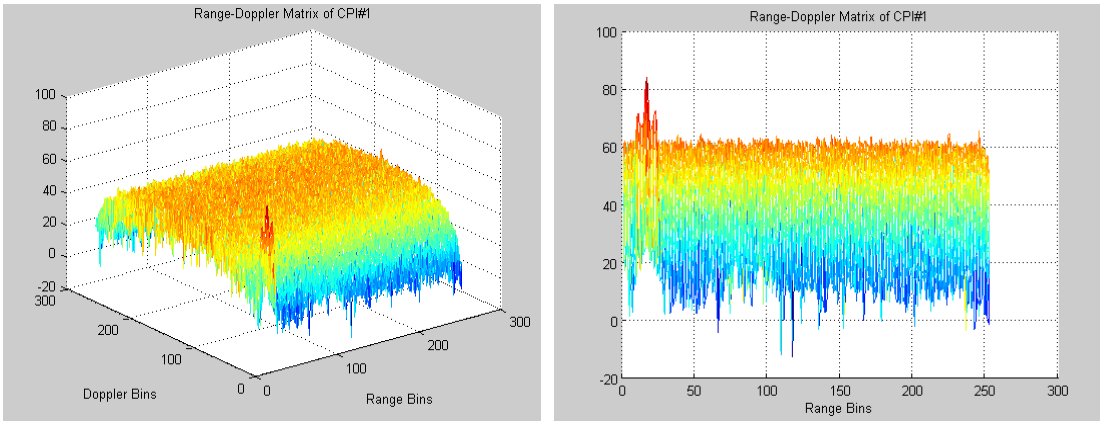

(a) View of 3 dimension (b) View of front side

Figure 3.15 One example for the output of FFT after matched filtering, MTI filtering and windowing

3.2.2.2.5 CFAR

Constant False Alarm Rate (CFAR) is defined as a set of techniques provide predictable detection and false alarm behaviour under clutter and other interferences. Cell Averaging CFAR (CA-CFAR) sets a threshold for each cell by averaging strength of the neighbouring cells. If neighbouring cells contain both

interference and some other statistics, it can be said that there is a potential target and if neighbouring cells only have interference, this cell does not contain a target [30]. The threshold value T for each bin is calculated according to Equation 3-3 where α is the multiplier which is a function of probability of false alarm, x_i is the testing cell, N is the number of averaging cells [30]:

$$T = \frac{\alpha}{\mathrm{N}} \sum_{i=1}^{\mathrm{N}} x_i \tag{3-3}$$

CFAR is applied to the range-Doppler matrix and the points which are above the threshold are assumed as target candidates and the point which has the highest signal strength is accepted as the target. CFAR applied to example in section 3.2.2.2.4. is shown in Figure 3.16. The points which are above the detection threshold are demonstrated with little black circles. The sides of the peaks are also very high; therefore, they also occur as candidate of targets. The candidate point which has the highest signal strength is defined as the target. The range and the Doppler bins of this point become the range bin and the Doppler bin of the target. In brief, at the end of this step, the range and Doppler bins of the target are obtained.

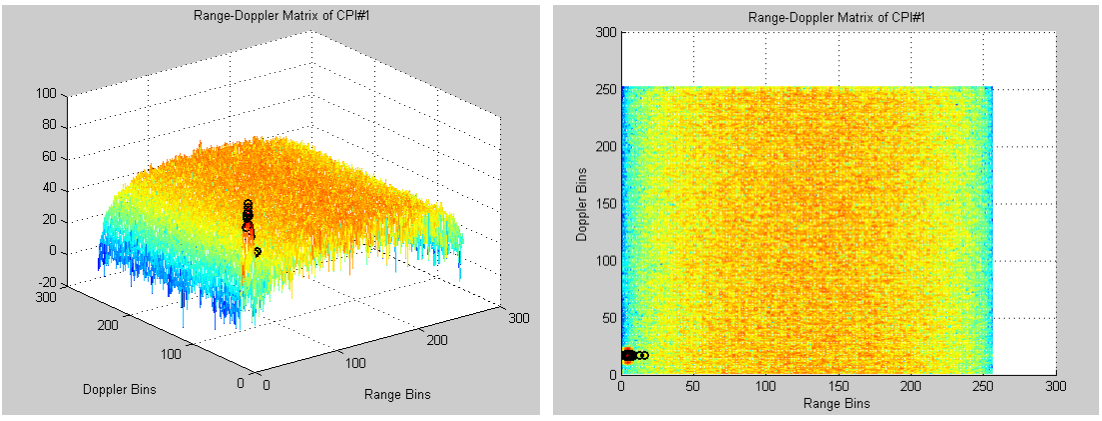

(a) View of 3 dimension (b) View of front side

Figure 3.16 One example for the output of CFAR

3.2.3 Feature Extraction on Experimental Human Data

The matched filtered matrix of the data is passed through the high pass filter and then windowed. After windowing, the columns of target range are extracted from windowed matrix and STFT is applied to obtain the spectrogram of human data. Features are extracted from spectrograms.

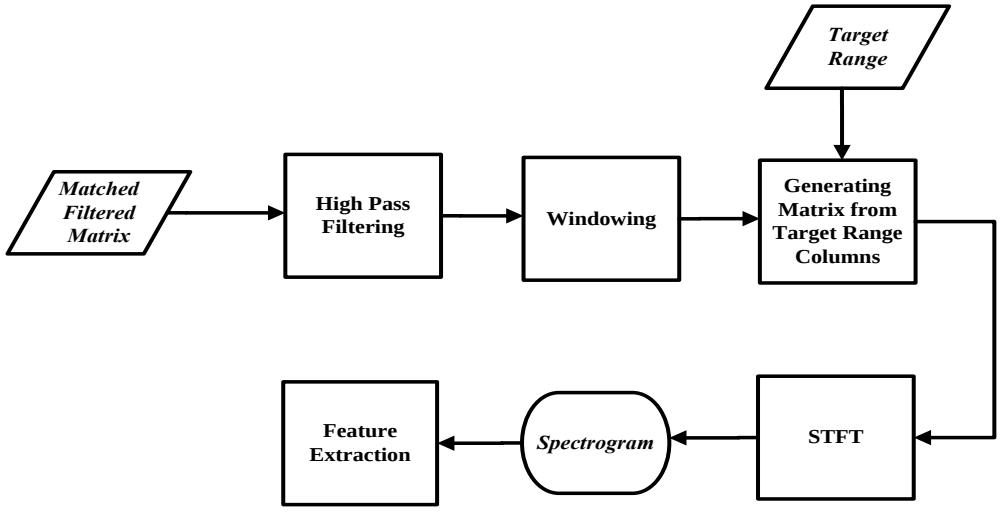

Figure 3.17 Block Scheme of micro Doppler processing part

3.2.3.1 High Pass Filtering

The background objects and environment cause strong clutter on the experimental data. To extract the useful data from the experimental data, this clutter must be suppressed. Radar returns for stationary objects are usually near zero mean Doppler and have very small bandwidths; therefore by using a notch filter, the clutter can be suppressed. The depth and width are the important parameters for designing notch filter to suppress the clutter efficiently [1].

In order to suppress the clutter, a high pass filter is designed with Matlab filter builder tool. Sampling frequency is chosen as 2000 Hz; stop frequency, which is the frequency at the edge of the end of the stop band, is entered as 10 Hz, pass frequency, which is the frequency at the edge of the start of the pass band, is chosen as 20 Hz. Moreover, amplitude attenuation in stop band is entered as 3 dB and amplitude of ripples allow in the pass band is chosen as 1 dB. These values are empirical values and the magnitude response of the designed high pass filter is seen in Figure 3.18. The phase response of this high pass filter is seen in Figure 3.19. This filter is a Direct-Form FIR (Finite Impulse Response) filter with 70 taps. It is capable of suppressing the clutter efficiently. The efficiency of this filter can be seen in Chapter 4 by examining the spectrograms before and after this high pass filter, such as Figure 4.3 which is spectrogram of human walking simulator with long radar pulse width before suppression and Figure 4.4 after suppression clutter.

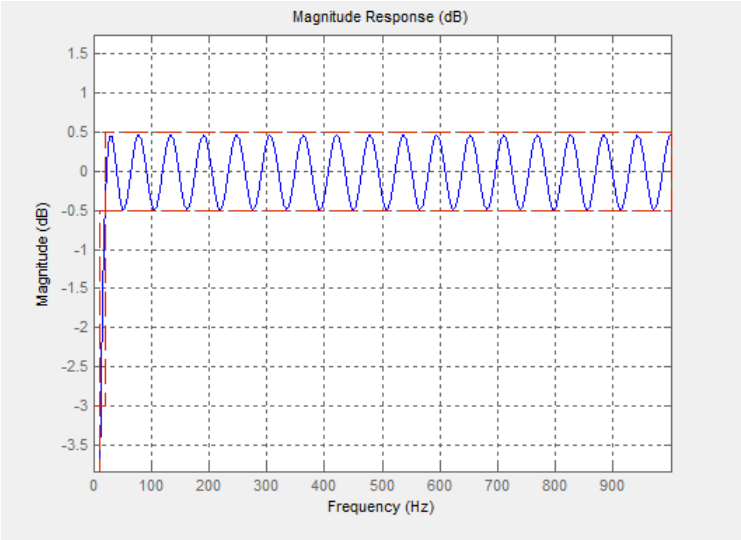

Figure 3.18 The magnitude response of the high pass filter to suppress the clutter

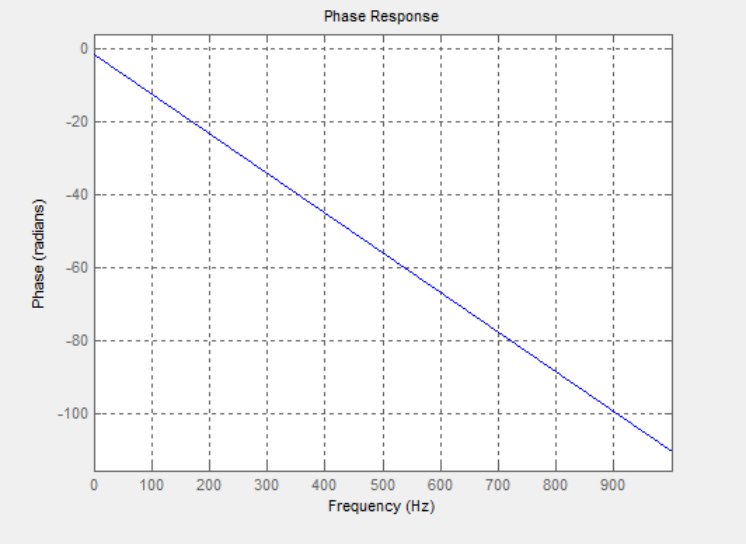

Figure 3.19 The phase response of the high pass filter to suppress the clutter

3.2.3.2 Windowing

The information about windowing is given in detail in section of 3.2.2.2.3. As mentioned in 3.2.2.2.3, Hamming window is used for windowing. For micro Doppler processing part, the same Hamming window is used after high pass filter.

3.2.3.3 Generating Matrix from Target Range Columns

It is known that at the end of matched filtering process, Pulse-Range Matrix which has data of range bins as its x component, pulse numbers as its y component, CPI numbers as its z component is obtained. For micro Doppler processing part, the matched filtered matrix is taken, high pass filter is applied to this matrix as explained in 3.2.3.1 and then windowing is applied as the section of 3.2.3.2. In addition, the output of section 3.2.2.2.5 which is the information of target range bin is taken. The range bins of the target are the only related information for each CPI. Therefore, the range column of target for each CPI is extracted and put side by side.

By this way, only the related range columns are separated from irrelevant part for human motions.

3.2.3.4 STFT

After the related range column matrix is obtained, the spectrogram should be obtained. As explained in 3.1.3**,** usage of STFT seems more appropriate than WVD to get the spectrogram of human motions and it is decided to be used as the time frequency transform.

STFT, which is explained in detail in 2.2.1, is applied to the related range columns matrix. In order to apply the STFT, the spectrogram function of MATLAB signal processing toolbox is used. The parameters of this function are chosen according to the requirements. The window is chosen as a Hamming window of length 256. The number of overlapping segments is adjusted to zero; overlapping segments are not preferred because of the test setup. NFFT is chosen as 256 and sampling frequency is adjusted to 1000 Hz. STFT is applied through the range columns. At the end of this step, the spectrogram of human motion is obtained.

3.2.3.5 Feature Extraction

Feature extraction methods and extracted features are explained in detail under the section of 3.1.2. In addition, micro Doppler features on the spectrogram of human walking is given in Figure 3.4.

The same feature extraction method, which is explained in section 3.1.2, is applied to the experimental data. The same six features, which are the torso Doppler frequency, the total bandwidth of the Doppler signal, the offset of the total Doppler, the bandwidth without micro Doppler, the normalized standard deviation of the Doppler signal strength, and the period of the limb motions are extracted from experimental spectrograms by using the same procedure. These features are extracted from the experimental data can be seen from Figure 3.20.

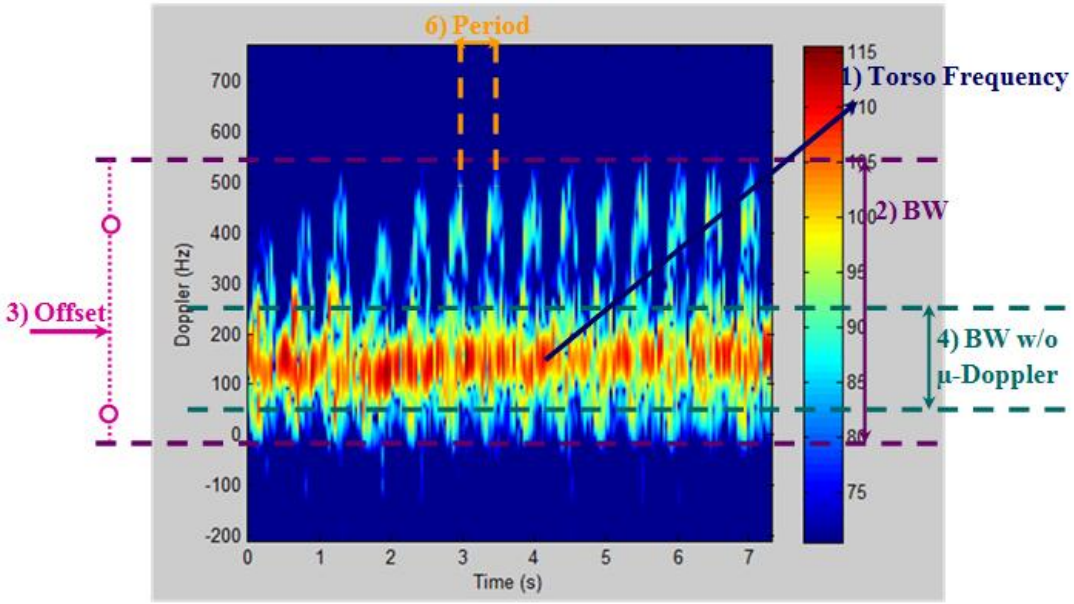

Figure 3.20 Demonstration of features on the experimental spectrogram

3.2.4 Micro Doppler Classification of Experimental Human Data Using Neural Network Classification

Neural network for classification can be viewed as a mapping function F: $R^d \rightarrow R^m$, where d is the dimension of the input, m is the dimension of output. The network is typically constructed such that an overall error measure is minimized. The input x is submitted to the neural network, the classification decision is made according to the neural network. For a two-class problem, the neural network classifier can be formulated as:

$$g(x) = P(w_1|x) - P(w_2|x) \tag{3-4}$$

The discriminating rule for classification between two classes of w_1 and w_2 is like assigning x to w_1 if g(x)> 0 or w_2 if g(x) < 0. Monotone increasing function of the posterior probability can be applied to replace the posterior probability in the

formula to form a different discriminant function but essentially the same classification rule [17].

For more classes, the network classifier can be formed as [32]:

$$if\ max_k\ P(C_k|x) \begin{cases} \geq \theta, then\ classify\ x \\ < \theta, then\ reject\ x \end{cases} \quad (3\text{-}5)$$

For the human motion classification problem, the input has 6 dimensions because feature extraction process requires 6 different features, which are torso frequency, bandwidth, offset, bandwidth without micro Dopplers, standard deviation and period. Each motion is repeated 7 times for 3 people; therefore, 21 samples are obtained for each motion. 9 samples of each motion are used as the training samples of the neural network. Neural network is constituted with 9 samples of each motion by using toolbox. The other 12 samples of each motion are entered as the input, which has 12x6 dimension, to the neural network. The output of the toolbox is the classes of the input motions. The results are presented in section 4.5.

It should be emphasized that classification is only made to get an idea about the possibility of discriminating human motions by a classifier. This classification part can be assumed as a preliminary for future studies.

By using the neural network toolbox of MATLAB, neural network classifier is applied to the extracted features to obtain an example performance.

CHAPTER 4

EXPERIMENTAL RESULTS

In the experimental part of the study, the basic issues which are examined can be listed as the effects of using different pulse widths, the effects of various forms of human walking, micro Doppler characteristics of human walking, running, crawling and creeping and the classification of human motions from micro Doppler signatures. In order to investigate these issues, an experimental data is collected from 5 different people by using a ground surveillance radar. For the analysis of effects of pulse widths on micro Doppler features, data is collected from 2 people; therefore, 14 data sets are collected in this part. In the second part of data collection, different human motions such as walking, running, crawling, creeping and various orientations of walking such as 0°, 30°, 60° are focused on and the data is collected from 3 different persons.

The recorded data is processed with the methods explained in Chapter 3. In this chapter, experimental results and discussions on the data characteristics are given and the analysis of each motion, the comparison between them, the classification results of motion types are presented.

4.1 Analysis of Effects of Using Different Pulse Widths of Radar

The radar system utilized for data acquisition can use variant pulse compression codes with different lengths. The use of different pulse compression codes with different pulse widths provides several options for working with different blind ranges. In order to examine the effects of range and pulse width on the spectrograms of human walking, the radar data is collected at two different ranges with two different pulse widths.

The range of the 1st target, who has 1.74 m height and 95 kg weight, is approximately 150 meters from the radar and the smallest pulse width (PW1) is chosen to utilize the smallest blind range. The target is asked to walk towards the radar and the radar data is recorded. Then, the experiment is repeated 7 times. After the raw data is processed as explained in Chapter 3, the human walking spectrograms for PW1 are calculated and one of the spectrograms of human walking towards the radar with the radar pulse width of PW1 is given in Figure 4.1.

When Figure 4.1 is examined, a strip is seen at the frequency band of -50 Hz and 50 Hz. The reason for this strip is ground clutter and in order to suppress the clutter effect on the spectrogram a high pass filter is designed and applied to the data as explained at Chapter 3. By filtering the experimental data with the designed high bass filter, the clutter effects on the spectrograms are diminished. The spectrograms of walking with radar pulse width of PW1 after suppression clutter is given in Figure 4.2; the other spectrograms of walking with radar pulse width of PW1 without clutter are given at Appendix A, Figure A.1.

After spectrograms of human walking with the radar pulse width PW1 without clutter are obtained, feature extraction process is applied on these spectrograms to observe the micro Doppler features of walking motion obtained with PW1. Feature extraction results of the spectrograms of human walking for the radar pulse width of PW1 for 7 data samples are listed at Table 4.1.

When Table 4.1 is inspected, it is seen that the average feature values of PW1 are calculated as torso frequency of 150,0045 Hz; bandwidth of 496,3697 Hz; offset of 161,9928 Hz; bandwidth without micro Doppler of 215,8521 Hz; standard deviation of 7,3275 and period of 0,5008 sec. These average values are used as the extracted features of walking with the radar pulse width of PW1.

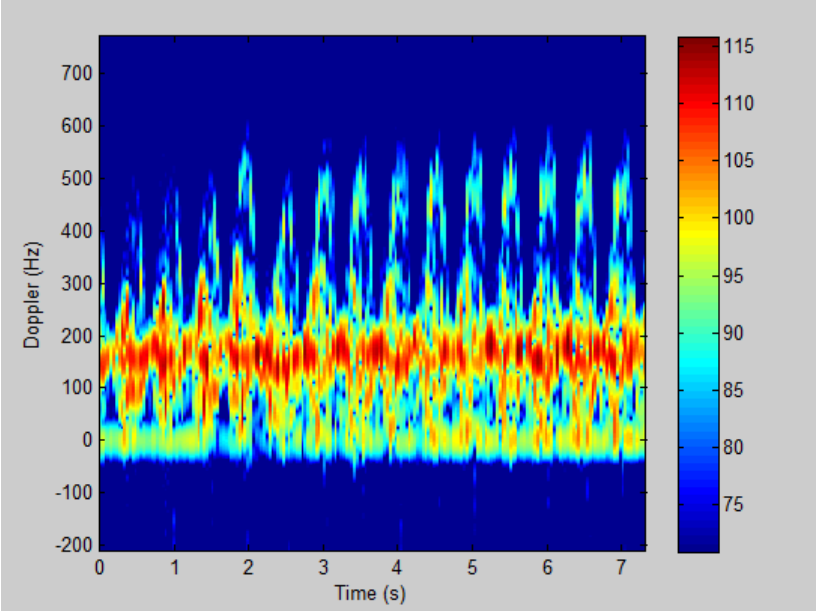

Figure 4.1 Spectrogram of human walking with radar pulse width of PW1 before clutter suppression

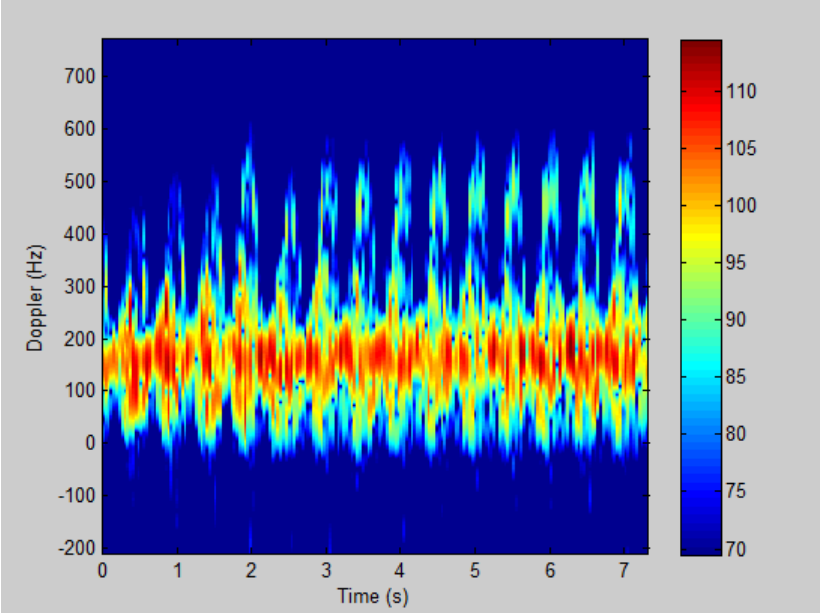

Figure 4.2 Spectrogram of human walking with radar pulse width of PW1 after clutter suppression

Table 4.1 Extracted micro Doppler features of human walking for PW1

PW1	Extracted Classification Features					
	Torso Frequency (Hz)	Bandwidth (Hz)	Offset (Hz)	Bandwidth w/o Micro Doppler (Hz)	Standard Deviation	Period (sec)
Sample-1	123,8969	451,2008	139,1031	217,9275	7,0347	0,4854
Sample-2	141,7595	479,4008	152,3379	197,4183	6,9329	0,5204
Sample-3	159,6973	511,8736	161,4346	223,9093	7,6562	0,5339
Sample-4	171,1331	531,5282	174,7912	245,2730	7,4759	0,5272
Sample-5	131,1299	479,4008	177,4467	209,3820	6,7807	0,4621
Sample-6	166,0107	525,5463	170,7598	211,9456	7,5393	0,4911
Sample-7	156,4041	495,6372	158,0762	205,1093	7,8727	0,4858

Secondly, the range of the 2nd target, who has 1.89 m height and 75 kg weight, is approximately 1000 meters from the radar and the PW2, which is approximately 5 times of PW1, is selected. The target is walked towards the radar. The data is recorded. The experiment is repeated this motion for 7 times. After raw data of human walking is processed as explained in Chapter 3, human walking spectrograms for PW2 are calculated and an example for the spectrograms is given in Figure 4.3.

When Figure 4.3 is examined, a strip corresponding to clutter is again seen at the frequency band of -50 Hz and 50 Hz. With high pass filtering, the clutter is depressed and shown in Figure 4.4; the other spectrograms of walking with radar pulse width of PW2 with clutter suppressed are given at Appendix-A, Figure A.2. Feature extraction results of the spectrograms of human walking for PW2 are listed at Table 4.2.

When Table 4.2 is inspected, it is seen that the average values of PW2 features are calculated as torso frequency of 171,7264 Hz; bandwidth of 468,5359 Hz; offset of 182,0902 Hz; bandwidth without micro Doppler of 183,8912 Hz; standard deviation of 7,4390 and period of 0,4206 sec. These average values are used as the extracted features of walking with the radar pulse width of PW2.

In order to make comparison between PW1 and PW2 by means of micro Doppler features, averages of extracted feature values for PW1 and PW2 are listed at Table 4.3.

Table 4.2 Extracted Micro Doppler features of human walking for PW2

PW2	Extracted Classification Features					
	Torso Frequency (Hz)	Bandwidth (Hz)	Offset (Hz)	Bandwidth w/o Micro Doppler (Hz)	Standard Deviation	Period (sec)
Sample-1	157,2665	497,3463	173,4687	206,1283	7,5194	0,3794
Sample-2	171,6486	499,0554	182,2150	190,5820	7,4938	0,4195
Sample-3	178,0418	520,4190	198,8082	173,4910	7,2233	0,4437
Sample-4	180,2862	489,6554	186,1246	169,2183	7,5111	0,4457
Sample-5	171,3685	405,9098	174,4643	175,2001	7,3953	0,4343
Sample-6	175,5712	392,2370	180,6747	188,8729	7,3620	0,4087
Sample-7	167,9020	475,1281	178,8759	183,7456	7,5683	0,4130

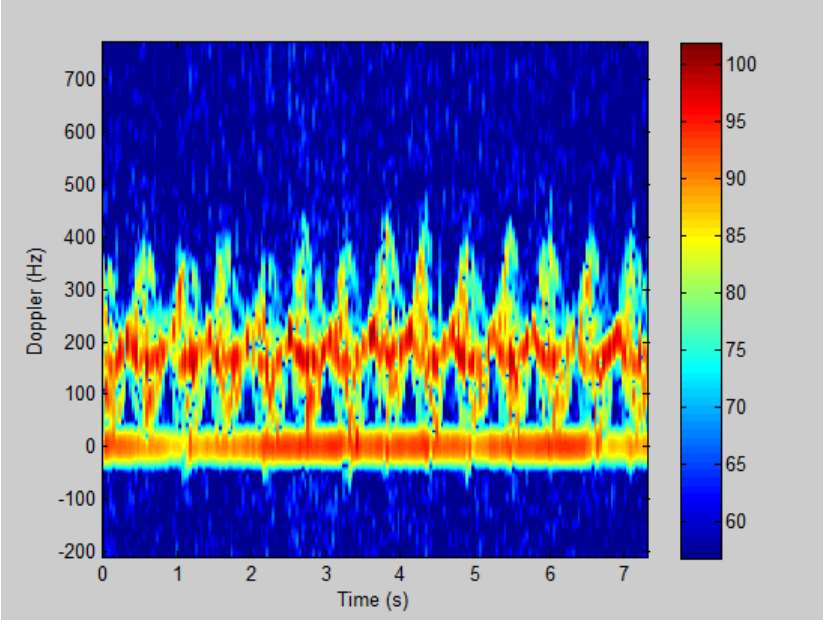

Figure 4.3 Spectrogram of human walking with radar pulse width of PW2 before clutter suppression

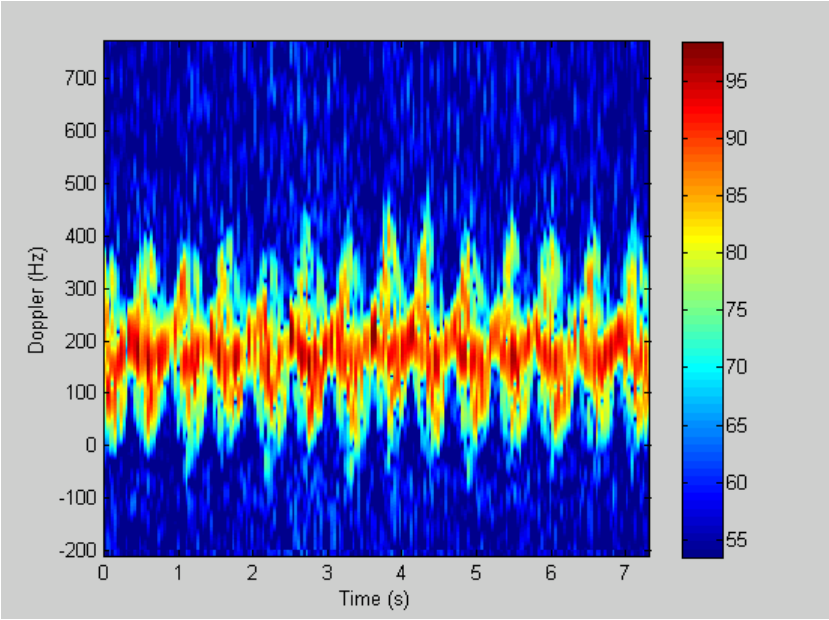

Figure 4.4 Spectrogram of human walking with radar pulse width of PW2 after clutter suppression

Table 4.3 Comparison between PW1 and PW2 by means of micro Doppler features

	Comparison of PW1 and PW2					
	Torso Frequency (Hz)	Bandwidth (Hz)	Offset (Hz)	Bandwidth w/o Micro Doppler (Hz)	Standard Deviation	Period (sec)
Average Values for PW1	150,0045	496,3697	161,9928	215,8521	7,3275	0,5008
Average Values for PW2	171,7264	468,5359	182,0902	183,8912	7,4390	0,4206

When extracted features of PW1 and PW2 are compared, it can be seen that the results are very similar to each other quantitively, which means that human walking at different ranges with different pulse widths provide similar feature values. The small differences between two pulse widths can be caused by having different physical characteristics and different walking signatures of two different target persons.

The range of the target to the radar and the change of the pulse lengths result in differences in SNR values. The possible reduction in SNR value can be calculated by using radar range Equation 4-1 [29]. For the first case, signal to noise ratio is abbreviated as $(S/N)_1$ and number of integrated pulses is demonstrated as n_1 and its range is 150 m. For the second case, the signal to noise ratio is abbreviated as $(S/N)_2$ and its pulse numbers is known as approximately 5 times of the pulse numbers of PW1 and given as $5.n_1$ and its range is 1000 m. It should be considered that because the spectrograms of PW1 and PW2 belong to 2 different targets and their RCS values are different, the calculation result can give an approximate result.

$$(S/N) = \frac{P_{av} \cdot G \cdot A \cdot \rho_a \cdot \sigma \cdot n \cdot E_i(n) \cdot F^4 \cdot e^{-2\alpha R}}{(4\pi)^2 \cdot R^4 \cdot k \cdot T_0 \cdot F_n \cdot (B \cdot \tau) \cdot f_p \cdot L_f \cdot L_s} \quad (4\text{-}1)$$

where

P_{av} : *Average transmit power, W*

G : *Antenna gain*

A : *Antenna area,* m^2

ρ_a : *Antenna aperture efficiency*

σ : *Radar cross section,* m^2

n : *Number of pulses integrated*

$E_i(n)$: *Integration efficiency*

F^4 : *Propagation factor*

α : *Attenuation coefficient, nepers per unit distance*

k : *Boltzmann's constant,* 1.38×10^{-23} *J/deg*

T_0 : *Standard temperature, 290 K*

F_n : *Noise figure of receiver*

B : *Bandwidth, Hz*

τ : *Pulse width, s*

f_p : *Pulse repetition frequency, Hz*

L_f : *Fluctuation loss*

L_s : *System loss*

$$(S/N)_1 = \frac{P_{av} \cdot G \cdot A \cdot \rho_a \cdot \sigma \cdot n_1 \cdot E_i(n) \cdot F^4 \cdot e^{-2\alpha \cdot R}}{(4\pi)^2 \cdot 50^4 \cdot k \cdot T_0 \cdot F_n \cdot (B \cdot \tau) \cdot f_p \cdot L_f \cdot L_s} \quad (4\text{-}2)$$

$$(S/N)_2 = \frac{P_{av} \cdot G \cdot A \cdot \rho_a \cdot \sigma \cdot 5 \cdot n_1 \cdot E_i(n) \cdot F^4 \cdot e^{-2\alpha \cdot R}}{(4\pi)^2 \cdot 1000^4 \cdot k \cdot T_0 \cdot F_n \cdot (B \cdot \tau) \cdot f_p \cdot L_f \cdot L_s} \quad (4\text{-}3)$$

The ratio of the Equations 4-2 and 4-3 gives the result that:

$$\frac{(S/N)_2}{(S/N)_1} = \frac{5 \cdot 150^4}{1000^4} = 0.0025$$

$$\Rightarrow \quad 10 \cdot \log\left(\frac{(S/N)_2}{(S/N)_1}\right) = 10 \cdot \log(0.0025) = -25.9666 dB$$

The increase of the range from 150 meters to 1000 meters and changing pulse width from PW1 to PW2 causes -25.9 dB reduction on the signal to noise ratio according to radar range equation. On the other hand, because the targets for two cases are different and their RCS values are different, there occurred deviation from the calculated value of 25.9 dB reduction.

The spectrograms of Figure 4.2 and Figure 4.4 are examined and it is seen from the spectrograms that maximum SNR value of PW1 is 115 dB and maximum SNR value of PW2 is 95 dB; which means that PW2 has approximately 20 dB smaller SNR values than PW1. This value is roughly consistent with the calculated SNR reduction.

4.2 Comparison between Simulated Human Walking Model and Experimental Human Walking Result

In Chapter 3, Chen's human walking simulator is examined and the simulator is modified according to the requirements of this thesis. The spectrogram of developed human walking simulator by using STFT is demonstrated at Figure 4.5. In addition to the simulated spectrogram of human walking, one of the spectrograms of experimental human walking with the azimuth angle of 0° and with the pulse width of PW1 is given in Figure 4.6 to make a comparison between the simulated and experimental results.

When Figure 4.5 and Figure 4.6 are examined, two spectrograms seem quite similar. The lines of the spectrogram of experimental human walking are more spread than the ones of simulator; this is expected because radar returns are

calculated from 17 points in the simulator; however, the spectrogram of experimental human walking is obtained from the return signal of all human body parts.

To better compare the simulated and experimental results by means of body parts of the human spectrograms, Figure 4.7 is prepared. In Figure 4.7, the shape of swinging foot is very consistent with simulated and experimental data. The shape and the amount of extension of fixed foot are also similar on both spectrograms. Even the torso seems spread in the experimental data, the general form and position of torso resembles the torso part of the simulator. Although knee has a distinctive shape on the spectrogram of the simulator, it is hard to discriminate knee from the experimental spectrogram. However, when it is examined in detail, the position and the shape of knee are again similar in both spectrograms. In brief, the simulated results resemble the experimental spectrogram quite closely in a qualitative sense.

In order to see the effectiveness of the simulator in the generation of selected micro Doppler features quantitively, the extracted feature values of human walking simulator by STFT and the average values of experimental human walking with PW1 are listed at Table 4.4.

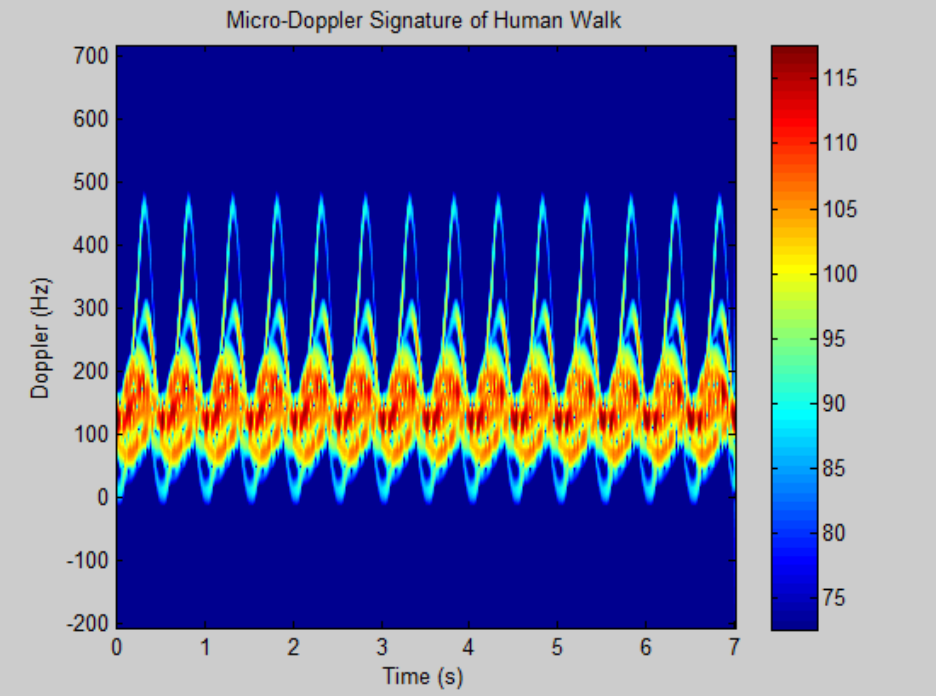

Figure 4.5 Spectrogram of human walking simulator by using STFT

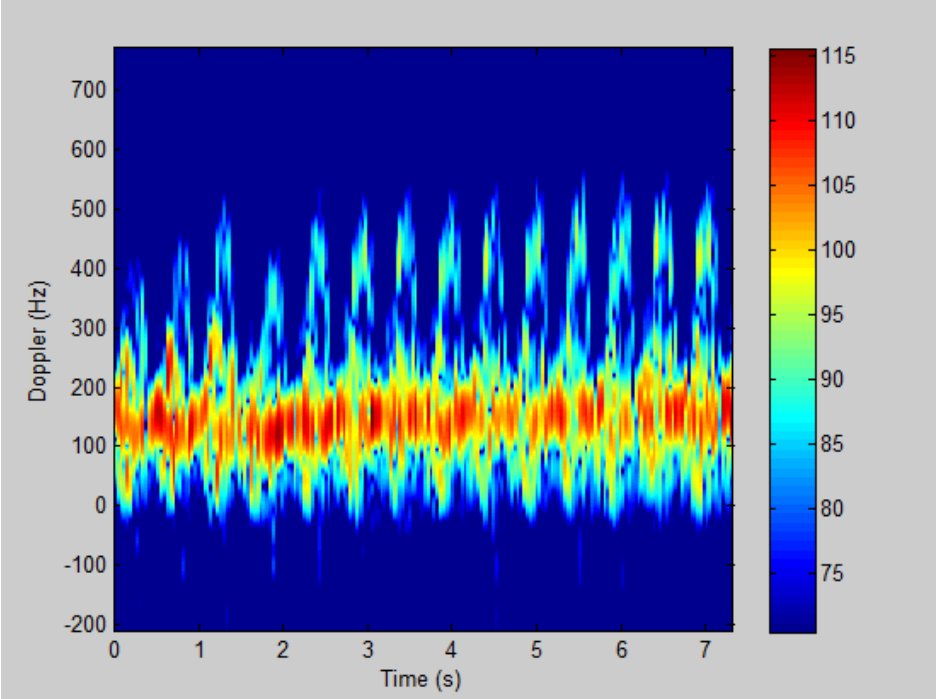

Figure 4.6 Spectrogram of experimental human walking with azimuth angle of 0°

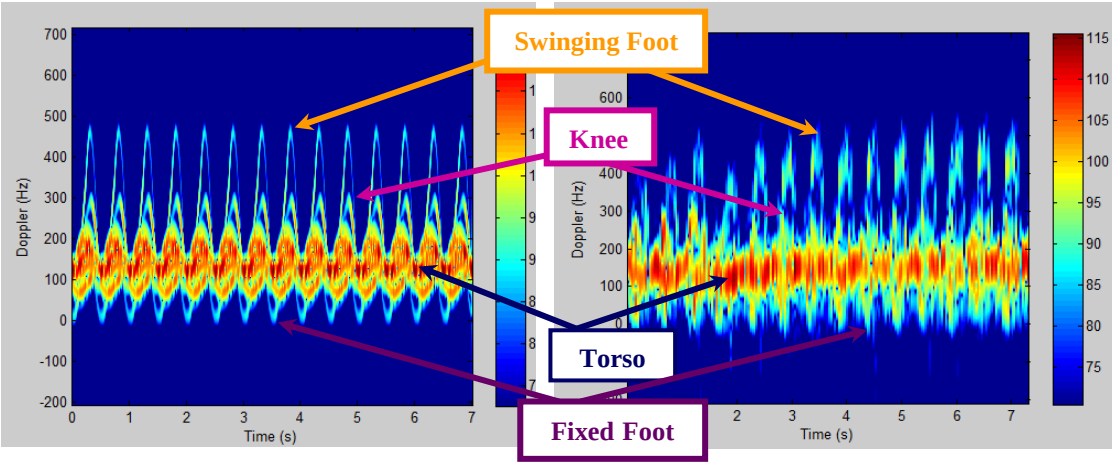

(a) Spectrogram of human walking simulator

(b) Spectrogram of experimental human walking

Figure 4.7 Spectrograms of human walking

Table 4.4 Comparison between human walking simulator by STFT and experimental human walking result by means of micro Doppler features

	Comparison of Simulator and Experimental Human Walking					
	Torso Frequency (Hz)	Bandwidth (Hz)	Offset (Hz)	Bandwidth w/o Micro Doppler (Hz)	Standard Deviation	Period (sec)
Human Walking Simulator with STFT	144,6971	497,9613	169,7528	227,9226	7,2021	0,5000
Experimental Human Walking with Azimuth Angle of 0°	150,0045	492,5445	168,0948	183,6850	7,4290	0,4594

When extracted features are investigated, it can be seen that the results of human walking simulator by using STFT is very similar to experimental human walking with azimuth angle of 0°. After the observation of spectrograms qualitatively and the examination of extracted features quantitively, it can be concluded that human walking simulator provides very similar results to experimental data; therefore, the given simulator is a beneficial tool to study human characteristics on radar.

4.3 Analysis of Different Types of Human Motions

Data for different human motions such as walking, running, crawling and creeping is collected. The collected data is processed and some features are extracted from the spectrograms as explained in Chapter 3. In addition, to understand the dependence of observed motion characteristics on the target, data is collected from 3 different persons for each type of motion. Moreover, to examine the effects of various orientations of human walking, the aspect angle of human to the line of sight of the radar is arranged as 0°, 30° and 60° and spectrograms for walking motions are obtained for these aspect angles. For all motions, the range of the target is adjusted to 150 meters from the radar and the smallest pulse width (PW1) is chosen to get the shortest blind range. Furthermore, in order to get more accurate results and prevent dependency on one motion of a human, each experiment is repeated for 7 times. In brief, the motion types of walking, running, crawling, creeping and walking aspect angles of 0°, 30°, 60° are analyzed by using 3 data sets from 3 persons with 7 repeats for each types of motion.

4.3.1 Walking

In order to characterize the micro Doppler response of human walking with respect to azimuth angle, the azimuth angles of the human target are arranged to 0°, 30°, 60° and data is collected and analyzed for these angles.

4.3.1.1 Walking with Azimuth Angle of 0°

The target azimuth angle is set to 0°. The range of the 1st person, who has 1.73 m height and 70 kg weight, is adjusted to approximately 150 meters from the radar and the shortest pulse width (PW1) is chosen to get the shortest blind range. 1st person is asked to walk towards the radar and this motion is repeated 7 times and raw data is recorded. After the raw data is processed as explained in Chapter 3, 1st person's walking spectrograms with the azimuth angle of 0° are obtained; one of these spectrograms and the spectrogram after clutter filtering are shown in Figure 4.8, and in Figure 4.9, respectively. The other spectrograms of 1st person's walking with the azimuth angle of 0° with clutter suppression are given at Appendix-B, Figure B.1.

After spectrograms of 1st person's walking with the azimuth angle of 0° with clutter suppressed are obtained, the feature extraction process is applied on these spectrograms to observe the micro Doppler features of 1st person's walking with the azimuth angle of 0°. Feature extraction results of the spectrograms of 1st person's walking with the azimuth angle of 0° are listed at Table 4.5.

When Table 4.5 is taken into consideration, it is seen that the average feature values of 1st person's walking with the azimuth angle of 0° are calculated as torso frequency of 188,6218 Hz; bandwidth of 557,5308 Hz; offset of 196,2589 Hz; bandwidth without micro Doppler of 235,0184 Hz; standard deviation of 7,3275 and period of 0,4607 sec. These average values are used as the extracted features of 1st person's walking with the azimuth angle of 0°.

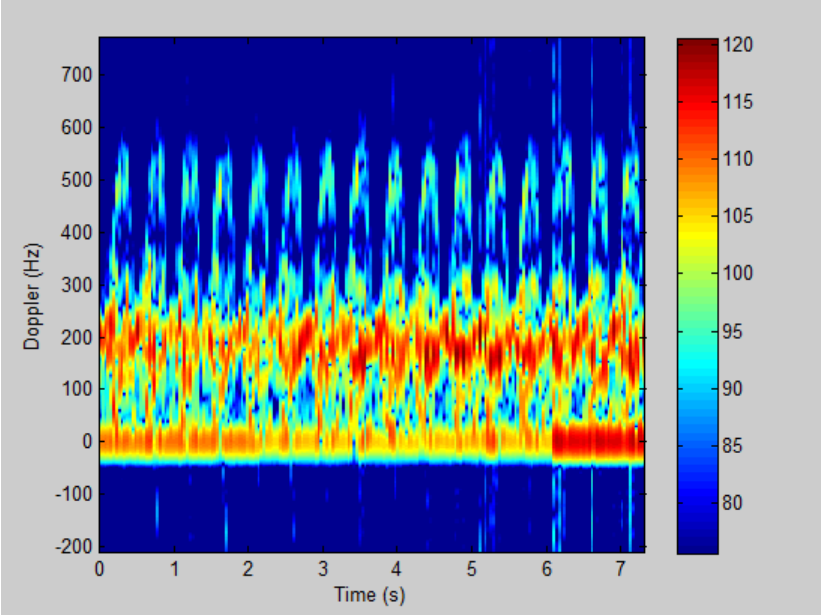

Figure 4.8 Spectrogram of 1st person's walking with azimuth angle of 0° before clutter suppression

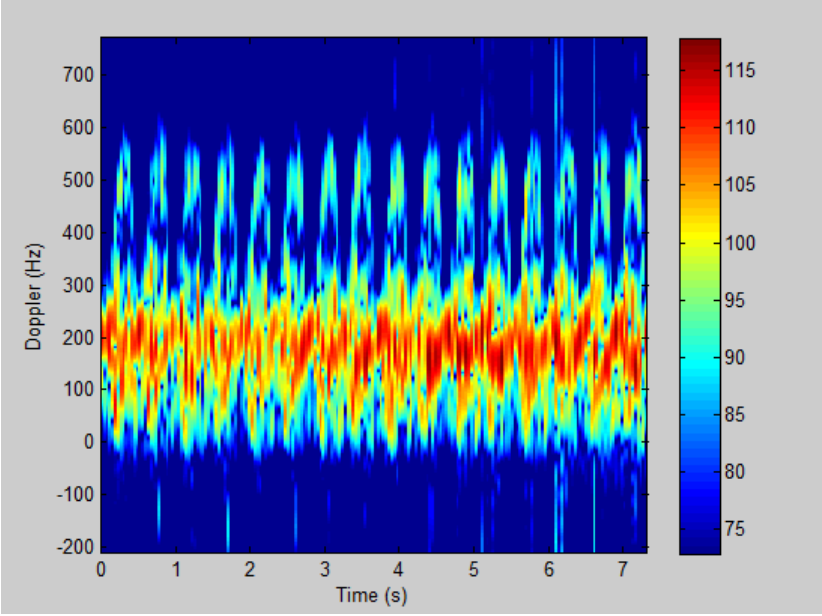

Figure 4.9 Spectrogram of 1st person's walking with azimuth angle of 0° after clutter suppression by using high pass filter

Table 4.5 Extracted micro Doppler features of 1st person's walking with 0°

1st Person's Walking with Azimuth Angle of 0°	Extracted Classification Features					
	Torso Frequency (Hz)	BW (Hz)	Offset (Hz)	BW w/o Micro Doppler (Hz)	STD	Period (sec)
Sample-1	188,3185	564,0009	196,1783	249,5457	7,0347	0,4045
Sample-2	208,3793	579,3828	202,8096	233,3093	6,9329	0,478
Sample-3	199,6267	583,6555	203,4719	245,273	7,6562	0,4632
Sample-4	191,4516	549,4736	196,1356	252,9639	7,4759	0,413
Sample-5	176,7542	532,3827	187,8401	170,0728	6,7807	0,5607
Sample-6	173,6054	549,4736	192,7238	252,1093	7,5393	0,4251
Sample-7	182,2167	544,3464	194,653	241,8548	7,8727	0,4806

The range of the 2nd person, who has 1.83 m height and 90 kg weight, is adjusted to approximately 150 meters from the radar and the smallest pulse width (PW1) is chosen to get the smallest blind range. 2nd person is asked to repeat the same motion.

The spectrogram of 2nd person before and after clutter suppression is given in Figure 4.10 and Figure 4.11, respectively.

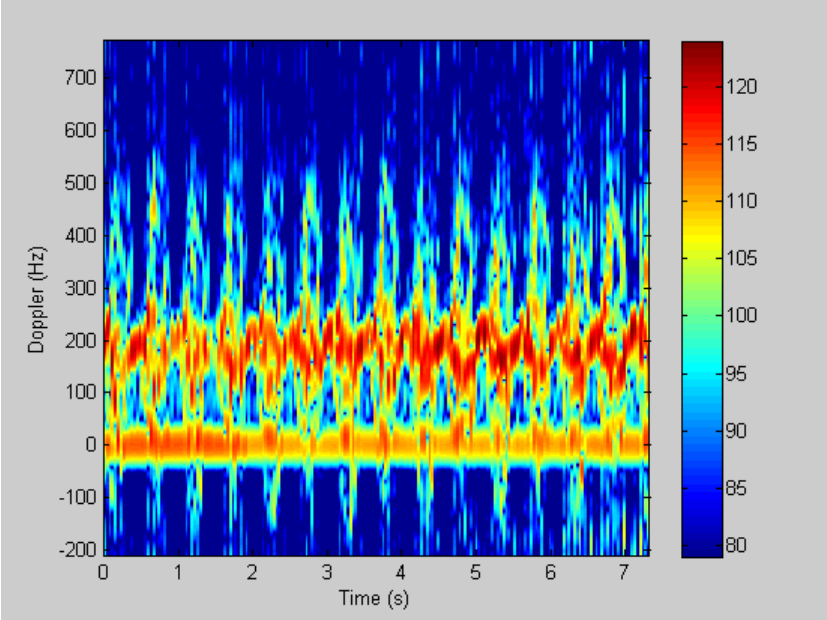

Figure 4.10 Spectrogram of 2nd person's walking with azimuth angle of 0° before clutter suppression

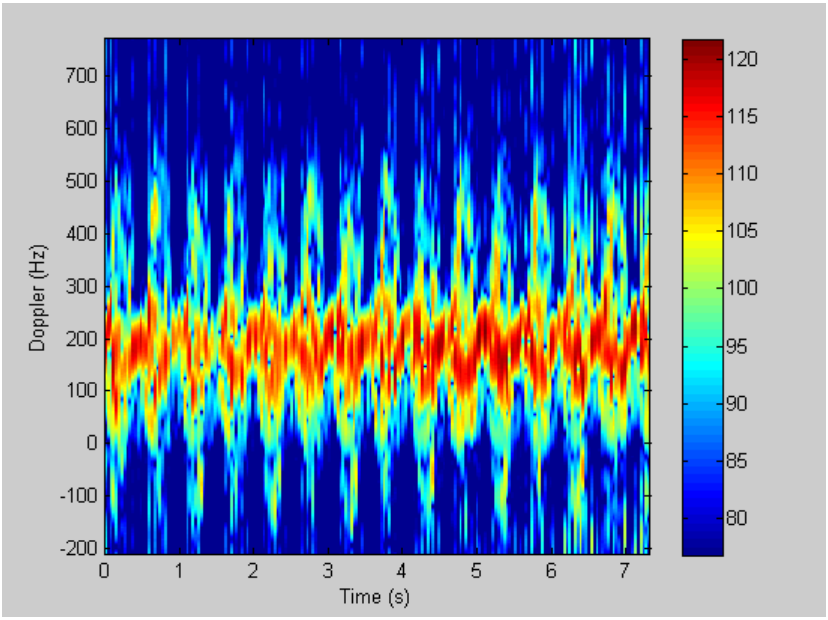

Figure 4.11 Spectrogram of 2nd person's walking with azimuth angle of 0° after clutter suppression

Table 4.6 Extracted micro Doppler features of 2nd person's walking with the azimuth angle of 0°

2nd Person's Walking with Azimuth Angle of 0°	Extracted Classification Features					
	Torso Frequency (Hz)	BW (Hz)	Offset (Hz)	BW w/o Micro Doppler (Hz)	STD	Period (sec)
Sample-1	171,9112	508,4554	184,6569	211,0911	7,5183	0,478
Sample-2	177,2271	568,2737	206,9243	217,9275	7,4109	0,4681
Sample-3	183,9676	543,4918	191,85	223,9093	7,8277	0,478
Sample-4	173,1720	540,0736	190,5426	198,2729	7,3794	0,4702
Sample-5	175,3219	526,4009	189,6966	215,3638	7,5487	0,4597
Sample-6	180,4487	573,401	193,3348	208,5275	7,3041	0,4623
Sample-7	179,3123	574,2555	199,15	204,2547	7,9367	0,4806

Table 4.6 shows the features generated for the 2nd person. From Table 4.6, it is seen that the average feature values of 2nd person's walking with the azimuth angle of 0° are calculated as torso frequency of 177,3373 Hz; bandwidth of 547,7646 Hz; offset of 193,7365 Hz; bandwidth without micro Doppler of 211,3353 Hz; standard deviation of 7,5608 and period of 0,4710 sec. These average values are used as the extracted features of 2nd person's walking with the azimuth angle of 0°.

The results for the 3rd person, who has 1.89 m height and 78 kg weight, is given in Figure 4.12 and Figure 4.13. Feature extraction results of the spectrograms of 3rd person's walking are listed at Table 4.7.

Table 4.7 Extracted micro Doppler features of 3rd person's walking with the azimuth angle of 0°

3rd Person's Walking with Azimuth Angle of 0°	Extracted Classification Features					
	Torso Frequency (Hz)	BW (Hz)	Offset (Hz)	BW w/o Micro Doppler (Hz)	STD	Period (sec)
Sample-1	205,2249	516,1463	207,9518	184,6001	7,8826	0,4698
Sample-2	219,9559	519,5645	212,0152	185,4547	8,0547	0,5015
Sample-3	225,4603	541,7827	221,9365	224,7638	8,1985	0,4989
Sample-4	224,8918	573,401	227,4142	190,582	7,8192	0,5818
Sample-5	231,4513	552,0373	225,4914	167,5092	7,7426	0,5272
Sample-6	234,4791	497,3463	224,936	176,0547	7,6555	0,4411
Sample-7	224,6487	501,619	217,527	172,6365	8,0687	0,4649

When features Table 4.7 for 3rd person, it is seen that the average feature values of 3rd person's walking with the azimuth angle of 0° are calculated as torso frequency of 223,7303 Hz; bandwidth of 528,8424 Hz; offset of 219,6103 Hz; bandwidth without micro Doppler of 185,9430 Hz; standard deviation of 7,9174 and period of 0,4979 sec. These average values are used as the extracted features of 3rd person's walking with the azimuth angle of 0°.

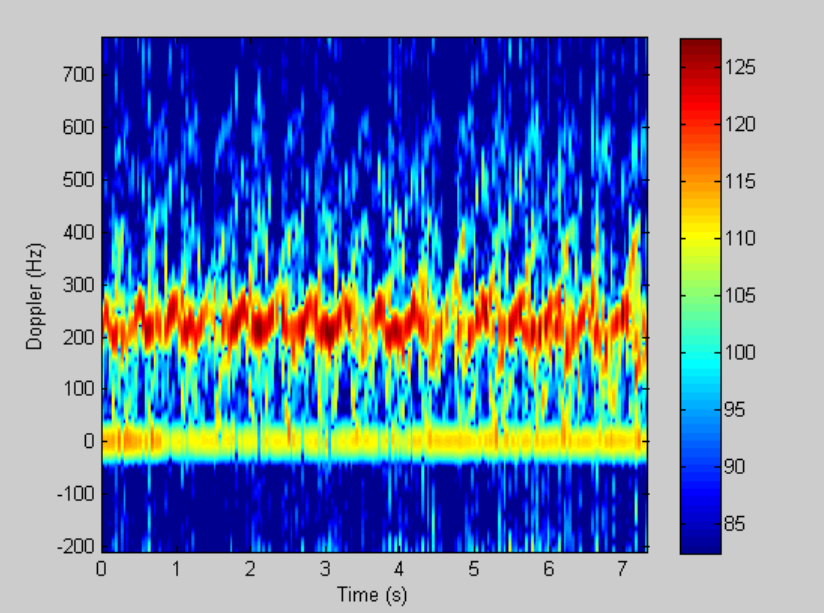

Figure 4.12 Spectrogram of 3rd person's walking with azimuth angle of 0° before clutter suppression

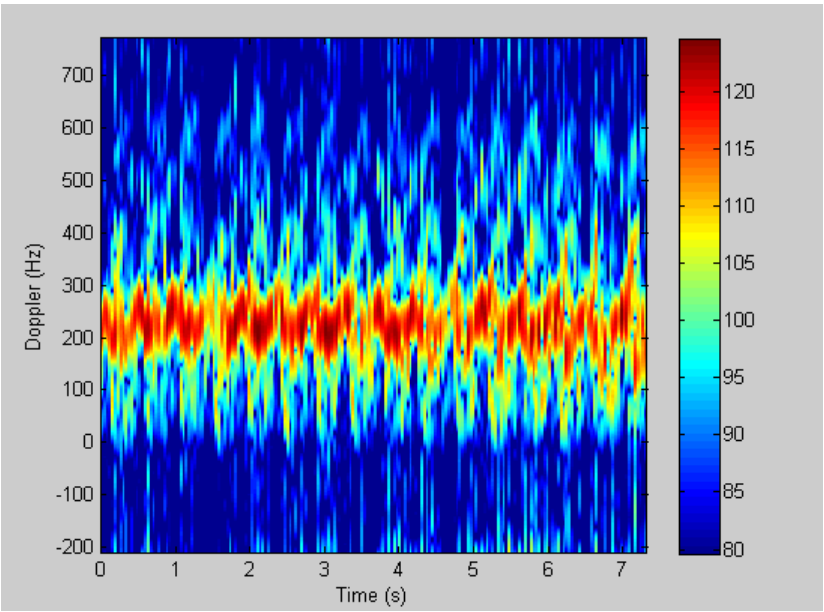

Figure 4.13 Spectrogram of 3rd person's walking with azimuth angle of 0° after clutter suppression

Table 4.8 Micro Doppler features of walking of 1st person, 2nd person and 3rd person

Walking with Azimuth Angle of 0°	Characteristics of 3 Persons' Walking with 0°					
	Torso Frequency (Hz)	BW (Hz)	Offset (Hz)	BW w/o Micro Doppler (Hz)	STD	Period (sec)
Average Values for 1st Person	188,6218	557,5308	196,2589	235,0184	7,3275	0,4607
Average Values for 2nd Person	177,3373	547,7646	193,7365	211,3353	7,5608	0,4710
Average Values for 3rd Person	223,7303	528,8424	219,6103	185,9430	7,9174	0,4979

In order to see whether every person has different walking characteristics and can be distinguished by using micro Doppler features, extracted feature values of 1st person's, 2nd person's and 3rd person's walking spectrograms are listed at Table 4.8. The followings can be extracted from Table 4.8:

- 3rd person has the largest torso frequency, which means that this person has the largest speed of walking.
- 1st person has the largest BW value, which can be explained that this person has the highest velocity of limb motions of walking.
- 3rd person has the largest offset value, which can be deduced that the forward and backward limb motions are more asymmetric than other persons' limb motions while walking.

- 1st person has the largest bandwidth without micro Doppler value, which can be concluded that this person has the largest bobbing motion of torso while walking.
- 3rd person has the largest standard deviation value, which means that dynamic range of the motion is bigger than others'; in other words, the signal strength bar consists of larger range of numbers.
- 3rd person has the largest period values, which means that the swing rate of limbs is smaller than others', which means that this person swings arms slowly.

In brief, when extracted features of walking spectrograms of the targets are taken into consideration, it is seen that each person has distinctive walking features, in other words each person has signatures of walking and identification of walking person could be done by looking at the walking spectrograms. In general, the extracted values of 3 person's walking are close to each other. It means that it is possible to group these values to obtain the features of walking with azimuth angle of 0°. By using the values at Table 4.8, the average values of 3 person's walking features are calculated as torso frequency of 196,5631 Hz; bandwidth of 544,7126 Hz; offset of 203,2019 Hz; bandwidth without micro Doppler of 210,7656 Hz; standard deviation of 7,6019 and period of 0,4765 sec. These average values are used as the extracted features of human walking with the azimuth angle of 0°.

4.3.1.2 Walking with Azimuth Angle of 30°

In order to arrange the azimuth angle of the target to the line of sight of the radar to 30°, walking path is calculated and marked on the field as seen in Figure 4.14.

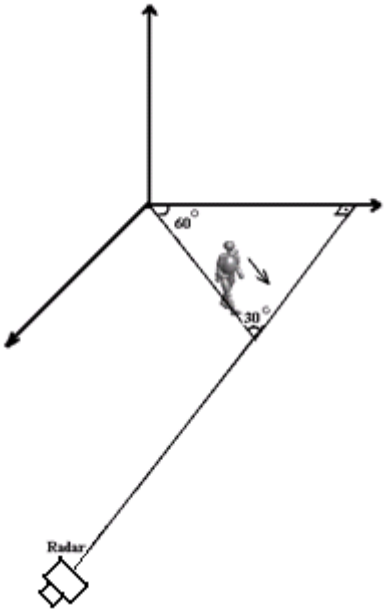

Figure 4.14 Walking path for the azimuth angle of 30°

1st person is asked to walk on the walking path which has azimuth angle of 30° to the radar and repeat this motion for 7 times to record raw data of human walking. After the raw data of human walking is processed as explained in Chapter 3, 1st person's walking spectrograms with the azimuth angle of 30° are obtained; one of these spectrograms is demonstrated at Figure 4.15. The clutter removed version is given in Figure 4.16. Feature extraction results of the spectrograms of 1st person's walking with the azimuth angle of 30° are listed at Table 4.9.

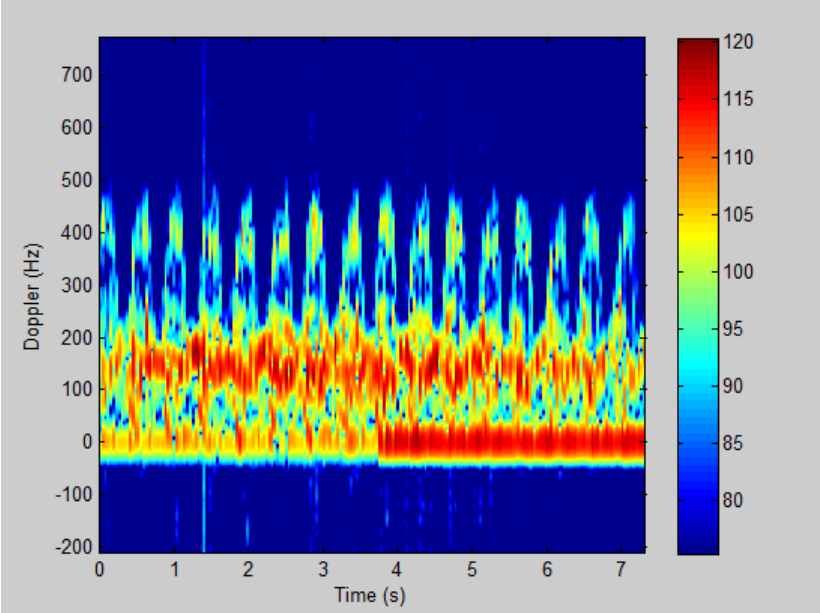

Figure 4.15 Spectrogram of 1st person's walking with azimuth angle of 30° before clutter suppression

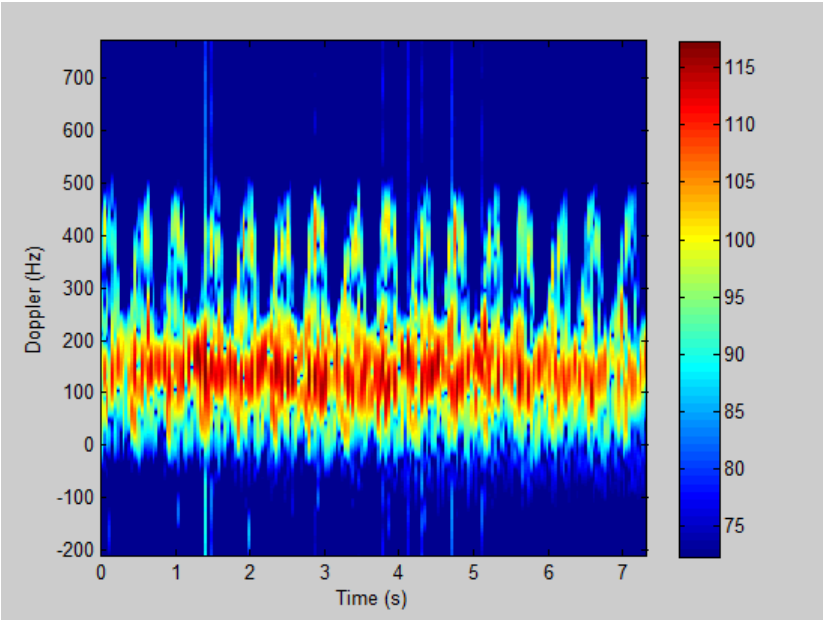

Figure 4.16 Spectrogram of 1st person's walking with azimuth angle of 30° after clutter suppression

When feature table (Table 4.9) is taken into consideration, it is seen that the average feature values of 1st person's walking with the azimuth angle of 30° are calculated as torso frequency of 146,5138 Hz; bandwidth of 483,0631 Hz; offset of 164,2824 Hz; bandwidth without micro Doppler of 209,5678 Hz; standard deviation of 7,1936 and period of 0,4397 sec. These average values are used as the extracted features of 1st person's walking with the azimuth angle of 30°.

Table 4.9 Extracted micro Doppler features of 1st person's walking with 30°

1st Person's Walking with Azimuth Angle of 30°	Extracted Classification Features					
	Torso Frequency (Hz)	BW (Hz)	Offset (Hz)	BW w/o Micro Doppler (Hz)	STD	Period (sec)
Sample-1	147,2549	492,219	171,5716	198,2729	7,2605	0,4274
Sample-2	151,7410	500,7645	165,5343	199,1274	7,1377	0,4258
Sample-3	142,6220	456,328	156,9461	212,2002	6,701	0,4519
Sample-4	153,2238	486,2372	167,9227	207,2366	7,4809	0,4473
Sample-5	141,7923	473,419	158,2279	201,4644	7,0022	0,4336
Sample-6	151,1185	488,8008	164,5409	219,6366	7,189	0,4597
Sample-7	137,8443	483,6735	165,233	229,0366	7,5839	0,432

The same experiment is repeated for 2nd and 3rd persons and results are given in Figure 4.17, Figure 4.18, Figure 4.19, and Figure 4.20. Feature extraction results for 2nd person and 3rd person are given in Table 4.10, and Table 4.11, respectively.

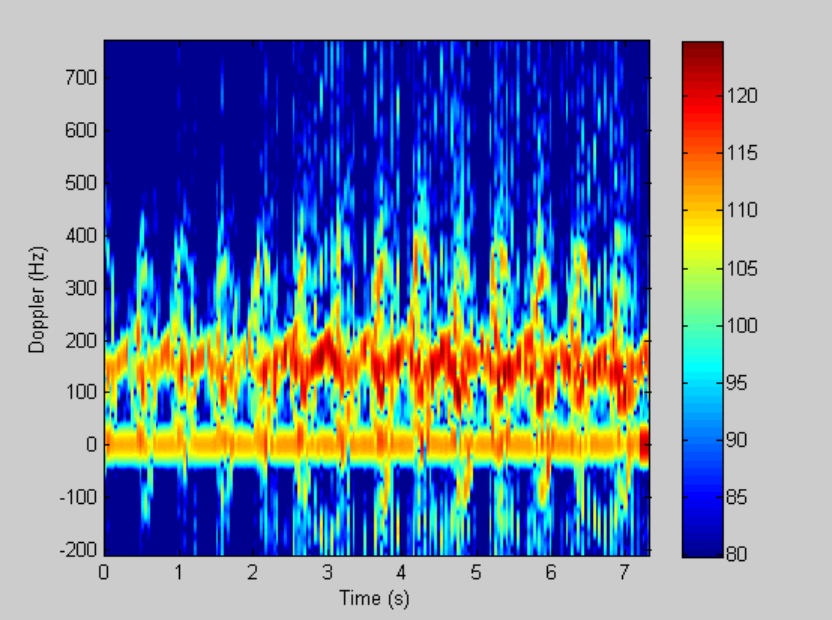

Figure 4.17 Spectrogram of 2nd person's walking with azimuth angle of 30° before clutter suppression

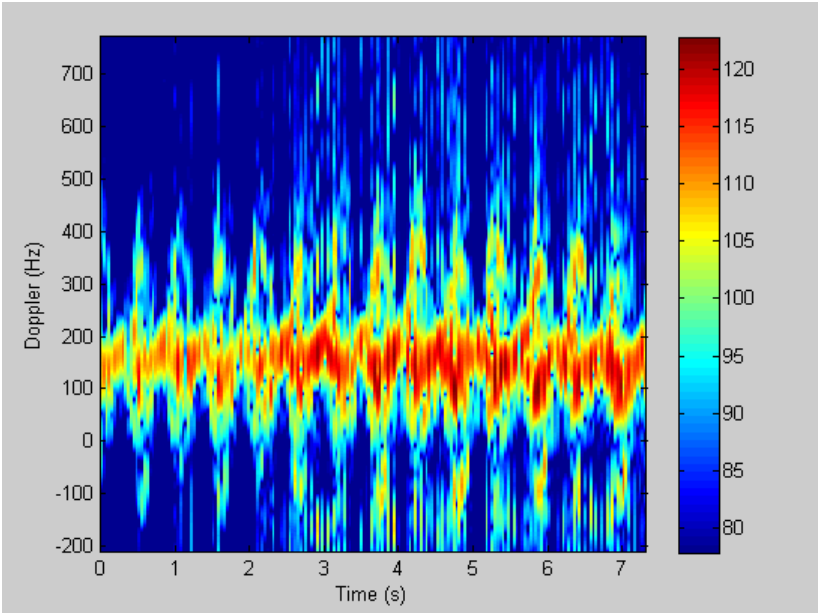

Figure 4.18 Spectrogram of 2nd person's walking with azimuth angle of 30° after clutter suppression

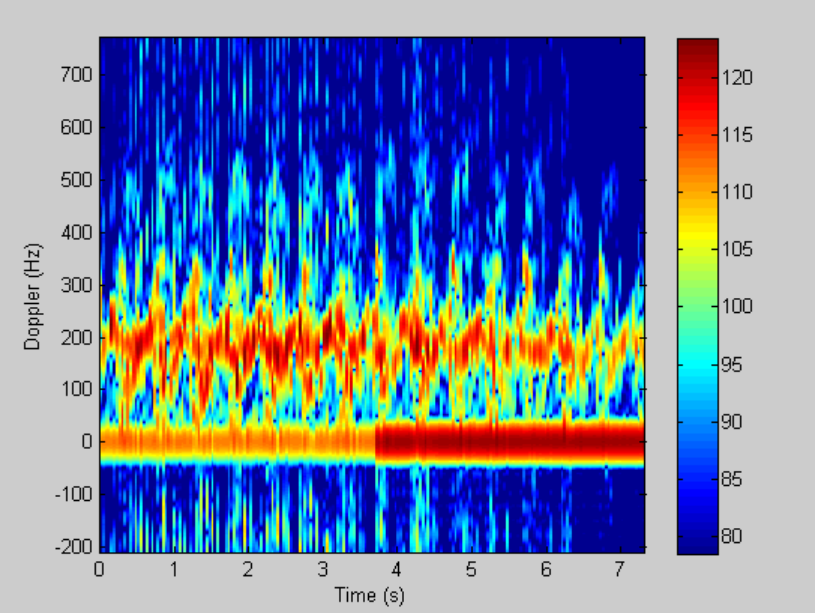

Figure 4.19 Spectrogram of 3rd person's walking with azimuth angle of 30° before clutter suppression

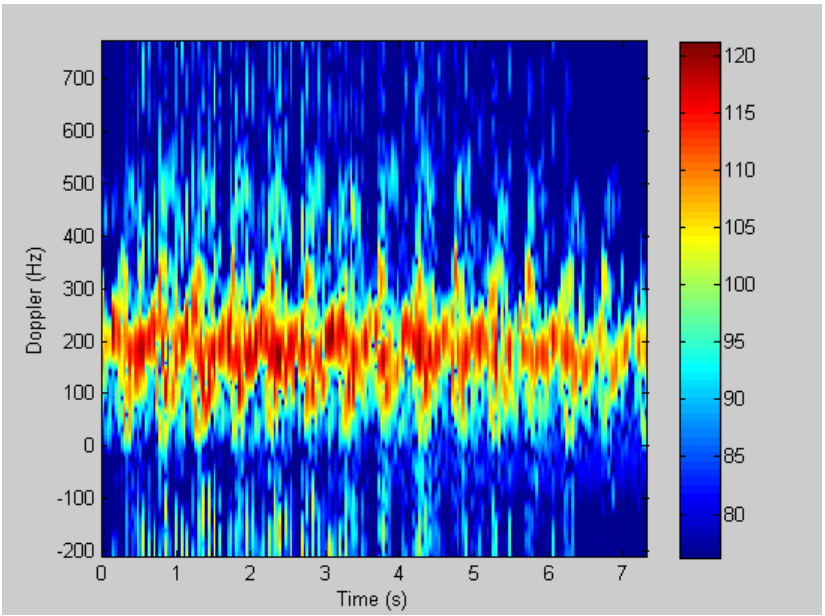

Figure 4.20 Spectrogram of 3rd person's walking with azimuth angle of 30° after clutter suppression

Table 4.10 Extracted micro Doppler features of 2nd person's walking with 30°

2nd Person's Walking with 30°	Extracted Classification Features					
	Torso Frequency (Hz)	BW (Hz)	Offset (Hz)	BW w/o Micro Doppler (Hz)	STD	Period (sec)
Sample-1	132,1308	457,1826	160,345	184,6001	7,6182	0,4681
Sample-2	131,8223	455,4735	164,5345	190,582	7,227	0,4656
Sample-3	129,6449	467,4371	162,3297	196,5638	7,2676	0,4672
Sample-4	137,0601	455,4735	167,269	183,7456	7,5437	0,4806
Sample-5	134,9041	478,5463	166,7819	181,6821	7,6145	0,478
Sample-6	145,1232	517,0009	164,5494	182,891	7,8533	0,4583
Sample-7	149,2950	538,3645	143,663	161,0183	7,5784	0,4795

Table 4.11 Extracted micro Doppler features of 3rd person's walking 30°

3rd Person's Walking with 30°	Extracted Classification Features					
	Torso Frequency (Hz)	BW (Hz)	Offset (Hz)	BW w/o Micro Doppler (Hz)	STD	Period (sec)
Sample-1	162,3580	507,6008	167,472	166,6547	7,7491	0,4422
Sample-2	168,3669	482,819	175,1757	168,3638	7,5866	0,4608
Sample-3	177,6670	518,71	187,6051	151,2728	7,7774	0,4571
Sample-4	185,7152	541,7827	179,739	146,1455	7,3417	0,4641
Sample-5	166,3749	485,3826	178,7883	144,4364	7,2722	0,4676
Sample-6	174,2694	531,5282	183,6678	171,7819	7,5521	0,5333
Sample-7	175,6928	524,6918	178,0949	160,6728	7,6724	0,4473

Table 4.12 Micro Doppler features of 1st person's, 2nd person's and 3rd person's walking with the azimuth angle of 30°

Walking with Azimuth Angle of 30°	Characteristics of 3 Persons' Walking with 30°					
	Torso Frequency (Hz)	BW (Hz)	Offset (Hz)	BW w/o Micro Doppler (Hz)	STD	Period (sec)
Average Values for 1st Person	146,5138	483,0631	164,2824	209,5678	7,1936	0,4397
Average Values for 2nd Person	137,1401	481,3541	161,3532	183,0118	7,5290	0,4710
Average Values for 3rd Person	172,9206	513,2164	178,6490	158,4754	7,5645	0,4675

In order to analyze whether every person has different walking characteristics and can be distinguished by using micro Doppler features, extracted feature values of 1st person's, 2nd person's and 3rd person's walking spectrograms are listed at Table 4.12. The followings can be extracted from Table 4.12:

- 3rd person has the largest torso frequency, which means that this person has the largest speed of walking at 30° approach angle.
- 3rd person has the largest BW value, which can be explained that this person has the highest velocity of limb motions of walking.
- 3rd person has the largest offset value, which can be deduced that the forward and backward limb motions are more asymmetric than other persons' limb motions while walking.
- 1st person has the largest bandwidth without micro Doppler value, which can be concluded that this person has the largest bobbing motion of torso while walking.

- 2nd person has the largest standard deviation value, which means that dynamic range of the motion is bigger than others'; in other words, the signal strength bar consists of larger range of numbers.
- 2nd person has the largest period values, which means that the swing rate of limbs is smaller than others', which means that this person swings arms slowly.

In brief, when extracted features of walking with 30° spectrograms of the targets are taken into consideration, it is seen that each person has distinctive walking features, in other words each person has signatures of walking and identification of walking person could be done by looking at the walking with 30° spectrograms. On the other hand, the extracted values of 3 persons' walking with 30° are close to each other. It means that it is possible to group these values to obtain the features of walking with azimuth angle of 30°. By using the values at Table 4.12, the average values of 3 persons' walking features are calculated as torso frequency of 152,1915 Hz; bandwidth of 492,5445 Hz; offset of 168,0948 Hz; bandwidth without micro Doppler of 183,6850 Hz; standard deviation of 7,4290 and period of 0,4594 sec. These average values are used as the extracted features of human walking with the azimuth angle of 30°.

4.3.1.3 Walking with Azimuth Angle of 60°

The experiment is repeated for the azimuth angle of 60°. Data is obtained from the same targets. Walking path is calculated and marked on the field as seen in Figure 4.21.

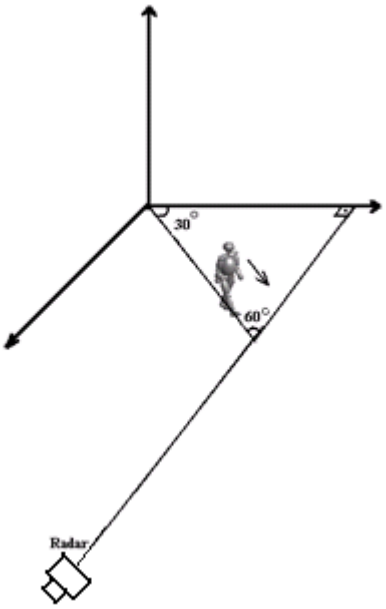

Figure 4.21 Walking path for the azimuth angle of 60°

The results for each target are given in Figure 4.22 and Figure 4.23 for 1st person; Figure 4.24 and Figure 4.25 for 2nd person; Figure 4.26 and Figure 4.27 for 3rd person. Feature extraction results of 1st person, 2nd person and 3rd person are given in Table 4.13, Table 4.14 and Table 4.15, respectively.

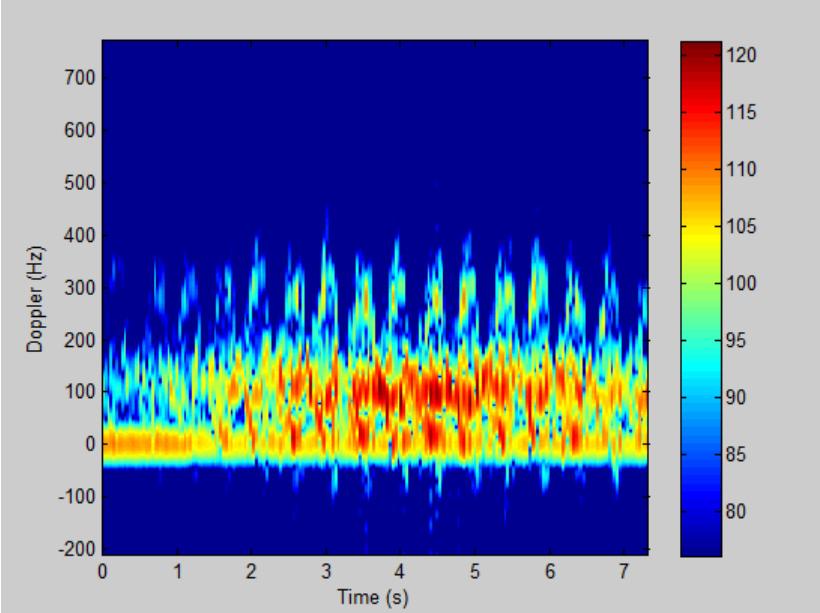

Figure 4.22 Spectrogram of 1st person's walking with azimuth angle of 60° before clutter suppression

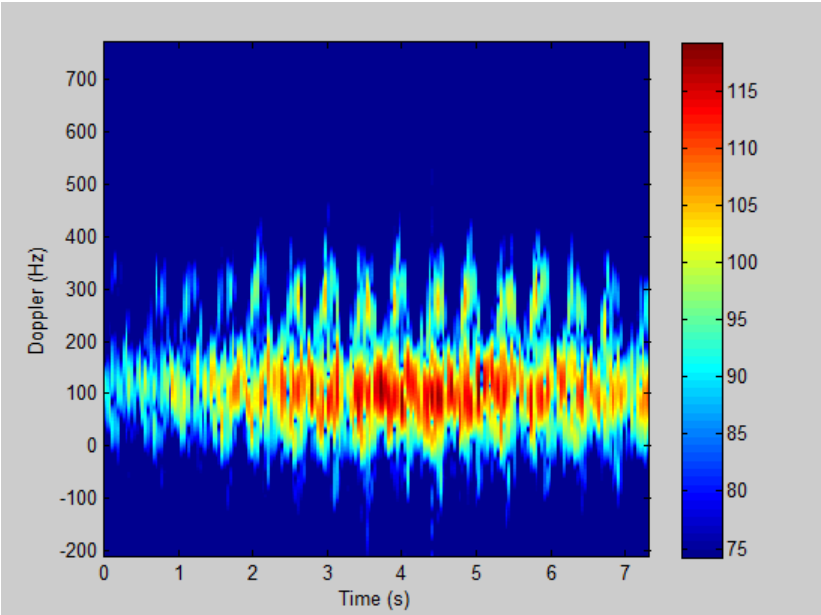

Figure 4.23 Spectrogram of 1st person's walking with azimuth angle of 60° after clutter suppression

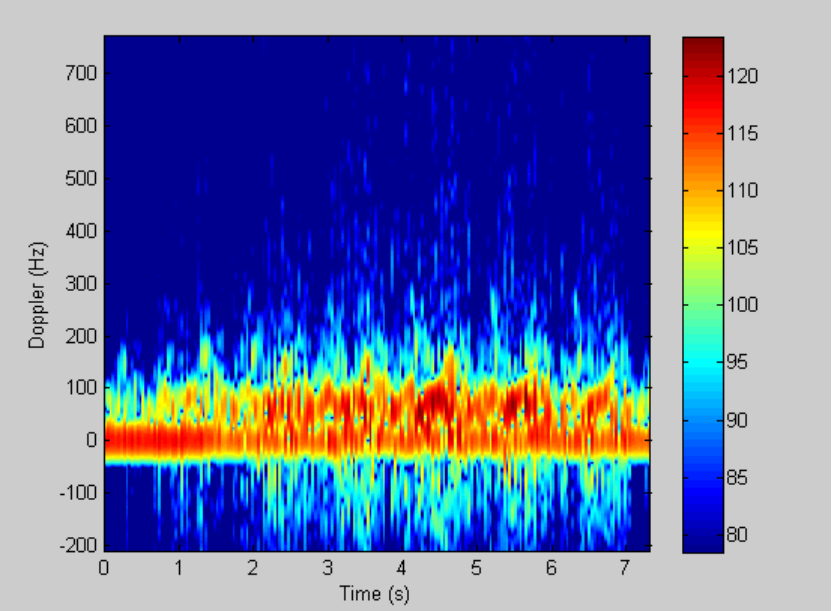

Figure 4.24 Spectrogram of 2nd person's walking with azimuth angle of 60° before clutter suppression

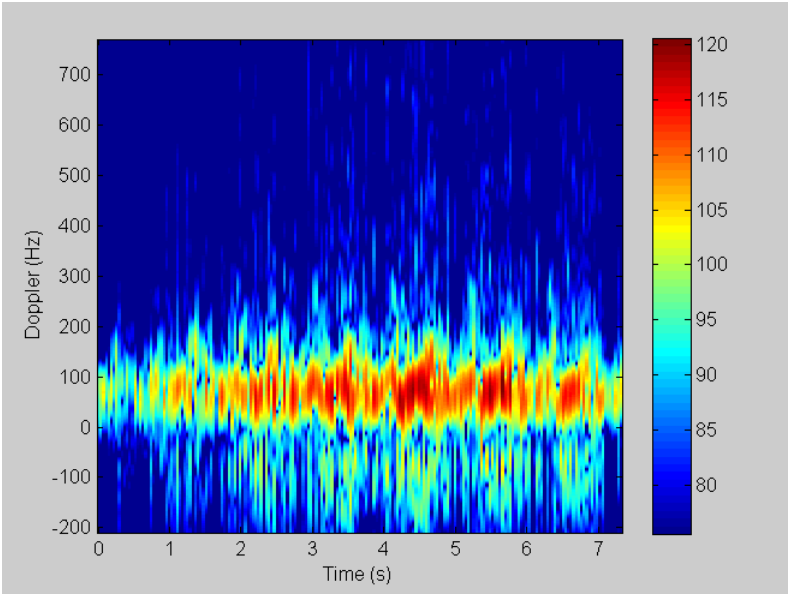

Figure 4.25 Spectrogram of 2nd person's walking with azimuth angle of 60° after clutter suppression

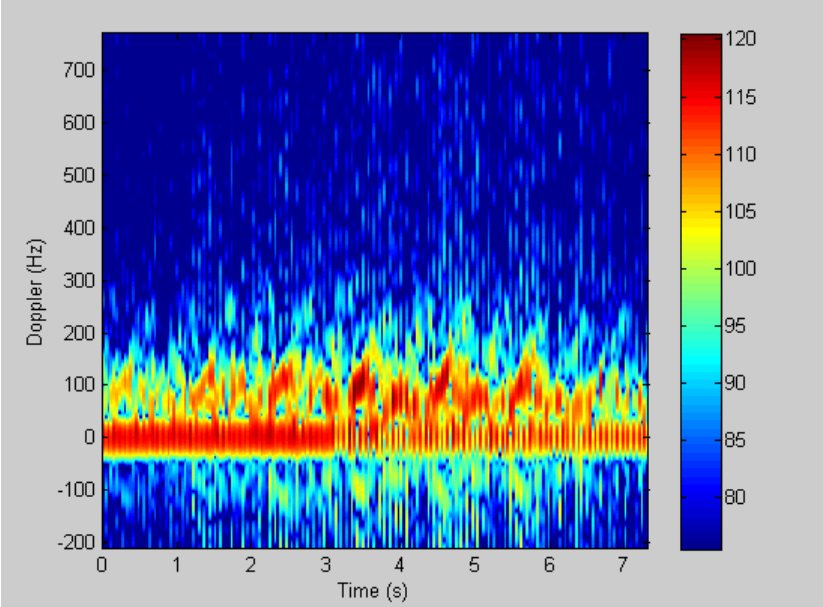

Figure 4.26 Spectrogram of 3rd person's walking with azimuth angle of 60° before clutter suppression

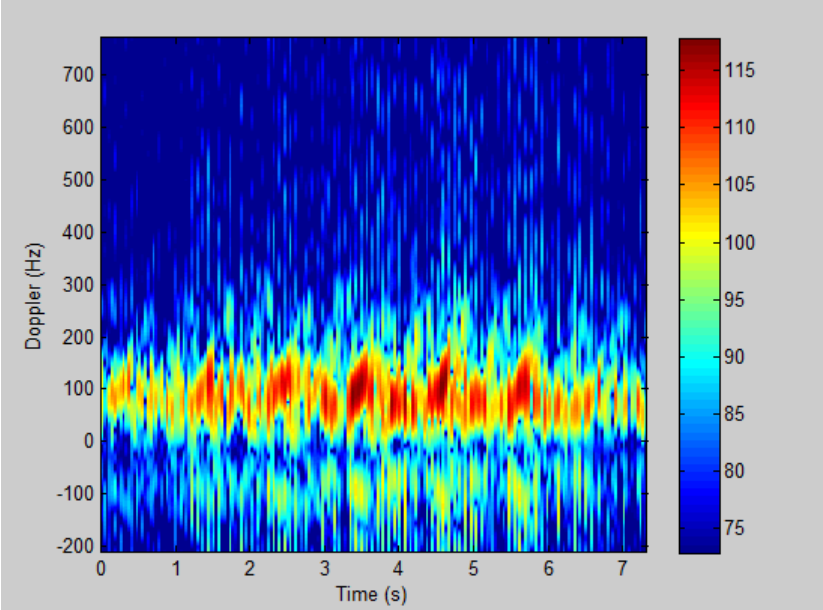

Figure 4.27 Spectrogram of 3rd person's walking with azimuth angle of 60° after clutter suppression

Table 4.13 Extracted micro Doppler features of 1st person's walking with 60°

1st Person's Walking with 60°	Extracted Classification Features					
	Torso Frequency (Hz)	BW (Hz)	Offset (Hz)	BW w/o Micro Doppler (Hz)	STD	Period (sec)
Sample-1	119,0730	392,237	92,5496	194,8547	7,5912	0,4434
Sample-2	110,3708	397,3643	114,6668	174,3456	7,3232	0,4632
Sample-3	104,7302	350,3642	110,962	165,8001	7,0711	0,4114
Sample-4	100,4464	351,2188	90,6375	179,982	6,7544	0,512
Sample-5	105,0493	355,4915	96,2668	185,4547	6,6828	0,448
Sample-6	98,9502	358,9097	98,0635	147,0001	7,2408	0,4713
Sample-7	98,0547	360,6188	102,834	185,0002	7,4075	0,4588

Table 4.14 Extracted micro Doppler features of 2nd person's walking with the azimuth angle of 60°

2nd Person's Walking with 60°	Extracted Classification Features					
	Torso Frequency (Hz)	BW (Hz)	Offset (Hz)	BW w/o Micro Doppler (Hz)	STD	Period (sec)
Sample-1	61,3783	194,8367	47,3846	151,2728	7,2711	0,4583
Sample-2	56,5033	200,8185	43,0264	167,5092	7,5757	0,4414
Sample-3	75,6878	223,8913	67,0776	173,491	6,8928	0,4109
Sample-4	79,3837	222,1822	65,8599	178,6183	7,0575	0,4486
Sample-5	81,4528	225,6004	71,7206	150,4183	6,9013	0,4461
Sample-6	69,7646	223,0367	65,0054	178,2729	7,5179	0,4195
Sample-7	74,6386	232,4368	68,5601	156,4001	7,2664	0,4251

Table 4.15 Extracted micro Doppler features of 3rd person's walking with the azimuth angle of 60°

3rd Person's Walking with 60°	Extracted Classification Features					
	Torso Frequency (Hz)	BW (Hz)	Offset (Hz)	BW w/o Micro Doppler (Hz)	STD	Period (sec)
Sample-1	77,1432	232,4368	64,8715	141,9817	7,0939	0,4109
Sample-2	81,9553	282,855	83,0983	123,9273	7,3159	0,4195
Sample-3	98,8749	269,1823	84,6925	162,7819	7,3851	0,4274
Sample-4	93,6406	266,6186	77,4964	142,7273	7,3873	0,4486
Sample-5	84,5033	282,855	70,9559	146,1635	7,2593	0,4242
Sample-6	80,9279	264,9095	80,5539	153,1456	6,8993	0,4457
Sample-7	97,3234	234,1458	74,4793	147,4673	6,6513	0,4127

Table 4.16 Micro Doppler features of 1st person's, 2nd person's and 3rd person's walking with the azimuth angle of 60°

Walking with Azimuth Angle of 60°	Characteristics of 3 Persons' Walking with 60°					
	Torso Frequency (Hz)	BW (Hz)	Offset (Hz)	BW w/o Micro Doppler (Hz)	STD	Period (sec)
Average Values for 1st Person	105,2392	366,6006	100,8543	176,0625	7,1530	0,4583
Average Values for 2nd Person	71,2584	217,5432	61,2335	165,1404	7,2118	0,4357
Average Values for 3rd Person	87,7669	261,8576	76,5925	145,4564	7,1417	0,4270

In order to analyze whether each person has different walking characteristics and can be distinguished by using micro Doppler features, the features of 1st person's, 2nd person's and 3rd person's walking spectrograms are given in Table 4.16. The followings can be extracted from Table 4.16:

- 1st person has the largest torso frequency, which means that this person has the largest speed of walking with 60°.
- 1st person has the largest BW value, which can be explained that this person has the highest velocity of limb motions of walking.
- 1st person has the largest offset value, which can be deduced that the forward and backward limb motions are more asymmetric than other persons' limb motions while walking.
- 1st person has the largest bandwidth without micro Doppler value, which can be concluded that this person has the largest bobbing motion of torso while walking.
- 2nd person has the largest standard deviation value, which means that dynamic range of the motion is bigger than others'; in other words, the signal strength bar consists of larger range of numbers.
- 1st person has the largest period values, which means that the swing rate of limbs is smaller than others', which means that this person swings arms slowly.
- 1st person has the largest value for 5 features, it can be caused that 2nd and 3rd persons' spectrograms are not clear enough as 1st person's spectrogram.

When the extracted features of walking with 60° spectrograms of the targets are taken into consideration, it is seen that each person has distinctive walking features, in other words each person has signatures of walking and identification of walking person could be done by looking at the walking with 60° spectrograms. On the other hand, the extracted values of 3 persons' walking with 60° are close to each other. It means that it is possible to group these values to obtain the features of

walking with azimuth angle of 60°. By using the values at Table 4.16, the average values of 3 person's walking features are calculated as torso frequency of 88,0882 Hz; bandwidth of 282,0005 Hz; offset of 79,5601 Hz; bandwidth without micro Doppler of 162,2197 Hz; standard deviation of 7,1688 and period of 0,4403 sec. These average values are used as the extracted features of human walking with the azimuth angle of 60°.

4.3.1.4 Comparison of Different Azimuth Angles

Figure 4.28 shows the spectrograms of a target walking at three different azimuth angles.

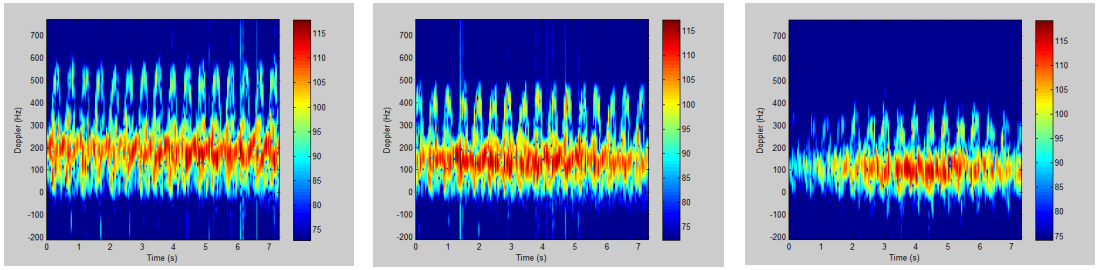

(a) Azimuth angle of 0° (b) Azimuth angle of 30° (c) Azimuth angle of 60°

Figure 4.28 One of the spectrograms of azimuth angles of 0°, 30°, 60°

It can be seen clearly in Figure 4.28 that when azimuth angle increases from 0° to 60°, the resolution of the limb motions on the spectrograms decreases. The limb motions that are very clear for the azimuth angle of 0° are blurred for the azimuth angle of 60°. In addition, where the walking person is outside the azimuth beam width, signal is not received with a proper SNR and walking signature is not formed at these parts of the spectrograms. Moreover, at the transition parts, where the person starts walking into the coverage of the azimuth beam width of the radar, the human motions on the spectrograms seem unclear as can be seen from Figure

4.28 (c). For example, at the spectrogram of the azimuth angle of 60°, the time intervals 0-2 sec and 6-7 sec can be assumed as transition parts and the walking signature is blurry for these time intervals. Further, as can be seen from Figure 4.28 that the Doppler spread and the torso frequency of the walking spectrograms decrease while the azimuth angle increases from 0° to 60°. Detailed analysis on the extracted features is given after presenting some numerical values of the features.

In order to compare the azimuth angles of 0°, 30°, 60° in terms of their micro Doppler features quantitively, the extracted feature values of human walking with 0°, 30°, 60° are listed at Table 4.17.

Table 4.17 Average values of the spectrograms of azimuth angles of 0°, 30°, 60°

	Comparison of azimuth angles					
	Torso Frequency (Hz)	BW (Hz)	Offset (Hz)	BW w/o Micro Doppler (Hz)	STD	Period (sec)
Average Values for 0°	196,5631	544,7126	203,2019	210,7656	7,6019	0,4765
Average Values for 30°	152,1915	492,5445	168,0948	183,6850	7,4290	0,4594
Average Values for 60°	88,0882	282,0005	79,5601	162,2197	7,1688	0,4403

The numerical results of the extracted features are consistent with the comments of spectrograms. Torso frequency is 196.6 Hz for the azimuth angle of 0°, it is 152.2 Hz for 30° and it is approximately 88 Hz for 60°; it means that the torso frequency, which depends on the human speed, decreases with the increasing

azimuth angles. It is known that if the azimuth angle is bigger than 0°, the human speed according to the radar becomes the radial component of the human speed. Therefore, it is reasonable that human speed becomes smaller for bigger azimuth angles than 0° and this makes the torso frequency values decrease while azimuth angles are increasing. Moreover, as can be seen from Table 4.17 that the bandwidth, which is related with the speed of the limbs, of the spectrograms decrease from 544,7 Hz to 282 Hz while the azimuth angles increases from 0° to 60°. It is reasonable because if there is an azimuth angle bigger than 0°, the limbs speed according to the radar is calculated as the radial components of the limbs speed; therefore, for the larger azimuth angles, smaller bandwidth values are obtained. Further, it is known that offset values depend on the symmetry of the limbs swings; because forward and backward limbs motions are symmetric while walking, offset values are very close to torso frequency values; therefore, the offset values are decreased from 210,8 Hz to 79,5 Hz as the azimuth angle increases from 0° to 60°; this decrease is resembling to the decrease of torso frequency. When the bandwidth without micro Doppler values are taken into consideration and it is seen that the values decrease from 274,5 Hz to 183,7 Hz and to 162,2 Hz, as the azimuth angle increases from 0° to 30° and then to 60°, respectively. The bandwidth without micro Doppler values depends only on the bandwidth of torso. The bobbing of torso can be seen partially; therefore, the bandwidth without micro Doppler value decreases, as the azimuth angle increases from 0° to 60°. Furthermore, when the standard deviation values are compared, it is seen that the standard deviations decrease as the azimuth angles increase from 0° to 60°; because the dynamic range of the walking spectrograms decreases as azimuth angle increases. When walking spectrograms with azimuth angles of 0°, 30°, 60° of one of the persons are examined such as Figure B.1, Figure B.4, Figure B.7, it is seen that the dynamic range values decreases from 0° to 60°; in other words the signal strength bar consists of smaller range of numbers while azimuth angle values are increasing from 0° to 60°. Finally, the period values are compared and it is seen that the period with the azimuth angle of 0° is 0,4765 sec; the period with the azimuth angle of 30° is 0,4594 sec; the period with the azimuth angle of 60° is 0,4403 sec. The period depends on the time

periods of limbs micro Doppler motions; and period values decrease as the azimuth angles are increasing. Even there seems a tendency of decreasing of period values while azimuth angles are increasing, the period values are very close to each other and it is not an efficient discriminative feature for azimuth angles of walking.

4.3.2 Running

The walking experiment is repeated for running. The same set targets are utilized. The results for each target are given in Figure 4.29 and Figure 4.30 for 1st person; Figure 4.31 and Figure 4.32 for 2nd person; Figure 4.33 and Figure 4.34 for 3rd person. Feature extraction results are given in Table 4.18 for 1st person,Table 4.19 for 2nd person, and Table 4.20 for 3rd person.

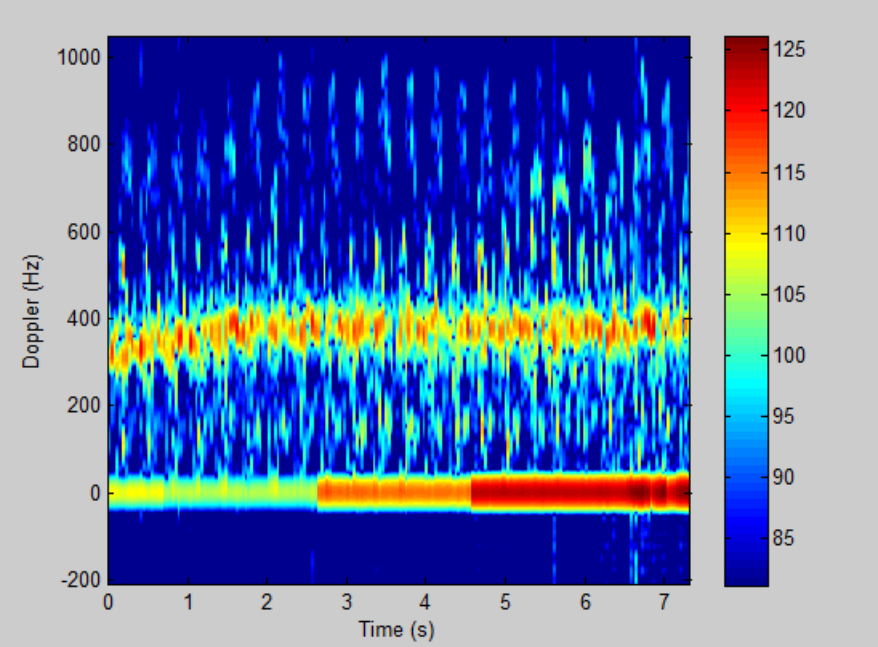

Figure 4.29 Spectrogram of 1st person's running before clutter suppression

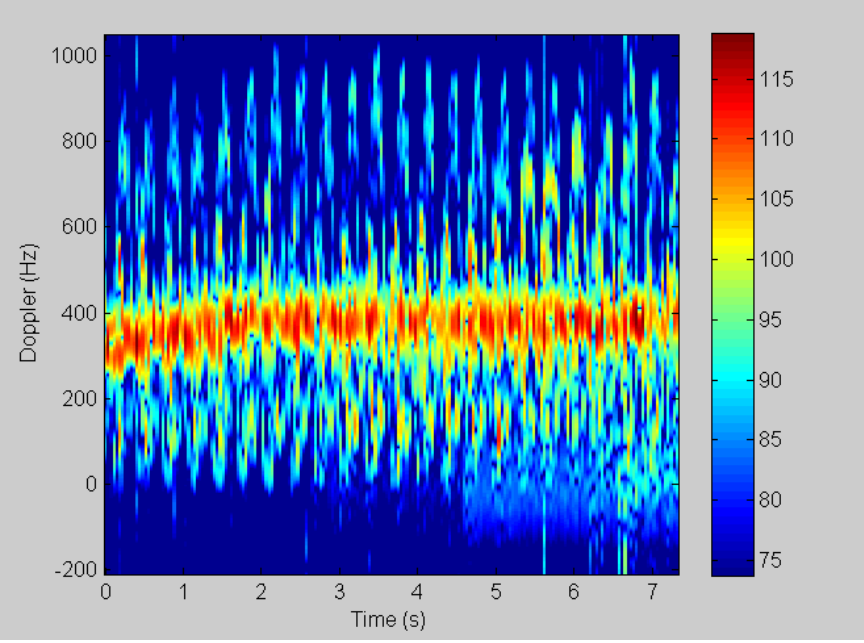

Figure 4.30 Spectrogram of 1st person's running after clutter suppression

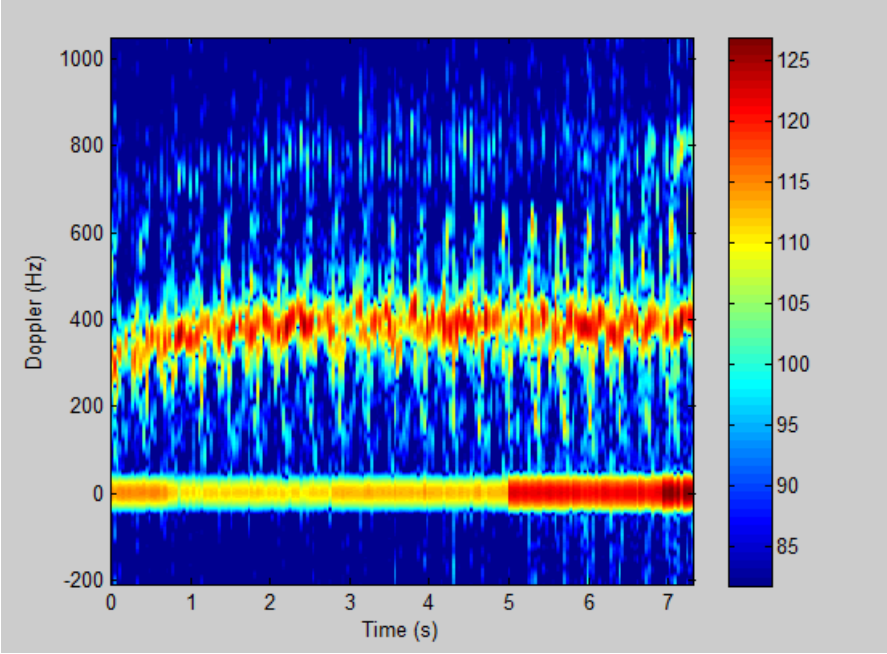

Figure 4.31 Spectrogram of 2nd person's running before clutter suppression

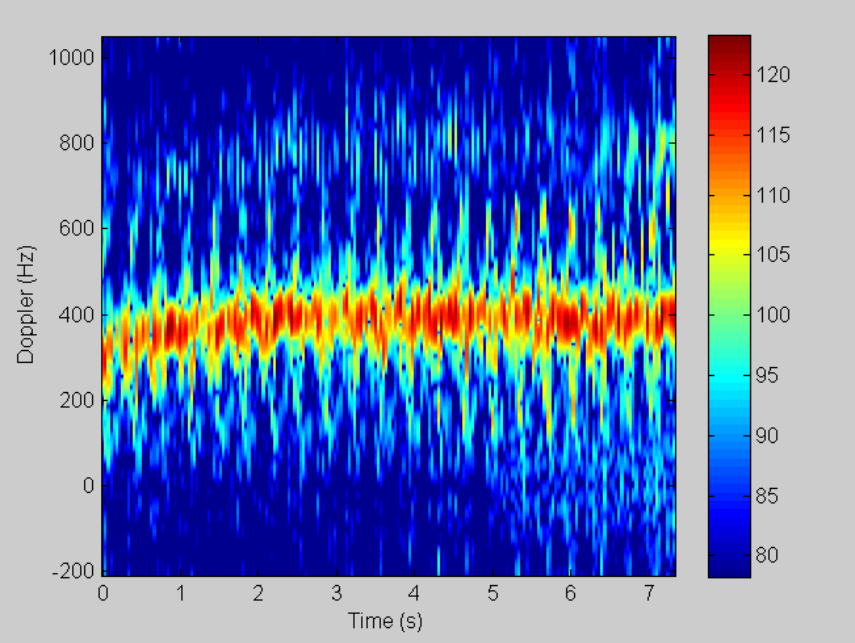

Figure 4.32 Spectrogram of 2nd person's running after clutter suppression

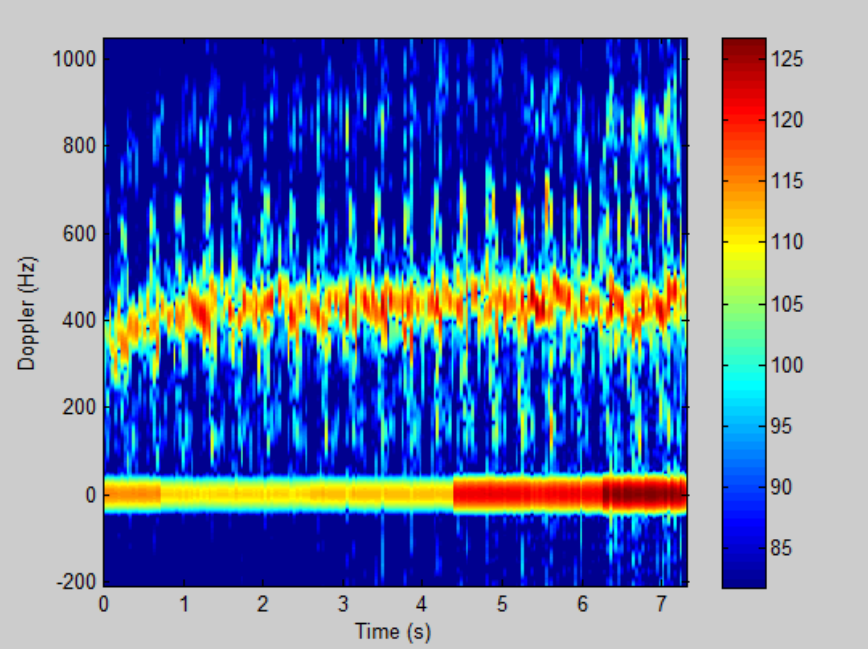

Figure 4.33 Spectrogram of 3rd person's running before clutter suppression

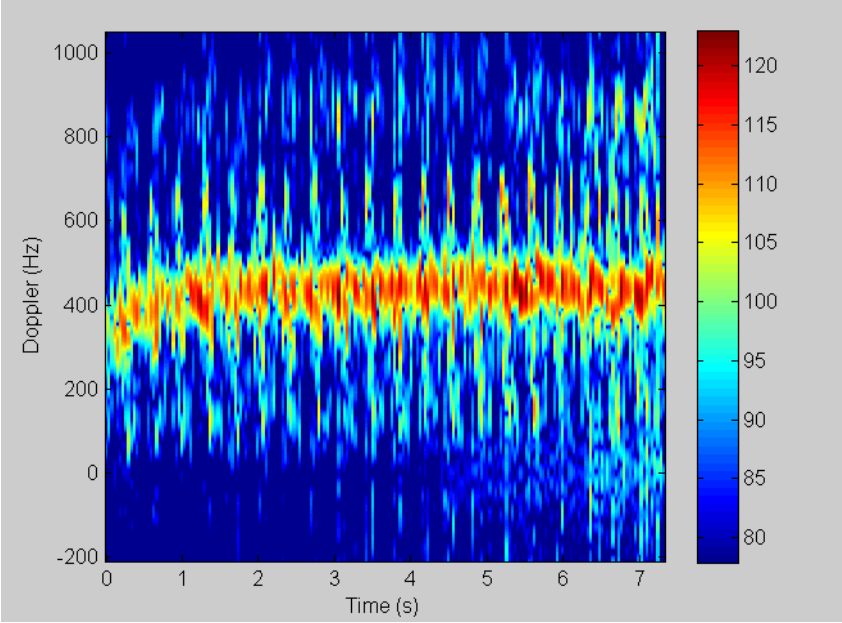

Figure 4.34 Spectrogram of 3rd person's running after clutter suppression

Table 4.18 Extracted micro Doppler features of 1st person's running

1st Person's Running	Extracted Classification Features					
	Torso Frequency (Hz)	BW (Hz)	Offset (Hz)	BW w/o Micro Doppler (Hz)	STD	Period (sec)
Sample-1	380,1706	902,4015	398,9338	255,5275	7,8702	0,2834
Sample-2	389,4716	935,7288	383,1035	233,3093	7,4923	0,2487
Sample-3	383,9130	911,8015	387,8289	239,2911	7,2425	0,2121
Sample-4	431,9843	940,8561	435,5609	258,9457	7,5138	0,3023
Sample-5	407,1131	937,4379	426,1481	259,8003	7,6994	0,2454
Sample-6	381,0525	919,1102	374,7611	281,182	7,0521	0,2873
Sample-7	368,6651	928,0559	382,1771	294,0002	7,8338	0,1933

Table 4.19 Extracted micro Doppler features of 2nd person's running

2nd Person's Running	Extracted Classification Features					
	Torso Frequency (Hz)	BW (Hz)	Offset (Hz)	BW w/o Micro Doppler (Hz)	STD	Period (sec)
Sample-1	410,8075	797,2922	436,8638	253,1456	8,377	0,2438
Sample-2	390,2012	787,8922	424,0245	255,1093	8,3113	0,3474
Sample-3	394,5899	804,1286	416,4435	259,382	8,216	0,3545
Sample-4	418,9271	859,6742	459,6701	272,6365	8,2526	0,1371
Sample-5	411,9509	843,4378	445,2105	288,8729	8,2111	0,416
Sample-6	377,4104	759,6922	411,8874	242,2002	8,6447	0,2438
Sample-7	388,9918	731,4921	401,0532	240,4911	8,4513	0,3047

Table 4.20 Extracted micro Doppler features of 3rd person's running

3rd Person's Running	Extracted Classification Features					
	Torso Frequency (Hz)	BW (Hz)	Offset (Hz)	BW w/o Micro Doppler (Hz)	STD	Period (sec)
Sample-1	456,0340	1181,838	485,0442	267,9275	7,4403	0,1536
Sample-2	451,6142	1075,875	454,4413	257,6729	7,1775	0,2294
Sample-3	480,4244	938,2925	499,0046	250,2365	7,5323	0,2057
Sample-4	433,9976	931,4741	466,058	243,1456	7,8137	0,2194
Sample-5	489,8894	940,0016	502,2197	225,6184	7,4507	0,1567
Sample-6	441,7595	1079,293	463,3675	217,9275	8,1102	0,3218
Sample-7	504,1508	1079,275	540,9536	246,9821	7,6958	0,3474

In order to analyze whether every person has different running characteristics and can be distinguished by using micro Doppler features, extracted average feature values of 1st person's, 2nd person's and 3rd person's running spectrograms are listed at Table 4.21. The followings can be extracted from Table 4.21:

- 3rd person has the largest torso frequency, which means that this person has the largest speed of running.
- 3rd person has the largest BW value, which can be explained that this person has the highest velocity of limb motions of running.
- 3rd person has the largest offset value, which can be deduced that the forward and backward limb motions are more asymmetric than other persons' limb motions while running.
- 1st person has the largest bandwidth without micro Doppler value, which can be concluded that this person has the largest bobbing motion of torso while running.

- 2nd person has the largest standard deviation value, which means that dynamic range of the motion is bigger than others'; in other words, the signal strength bar consists of larger range of numbers.
- 2nd person has the largest period values, which means that the swing rate of limbs is smaller than others', which means that this person swings arms slowly.

Table 4.21 Micro Doppler features of 1st person's, 2nd person's and 3rd person's running

Running	Characteristics of 3 Persons' Running					
	Torso Frequency (Hz)	BW (Hz)	Offset (Hz)	BW w/o Micro Doppler (Hz)	STD	Period (sec)
Average Values for 1st Person	391,7672	925,0560	398,3591	260,2937	7,5292	0,2532
Average Values for 2nd Person	398,9827	797,6585	427,8790	258,8339	8,3520	0,2925
Average Values for 3rd Person	465,41	1032,2926	487,2984	244,2158	7,6029	0,2334

When extracted features of running spectrograms of the targets are taken into consideration, it is seen that each person has distinctive running features, in other words each person has signatures of running and identification of running person could be done by looking at the running spectrograms. On the other hand, the extracted values of all people's

running are close to each other. It means that it is possible to group these values to obtain the features of running. By using the values at Table 4.21, the average values of 3 persons' running features are calculated as torso frequency of 418,7199 Hz; bandwidth of 918,3357 Hz; offset of 437,8455 Hz; bandwidth without micro Doppler of 254,4478 Hz; standard deviation of 7,8280 and period of 0,2597 sec. These average values are used as the extracted features of human running.

4.3.3 Crawling

The experiment is repeated for crawling. The same set targets are utilized. The results for each target are given in Figure 4.35 and Figure 4.36 for 1st person; Figure 4.37 and Figure 4.38 for 2nd person; Figure 4.39 and Figure 4.40 for 3rd person. Feature extraction results of 1st person, 2nd person, 3rd person are given in Table 4.22, Table 4.23 and Table 4.24, respectively.

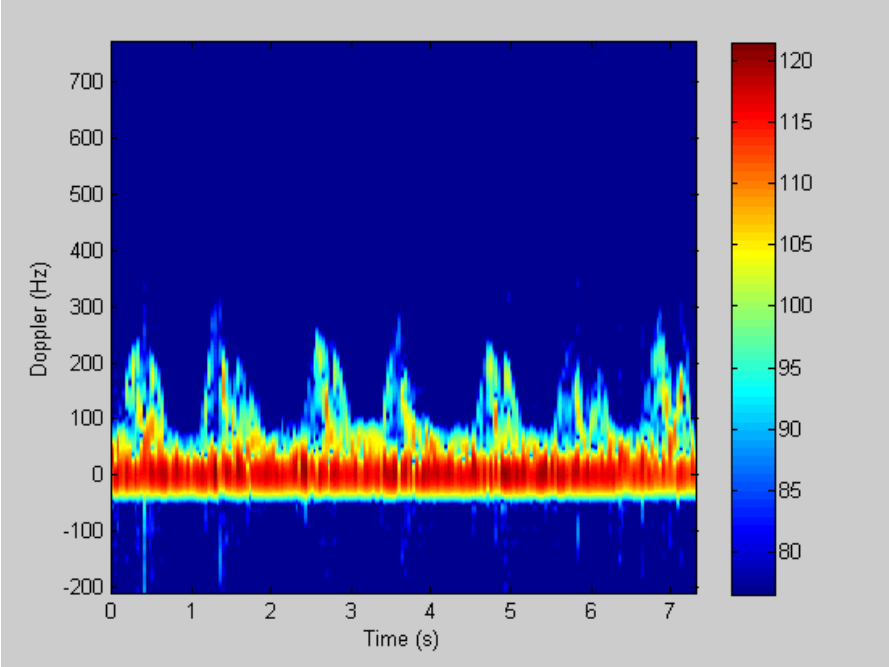

Figure 4.35 Spectrogram of 1st person's crawling before clutter suppression

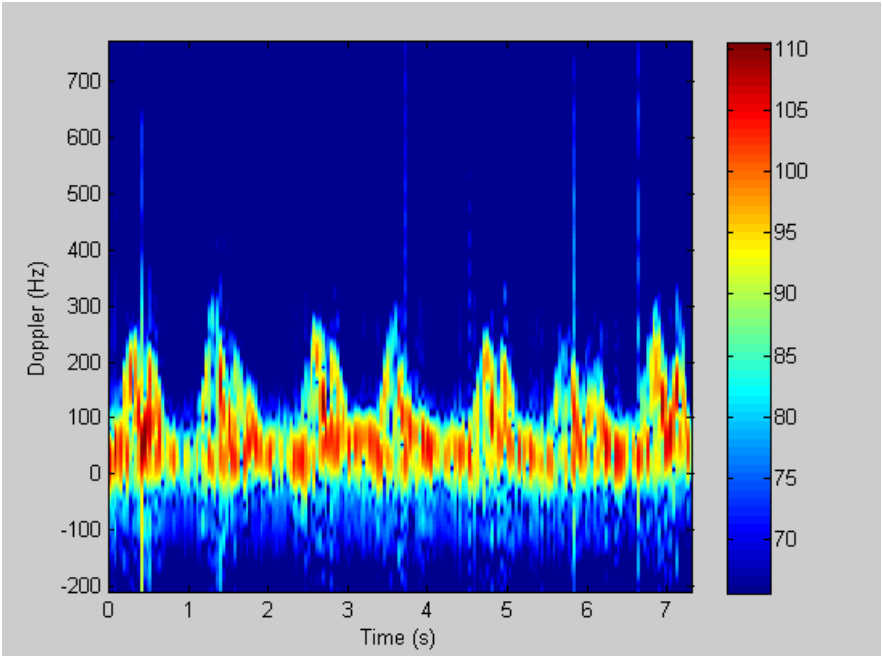

Figure 4.36 Spectrogram of 1st person's crawling after clutter suppression

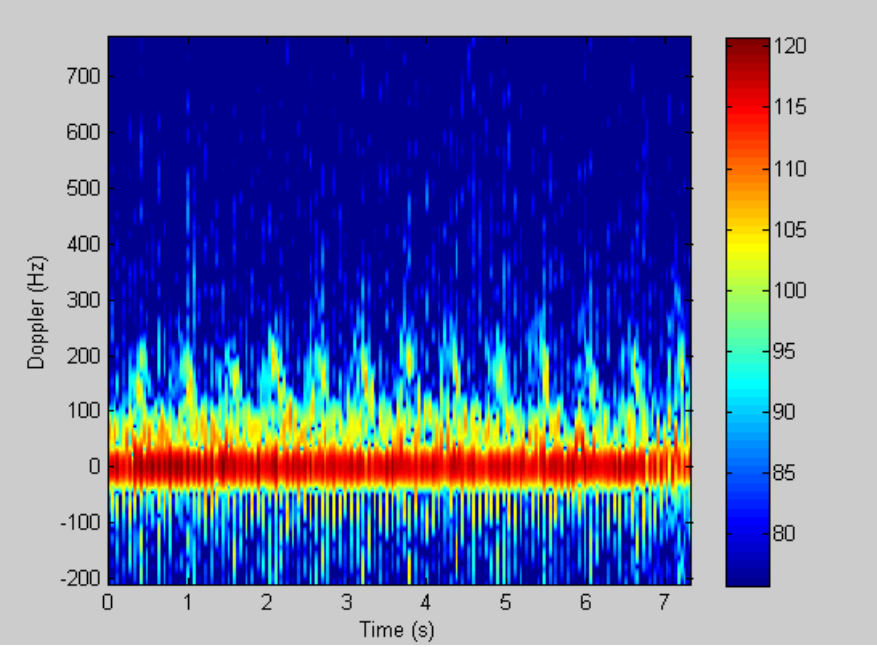

Figure 4.37 Spectrogram of 2nd person's crawling before clutter suppression

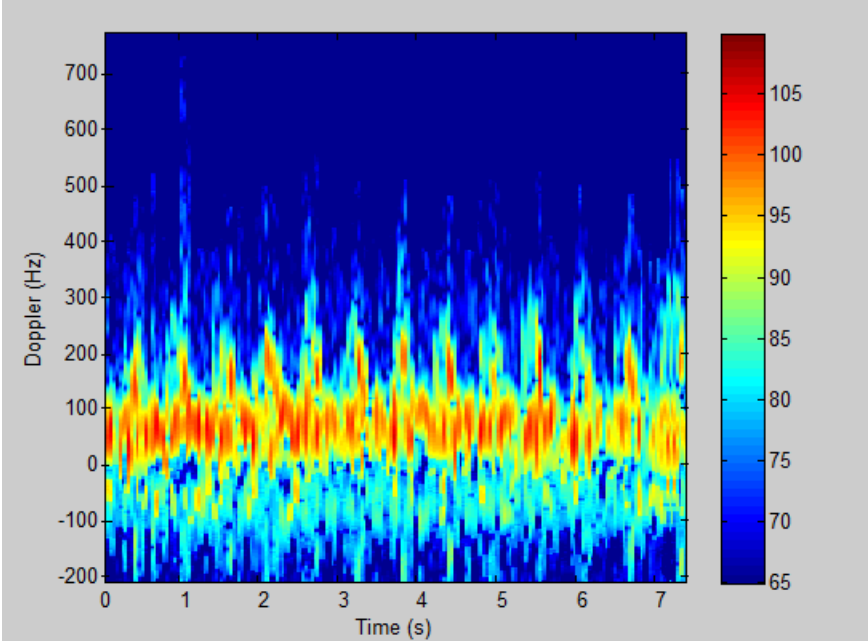

Figure 4.38 Spectrogram of 2nd person's crawling after clutter suppression

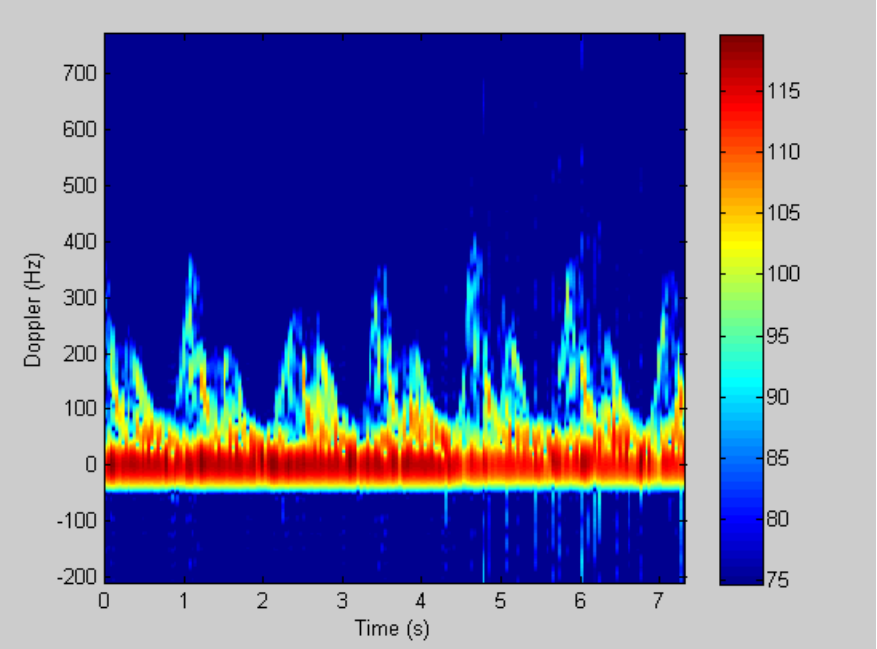

Figure 4.39 Spectrogram of 3rd person's crawling before clutter suppression

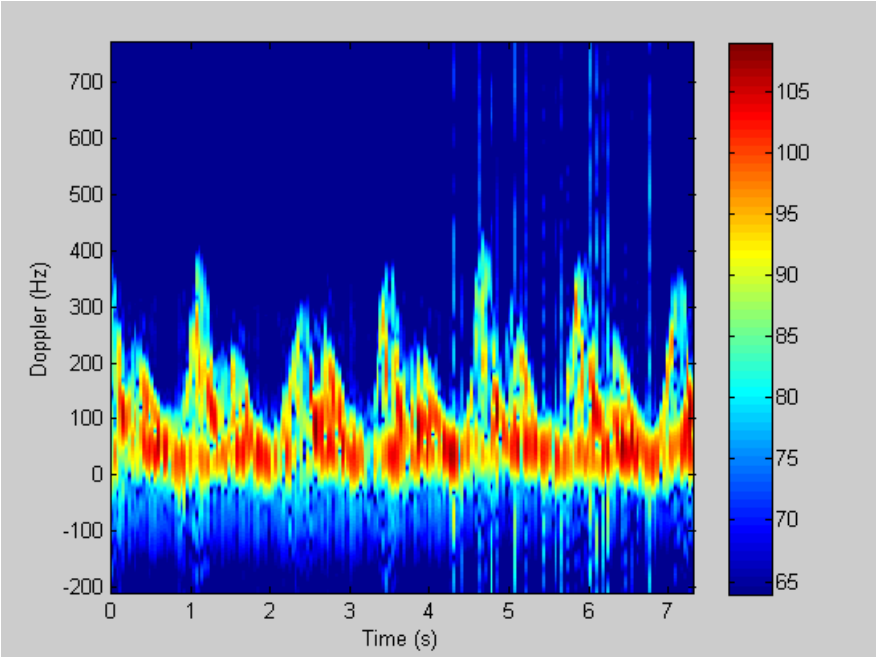

Figure 4.40 Spectrogram of 3rd person's crawling after clutter suppression

Table 4.22 Extracted micro Doppler features of 1st person's crawling

1st Person's Crawling	Extracted Classification Features					
	Torso Frequency (Hz)	BW (Hz)	Offset (Hz)	BW w/o Micro Doppler (Hz)	STD	Period (sec)
Sample-1	62,6724	264,055	66,8662	92,6547	7,015	0,909
Sample-2	69,8983	280,2914	68,3424	87,6728	6,7213	0,8822
Sample-3	83,5910	337,546	76,1679	89,2728	7,1406	0,9769
Sample-4	63,2807	372,5824	74,0572	80,0909	7,0911	0,9935
Sample-5	83,8523	296,5278	70,263	78,6183	6,7773	0,9089
Sample-6	74,6322	316,1823	72,0404	84,1092	7,24	0,9038
Sample-7	84,7743	291,4005	68,9213	80,2001	6,8395	0,8672

Table 4.23 Extracted micro Doppler features of 2nd person's crawling

2nd Person's Crawling	Extracted Classification Features					
	Torso Frequency (Hz)	BW (Hz)	Offset (Hz)	BW w/o Micro Doppler (Hz)	STD	Period (sec)
Sample-1	58,7334	333,2733	107,4999	123,4729	7,0616	0,413
Sample-2	66,5104	303,3641	102,9943	129,0366	7,8635	0,3772
Sample-3	80,2157	308,4914	115,3766	110,2365	7,6741	0,4754
Sample-4	78,2368	358,9097	119,3012	105,9638	6,5781	0,473
Sample-5	88,3823	316,1823	104,5154	113,6547	7,2161	0,4559
Sample-6	72,8886	290,5459	106,7115	115,8284	7,217	0,473
Sample-7	81,4562	249,5277	98,76	129,8911	6,7545	0,5067

Table 4.24 Extracted micro Doppler features of 3rd person's crawling

3rd Person's Crawling	Extracted Classification Features					
	Torso Frequency (Hz)	BW (Hz)	Offset (Hz)	BW w/o Micro Doppler (Hz)	STD	Period (sec)
Sample-1	89,4666	358,9097	94,2843	96,491	6,9856	0,9752
Sample-2	82,4535	468,2917	106,4958	83,7456	7,5897	1,1032
Sample-3	73,4464	372,5824	89,0908	77,7638	7,3514	0,9926
Sample-4	74,6322	358,9097	96,7411	74,7092	7,5496	0,9142
Sample-5	78,3997	440,9462	93,684	76,9092	7,4892	0,9264
Sample-6	76,8136	372,5824	98,0785	65,8001	7,0236	0,9769
Sample-7	65,4024	406,7643	95,9336	64,9456	6,9475	0,9926

In order to analyze whether each person has different crawling characteristics and can be distinguished by using micro Doppler features, extracted feature values of 1st person's, 2nd person's and 3rd person's crawling spectrograms are listed at Table 4.25. The followings can be extracted from Table 4.25:

- 3rd person has the largest torso frequency, which means that this person has the largest speed of crawling.
- 3rd person has the largest BW value, which can be explained that this person has the highest velocity of limb motions of crawling; the fact that 3rd person has the largest BW can also be realized by looking at the spectrograms.
- 2nd person has the largest offset value, which can be deduced that the forward and backward limb motions are more asymmetric than other persons' limb motions while crawling.

- 2nd person has the largest bandwidth without micro Doppler value, which can be concluded that this person has the largest bobbing motion of torso while crawling.
- 3rd person has the largest standard deviation value, which means that dynamic range of the motion is bigger than others'; in other words, the signal strength bar consists of larger range of numbers.
- 3rd person has the largest period values, which means that the swing rate of limbs is smaller than others', which means that this person's arm movements are slowly.

Table 4.25 Micro Doppler features of 1st person's, 2nd person's and 3rd person's crawling

Crawling	Characteristics of 3 Persons' Crawling					
	Torso Frequency (Hz)	BW (Hz)	Offset (Hz)	BW w/o Micro Doppler (Hz)	STD	Period (sec)
Average Values for 1st Person	74,6716	308,3693	70,9512	84,6598	6,9750	0,9202
Average Values for 2nd Person	75,2033	308,6135	107,8798	118,2977	7,1950	0,4535
Average Values for 3rd Person	77,2306	396,9981	96,3297	77,1949	7,2767	0,9830

When extracted features of crawling spectrograms of the targets are taken into consideration, it is seen that each person has distinctive crawling features, in other words each person has signatures of crawling and identification of crawling person could be done by looking at the crawling spectrograms. On the other hand, the extracted values of 3 persons' crawling are close to each other. It means that it is possible to group these values to obtain the features of crawling. By using the values at Table 4.25, the average values of 3 persons' crawling features are calculated as torso frequency of 75,7019 Hz; bandwidth of 337,9936 Hz; offset of 91,7203 Hz; bandwidth without micro Doppler of 93,3842 Hz; standard deviation of 7,1489 and period of 0,7856 sec. These average values are used as the extracted features of human crawling.

4.3.4 Creeping

The experiment is repeated for creeping. The same set targets are utilized. The results for each target are given in Figure 4.41 and Figure 4.42 for 1st person; Figure 4.43 and Figure 4.44 for 2nd person; Figure 4.45 and Figure 4.46 for 3rd person. Feature extraction results of 1st person, 2nd person and 3rd person are given in Table 4.26, Table 4.27, and Table 4.28, respectively.

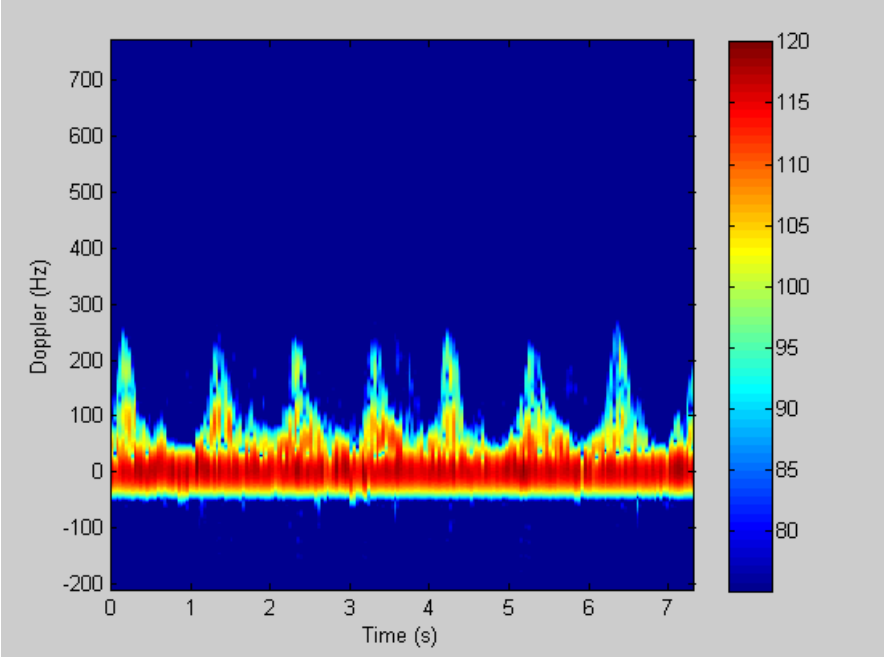

Figure 4.41 Spectrogram of 1st person's creeping before clutter suppression

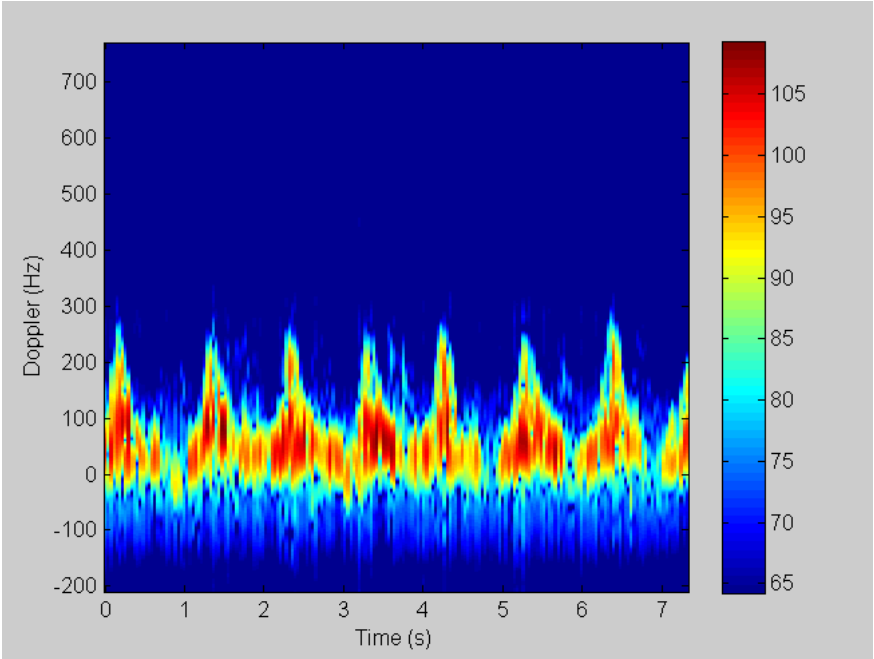

Figure 4.42 Spectrogram of 1st person's creeping after clutter suppression

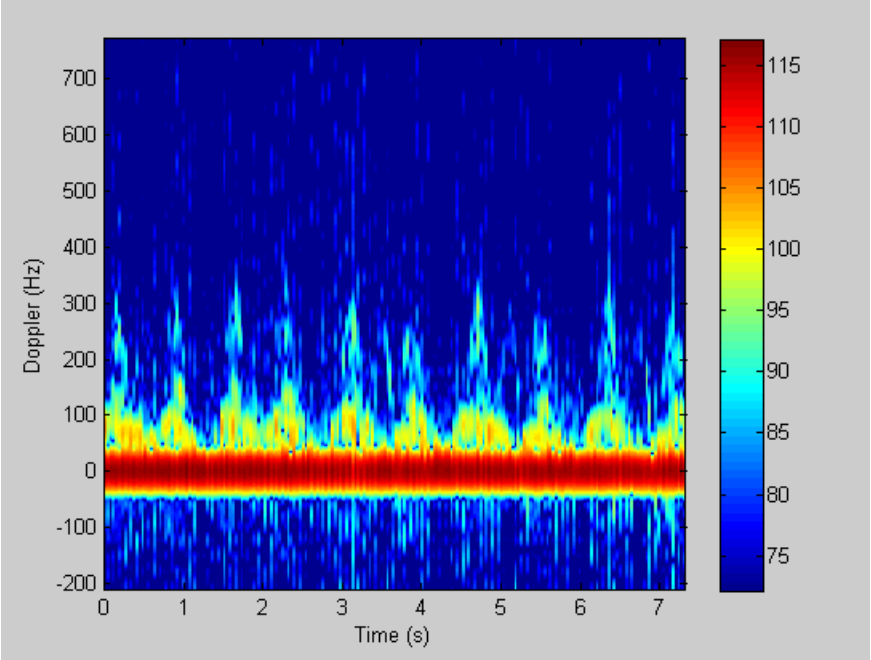

Figure 4.43 Spectrogram of 2nd person's creeping before clutter suppression

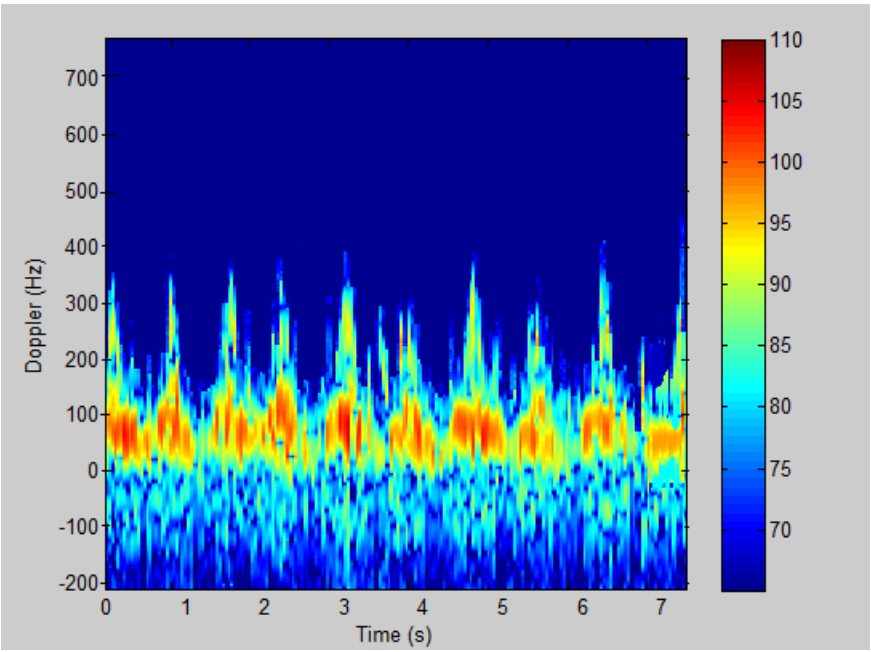

Figure 4.44 Spectrogram of 2nd person's creeping after clutter suppression

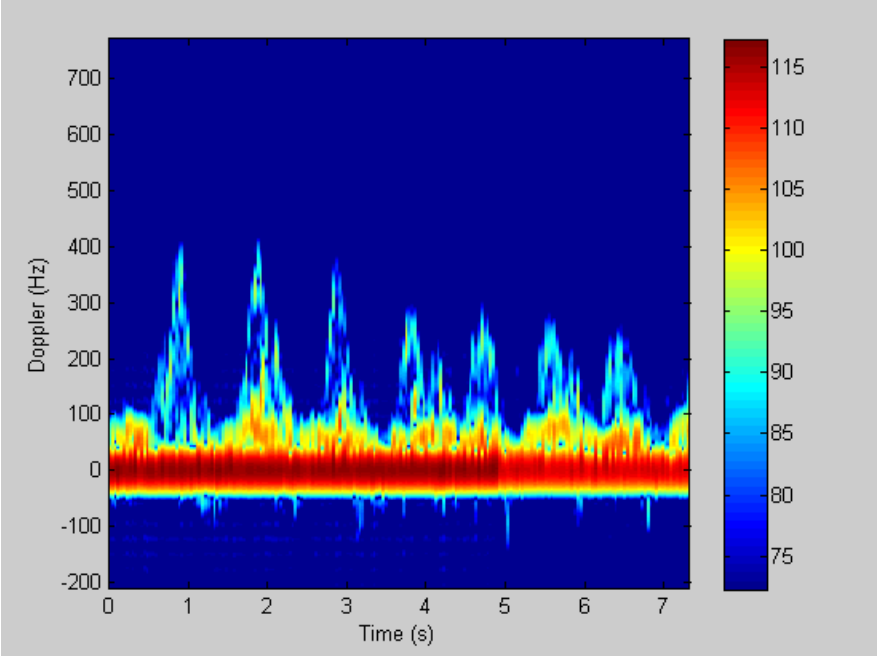

Figure 4.45 Spectrogram of 3rd person's creeping before clutter suppression

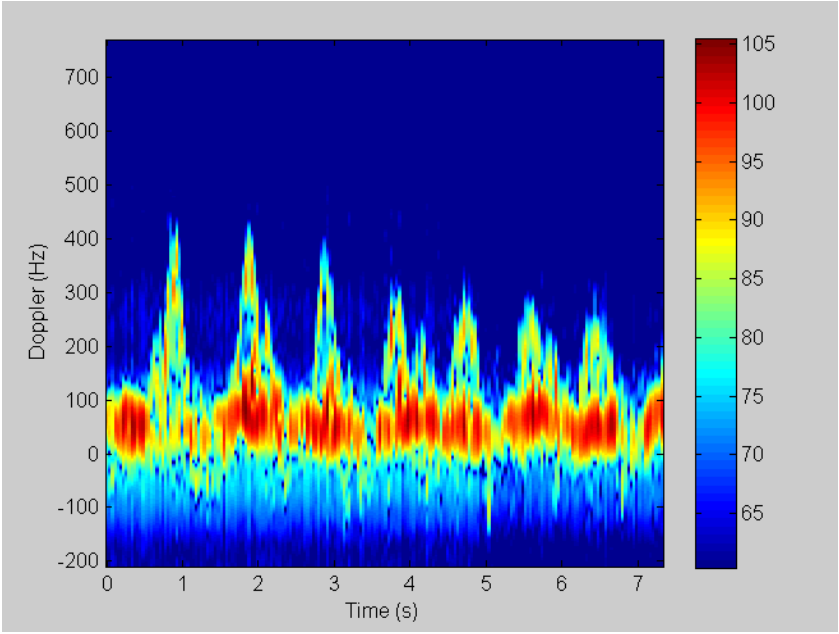

Figure 4.46 Spectrogram of 3rd person's creeping after clutter suppression

Table 4.26 Extracted micro Doppler features of 1st person's creeping

1st Person's Creeping	Extracted Classification Features					
	Torso Frequency (Hz)	BW (Hz)	Offset (Hz)	BW w/o Micro Doppler (Hz)	STD	Period (sec)
Sample-1	67,6129	283,7096	49,9376	75,9091	6,7051	0,8986
Sample-2	68,6207	277,7277	54,6077	51,2728	6,6089	0,8672
Sample-3	70,6341	324,7278	60,2456	71,7819	7,0318	0,8777
Sample-4	69,5540	294,8187	57,2696	72,6414	7,0258	0,9665
Sample-5	65,3213	340,9642	58,9894	44,9273	7,1972	1,0135
Sample-6	75,9490	260,6368	50,6853	60,6752	6,5627	0,9351
Sample-7	66,6143	272,6005	55,6844	41,6364	7,3175	0,8881

Table 4.27 Extracted micro Doppler features of 2nd person's creeping

2nd Person's Creeping	Extracted Classification Features					
	Torso Frequency (Hz)	BW (Hz)	Offset (Hz)	BW w/o Micro Doppler (Hz)	STD	Period (sec)
Sample-1	80,2557	308,4914	98,4523	105,1093	7,1173	0,6483
Sample-2	79,5086	316,1823	99,8773	101,6911	5,7802	0,5041
Sample-3	86,3680	338,4006	92,9768	111,9456	6,5426	0,4989
Sample-4	56,4886	352,9279	97,3585	82,891	7,1851	0,6912
Sample-5	55,9299	329,8551	102,473	117,9275	7,3003	0,4535
Sample-6	65,1513	323,0187	91,9022	70,0728	6,804	0,5429
Sample-7	74,8722	345,2369	94,1668	83,7456	6,4036	0,5067

Table 4.28 Extracted micro Doppler features of 3rd person's creeping

3rd Person's Creeping	Extracted Classification Features					
	Torso Frequency (Hz)	BW (Hz)	Offset (Hz)	BW w/o Micro Doppler (Hz)	STD	Period (sec)
Sample-1	67,6292	336,6915	86,8946	61,5274	6,873	1,0483
Sample-2	65,3342	421,2916	79,7869	72,163	7,3855	0,9362
Sample-3	72,4780	417,8734	77,3386	84,982	7,6252	1,0605
Sample-4	76,0247	528,11	95,8332	80,5636	7,6743	1,0971
Sample-5	71,7115	489,6554	88,1508	61,5274	7,19	0,9947
Sample-6	95,0350	464,8735	71,7777	51,3637	7,2643	1,3409
Sample-7	84,9409	561,4373	87,7598	58,6182	7,5108	1,2433

When the spectrograms crawling and creeping before and after suppression clutter are examined, it is seen that high pass filter distorts the spectrograms of these motions more than spectrograms of walking and running; it makes sense because creeping is a much slower motion than others and the clutter is much more induced to the creeping spectrograms than others; therefore, the high pass filter which is designed to suppress the clutter causes some distortions on the spectrograms of creeping. On the other hand, micro Doppler features can be extracted despite these distortions.

Table 4.29 Micro Doppler features of 1st person's, 2nd person's and 3rd person's creeping

Creeping	Characteristics of 3 Persons' Creeping					
	Torso Frequency (Hz)	BW (Hz)	Offset (Hz)	BW w/o Micro Doppler (Hz)	STD	Period (sec)
Average Values for 1st Person	69,1866	293,5979	55,3457	59,8349	6,9213	0,9210
Average Values for 2nd Person	71,2249	330,5876	96,7438	96,1976	6,7333	0,5494
Average Values for 3rd Person	76,1648	459,9904	83,9345	67,2493	7,3604	1,1030

In order to analyze whether every person has different creeping characteristics and can be distinguished by using micro Doppler features, extracted feature values of 1st person's, 2nd person's and 3rd person's creeping spectrograms are listed at Table 4.29. The followings can be extracted from Table 4.29:

- 3rd person has the largest torso frequency, which means that this person has the largest speed of crawling.
- 3rd person has the largest BW value, which can be explained that this person has the highest velocity of limb motions of creeping; the fact that 3rd person has the largest BW can also be realized by looking at the spectrograms.

- 2nd person has the largest offset value, which can be deduced that the forward and backward limb motions are more asymmetric than other persons' limb motions while creeping.
- 2nd person has the largest bandwidth without micro Doppler value, which can be concluded that this person has the largest bobbing motion of torso while creeping.
- 3rd person has the largest standard deviation value, which means that dynamic range of the motion is bigger than others'; in other words, the signal strength bar consists of larger range of numbers.
- 3rd person has the largest period values, which means that the swing rate of limbs is smaller than others', which means that this person's arm movements are slowly.

When extracted features of creeping spectrograms of the targets are taken into consideration, it is seen that each person has distinctive creeping features, in other words each person has signatures of creeping and identification of creeping person could be done by looking at the creeping spectrograms. On the other hand, the extracted values of 3 persons' creeping are close to each other. It means that it is possible to group these values to obtain the features of creeping. By using the values at Table 4.29, the average values of 3 persons' creeping features are calculated as torso frequency of 72,1921 Hz; bandwidth of 361,3919 Hz; offset of 78,6747 Hz; bandwidth without micro Doppler of 74,4273 Hz; standard deviation of 7,0050 and period of 0,8578 sec. These average values are used as the extracted features of human.

4.4 Analysis of Different Types of Human Motions

After the spectrograms and extracted micro Doppler features of human motions like walking, running, crawling, creeping are analyzed, the comparison of the spectrograms and the extracted features is required to comprehend whether different motions could be distinguished or not. First of all, in order to make the examination of the spectrograms of different motions easy for comparison, one of the spectrograms of each motions are given in Figure 4.47.

It is seen from Figure 4.47 that the spectrograms of human motions such as walking, running, crawling and creeping have different motion characteristics. The Doppler signatures provide distinguishing the type of motions by only looking at them. It is known that the torso produces the strongest return in each spectrogram, while arm and leg movements surround the torso with the periodic micro-Doppler modulations. Walking and running spectrograms are discriminated from crawling and creeping spectrograms at first look because of several reasons. First of all, torso frequency of crawling and creeping signatures are positioned around 0 Hz. Secondly, due to the fact that there is no back swing in these motions, negative Doppler signatures do not occur; therefore, micro Dopplers skew towards the positive with respect to the torso frequency. Thirdly, these motions have narrower Doppler signal spread. Lastly, the period of these motions are longer. With the help of these deductions, crawling and creeping signatures are discriminated from others. Even crawling and creeping are very close to each other, they can also be distinguished. In crawling, there are two consecutive positive modulations for each micro Doppler peak; on the other hand, there is only one positive modulation for each micro Doppler peak in creeping. This can be explained with the difference of arm and knee motions. In crawling, there are two consecutive positive modulations for each peak in the spectrogram; however, in creeping, the arm movements are dominant motions, which produce only one positive modulations for each peak.

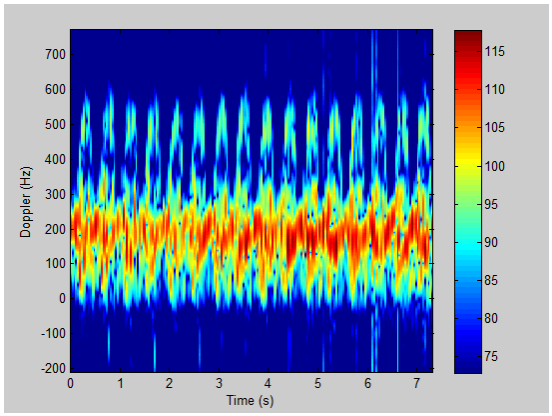

(a) Walking with 0°

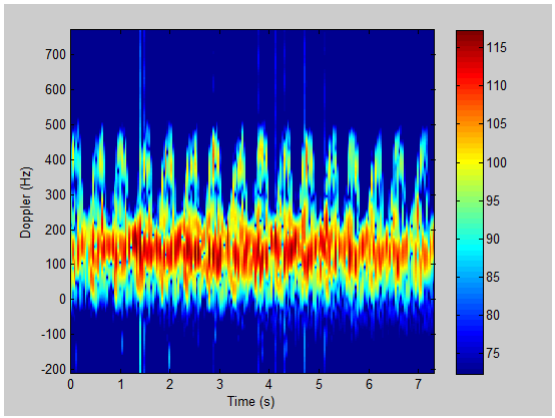

(b) Walking with 30°

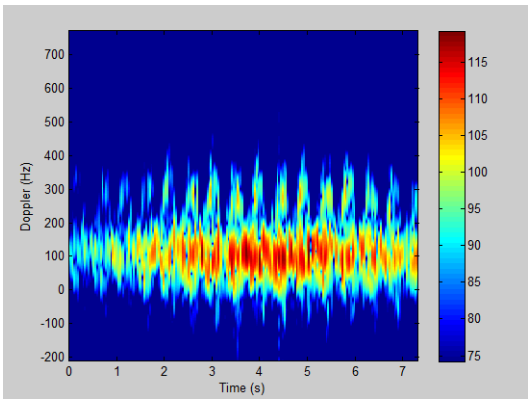

(c) Walking with 60°

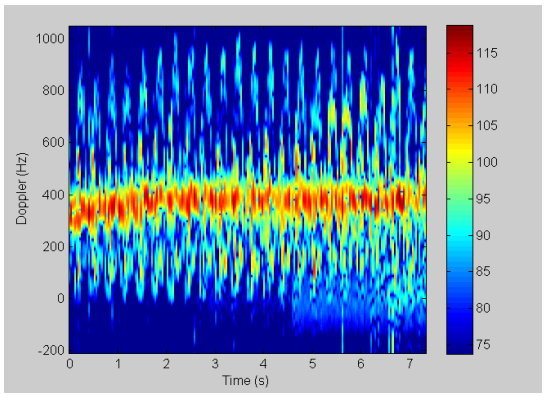

(d) Running

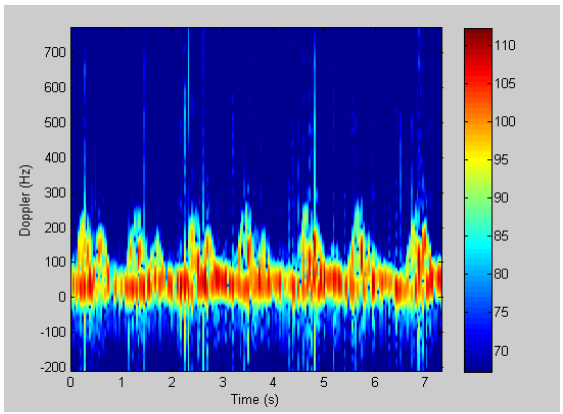

(e) Crawling

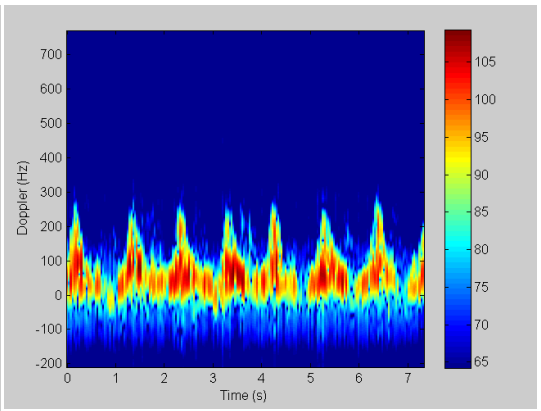

(f) Creeping

Figure 4.47 Spectrogram of different types of human motions

Walking and running signatures can be discriminated from the spectrograms by using the following method. Firstly, torso frequency of running is positioned around 400 Hz, which is higher than the frequency of walking. Secondly, running has a wider Doppler spread compared to walking. Lastly, the period of running is shorter than walking period. These three features are sufficient to discriminate running from walking. In addition, the discrimination methods of walking for three different azimuth angles is given are Chapter 4.3.1.4.

In order to compare different types of human motions quantitively, average values for walking with azimuth angles of 0°, 30°, 60°, running, crawling and creeping are presented at Table 4.30.

Table 4.30 Average values of the spectrograms of different human motions

	Comparison of Different Human Motions					
	Torso Frequency (Hz)	BW (Hz)	Offset (Hz)	BW w/o Micro Doppler (Hz)	STD	Period (sec)
Running	418,7199	918,3357	437,8455	254,4478	7,8280	0,2597
Walking with 0°	196,5631	544,7126	203,2019	210,7656	7,6019	0,4765
Walking with 30°	152,1915	492,5445	168,0948	183,6850	7,4290	0,4594
Walking with 60°	88,0882	282,0005	79,5601	162,2197	7,1688	0,4403
Crawling	75,7019	337,9936	91,7203	93,3842	7,1489	0,7856
Creeping	72,1921	361,3919	78,6747	74,4273	7,0050	0,8578

The numerical results of extracted features of different human motions are consistent with the spectrograms. Among all motions running has the largest torso frequency of 418.7 Hz; which makes sense because torso frequency depends on the human speed and it is obvious that human speed is the highest for running. Torso frequency values of walking 196.5 Hz, 152.2 Hz and 88 Hz are lower than running, higher than crawling and creeping values as expected; because the human speed is lower than running, but higher than crawling and creeping. When the torso frequency values of crawling and creeping are compared, it is seen that these values are close to each other; which means that average human speed is similar for crawling and creeping. The torso frequency of crawling is slightly higher than creeping as expected.

Among all motions, running has the largest bandwidth value of 918,3357 Hz; which makes sense because bandwidth depends on the limbs speed and it is obvious that limbs speed is the highest for running. Bandwidth values of walking 544,7126 Hz, 492.5445 Hz and 282.0005 Hz are lower than running; because limbs speed is lower than running. The bandwidth value for walking with azimuth angle of 60° is narrower than bandwidth values of crawling and creeping. In fact, the expectation is opposite because walking must have wider bandwidth than crawling and creeping; however, when the spectrograms of walking with azimuth angle of 60° are examined, it is seen that these spectograms are blurred. Therefore, because of the unclear spectrograms of walking with 60°, the feature extraction from these spectrograms might have some deviations. Moreover, when the bandwidth value of crawling of 337.9936 Hz and the bandwidth value of creeping of 361.3919 Hz are compared, it is seen that creeping bandwidth value is higher than crawling value; while the opposite is expected. Different creeping styles of human subjects can cause this result; such as 3rd persons' creeping spectrograms have very high bandwidths.

It is known that if the motion is symmetric, the offset value converges to the torso frequency. Because walking is more symmetric motion than others, the offset value of walking of 203 Hz is very close to torso frequency of 196,2088 Hz. It is seen that crawling is more asymmetric motion than others, there is approximately

20 Hz of difference between the offset value of crawling of 91,7203 Hz and the torso frequency of 72,0466 Hz. It is also realized the offset values of walking with azimuth angle of 60° of 79,5601 Hz are smaller than the torso frequency of 89,0402 Hz; the unclear spectrograms of walking with 60°, the feature extraction from these spectrograms might cause these deviations. In the light of these explanations, it is seen that running has the largest offset value of 437,8455 Hz. After running, walking offset values are higher than others, except the walking with 60° because of the deviations of features from blurred spectrograms. Lastly, it is seen that crawling offset is bigger than creeping value. Actually, creeping is an asymmetric motion and it is expected that the offset value is much different than 5.4 Hz; however, it can be said that different creeping styles of human subjects may cause this result.

Among all motions, running has the largest value of bandwidth without micro Doppler 254,4478 Hz; which makes sense because this feature depends on the bobbing motion of the human and it is obvious that bobbing motion is the highest for running. Bandwidth without micro Doppler values of walking of 210,7656 Hz, 183.6850 Hz and 162.2197 Hz are lower than running, higher than crawling and creeping values, as expected; the bobbing motion is smaller than running but larger than crawling and creeping. The bandwidth without micro Doppler value is 93,3842 Hz for crawling. Among all motions, creeping has the smallest bandwidth without micro Doppler value of 74,4273 Hz; which makes sense as bobbing motion is very small for the creeping. When the bandwidth without micro Doppler values are taken into account, it is seen that these values are disjoint; which means that bandwidth without micro Doppler values is one of the efficient discriminative features.

Among all motions, running has the largest standard deviation of 7.828; which makes sense because the standard deviation depends on the dynamic range of the motion and it is obvious that dynamic range has the highest value for running; in other words, the signal strength bar of running consists of largest range of numbers. Standard deviation values of walking of 7.6019, 7.4290 and 7.1688 are lower than running, and higher than crawling and creeping values as expected; because the dynamic range is lower than running but higher than crawling and creeping. The

standard deviation value is 7,1489 for crawling. Among all motions, creeping has the smallest standard deviation value of 7.0050; which can be seen from the spectrograms that creeping has the smallest dynamic range, in other words the smallest range numbers for signal strength. When the standard deviation values are taken into account, it is seen that the standard deviation values are very close to each other; which means that standard deviation is not a very discriminative feature.

Among all motions, creeping has the longest period of 0,8578 sec; which makes sense because period depends on the swing rate of human limbs and it is obvious that human subject has the smallest swing rate for creeping. The swing rate for crawling is higher than creeping, which makes the period of the crawling as 0.7856 sec, which is shorter than creeping period. Period values of walking of 0.4765 sec, 0.4594 sec and 0.4403 sec are shorter than crawling but longer than running as expected; the limbs walking swing rate is higher than crawling but smaller than running. Running has the shortest period value of 0.2597 sec, which makes sense because the swing rate is very high for running. Although there is a logic between the period values; the feature of period is not a very efficient feature for classification of motions. One reason for this fact is that while searching the peaks from the complex spectrograms, there can be errors on the calculation of the peak numbers. In addition, the period values are very close to each other; which means that period is not a very discriminative feature.

When Table 4.30 is examined, it can be deduced that torso frequency is very distinctive feature. For the symmetric motions, offset values are close to torso frequency values; therefore, they can be also assumed as distinguishing. The bandwidth and bandwidth without micro Doppler features are very separated and they can be used as distinguishing features. On the other hand, standard deviation and period values are too close to each other for different motion types.

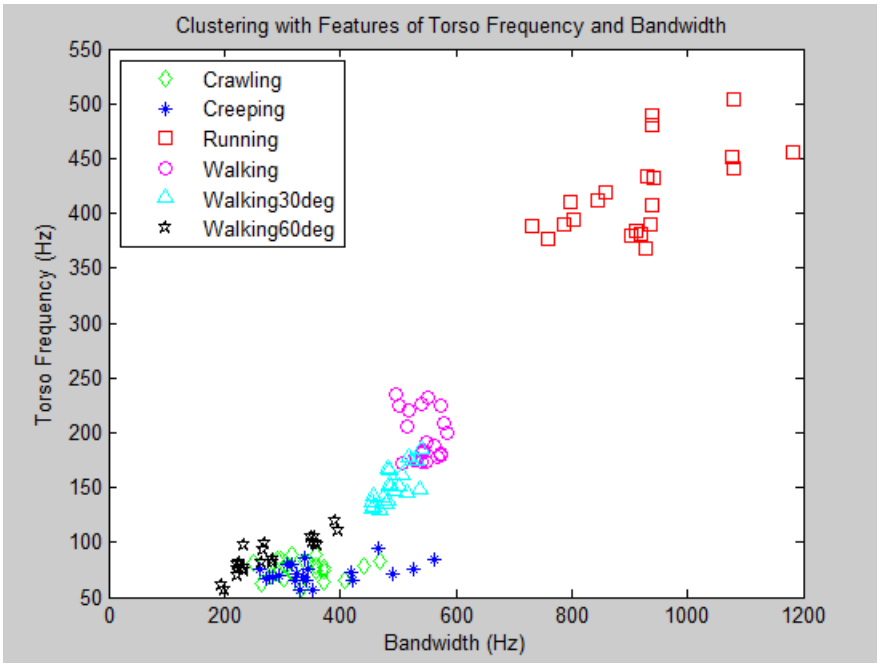

Figure 4.48 Clustering with micro Doppler features of torso frequency and BW

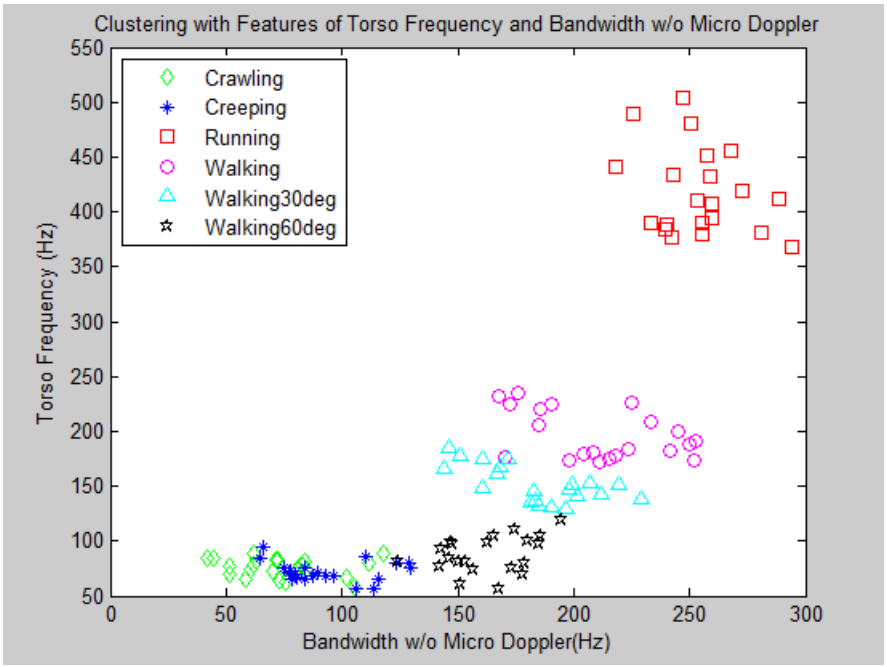

Figure 4.49 Clustering with micro Doppler features of torso frequency and BW w/o Micro Doppler

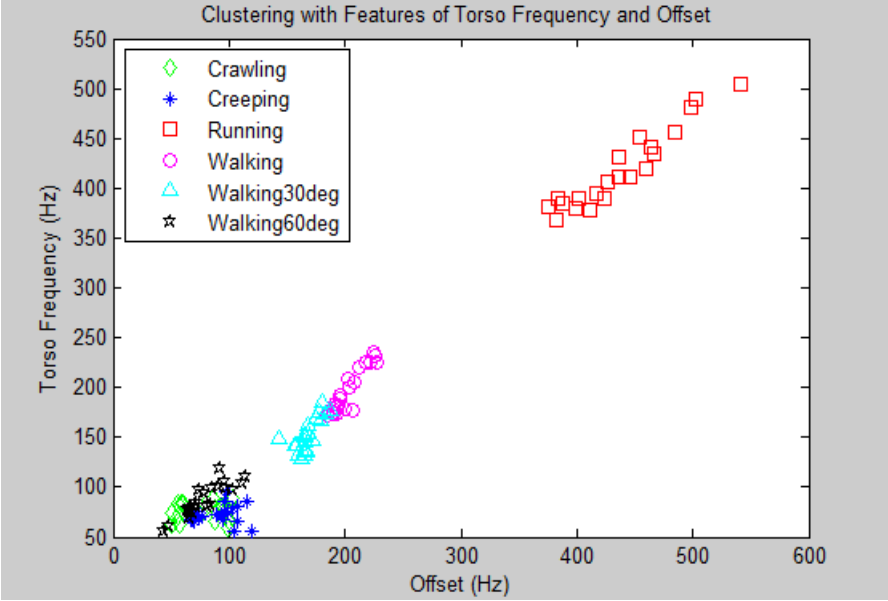

Figure 4.50 Clustering with micro Doppler features of torso frequency and offset

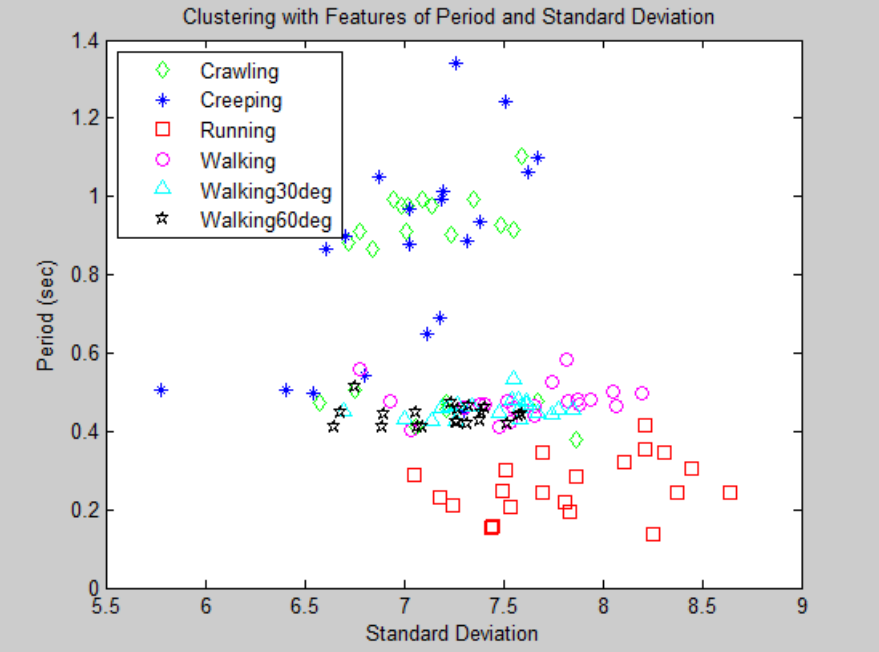

Figure 4.51 Clustering with micro Doppler features of period and standard deviation

In order to visualize the efficiency of extracted features, the experimental data for a pair of features is plotted. First, it is decided that torso frequency is the most efficient feature; because the separation is more precise for torso frequency, except crawling and creeping; however, the crawling and creeping results are too close for every features, not only for torso frequency. To examine the efficiency of bandwidth, the clustering figure with torso frequency and bandwidth is generated as can be seen in Figure 4.48. Bandwidth without micro Doppler affects are demonstrated at clustering figure with torso frequency and bandwidth without micro Doppler in Figure 4.49. For the efficiency of offset, clustering with torso frequency and offset is given in Figure 4.50. Lastly, the clustering figure with standard deviation and period is presented in Figure 4.51. When these figures are examined, several observations can be made:

- The crawling and creeping values are mostly the same for every features. Walking with 60° features may not be reliable because of the blurred spectrograms and it may have similar values with creeping and crawling. Therefore, the discrimination of these motions cannot be done with these features.
- The effectiveness of torso frequency is obvious from the first three graphs; because running, walking with 0° and 30° can be separated easily with the help of their torso frequencies; in short, the most discriminative feature is torso frequency.
- It seems that the offset value is second efficient feature for classification.
- The bandwidth value can be considered at the third place; because three classes mixed too much for this feature.
- Bandwidth width without micro Doppler has the fourth place in the list of classification performance of features.
- Period is the feature at the fifth place; at least running, group of walking and pair of crawling and creeping can be discriminated.
- The least effective feature seems standard deviation; whose values are similar for nearly all classes.

4.5 Classification of Human Motions

It is seen from Table 4.30 Average values of the spectrograms of different human motions and clustering figures of Figure 4.48, Figure 4.49, Figure 4.50 and Figure 4.51 that classification performance for each class differs. First of all, running can be discriminated from other motions easily; because running features are more distinctive than others. Second, walking can also be separated from others; however, for some data, results of walking with 0° and 30° interfere partially. Third, walking with 60° cannot be discriminated from crawling and creeping results. Moreover, results of walking with 60° are similar to 30° for some data. Lastly, crawling and creeping results are almost the same each other; and cannot be discriminated.

In order to examine these results by using a classification tool, neural network is trained. First, although it is known that there are not sufficient amount of data to train the neural network effectively; this tool is used to obtain a general opinion with the hope that it can be a basic for future work. Three of each person's results for each motion are defined as the training data; in other words, training data set consists of 54 data, which comprises 3 data for 6 motion types from 3 persons. Neural network is constituted according to this training data set. Four of each person's results for each motion are defined as the test data; in other words, for each motion 12 data, which consists of 4 data for each person is used as test data. Firstly, 12 running test data are entered to the neural network. The output of the neural network is obtained that 11 of them are running, 1 of them is walking; they can be expressed in percentage as 91.67% of running, 8.33% of walking. Then, 12 walking with 0° test data are used. The outputs are like that 10 of them are walking with 0°, and 2 of them are walking with 30°; the percentages of output are 83.33% of walking with 0°, 16.67% of 30°. After that, 12 walking with 30° test data are entered to the neural network. The results show that 9 of them are walking with 30°, 3 of them are walking with 0°, and can be expressed in percentage as 75% of walking with 30°, 25% of 0°. In addition, 12 walking with 60° test data are entered to the neural network. The output of the neural network gives that 7 of them are

walking with 60°, 1 of them is walking with 30°, 2 of them are crawling, 2 of them are creeping; which means that in percentages of 58.33% of walking with 60°, 8.33% of walking with 30°, 16.67% of crawling and 16.67% of creeping. Moreover, 12 crawling test data are used. The outputs are 6 of them are crawling, 6 of them are creeping; which means that 50% of crawling and 50% of creeping. The result is vice versa for creeping is that for 12 creeping test data; which is 50% of creeping and 50% of crawling. These results are given at Table 4.31 that Act represents the actual motion type and Est represents the estimation of the neural network.

Table 4.31 The percentage of neural network classification results for each motion

Est\Act	Running	Walking with 0°	Walking with 30°	Walking with 60°	Crawling	Creeping
Running	91.67	0	0	0	0	0
Walking with 0°	8.33	83.33	25.00	0	0	0
Walking with 30°	0	16.67	75.00	8.33	0	0
Walking with 60°	0	0	0	58.33	0	0
Crawling	0	0	0	16.67	50.00	50.00
Creeping	0	0	0	16.67	50.00	50.00

The results of Table 4.31 agree with the comments in section 4.5. First, running can be classified with the highest performance. Second, classification of walking with 0° and 30° is sufficient enough. Third, because of the angular effects, walking cannot be distinguished effectively for 60°. Lastly, crawling and creeping could not be discriminated from each other with these features. In brief, running, walking classes are discriminated from crawling and creeping classes by using neural network; however, crawling and creeping results are hard to distinguish from extracted features of micro Doppler.

It should be emphasized that classification by using classifiers is not one of the main objects of this thesis. In this thesis, the features from micro Doppler signatures are extracted and it is demonstrated that the human motions can be distinguishable. Classification is only made to get an idea about the possibility of discriminating human motions by a classifier. By using the neural network toolbox of MATLAB, neural network classifier is applied to the extracted features to obtain an example performance. The real classification performance by using classifiers should be studied in more detailed.

CHAPTER 5

CONCLUSION

The classification of human motions from micro Doppler features is examined in this thesis. The followings are the conclusions drived from the study:

- The human walking simulator by V. Chen is examined and it is deduced that this simulator is consistent with experimental human walking data.
- The time-frequency transformations to obtain spectrograms of human walking are examined and applied to the human walking simulator. It is seen that STFT is a more appropriate time-frequency distribution for human walking than WVD. (The cross-terms of difficulties in the processing of multicomponent human walking data.)
- The effects of target range and the pulse compression codes are analyzed. It is seen that when the distance of the target person changes from 150 meters to 1000 meters and the pulse compression codes are changed, the extracted features give very similar results, there occur differences only on SNR values on the spectrograms.
- The effects of azimuth angles on human walking spectrogram are analyzed by considering the experimental data of human walking with azimuth angles of 0°, 30° and 60°. It is deduced that when azimuth angle is approaching to 90°, the micro Doppler effects are hard to discriminate from the spectrograms.
- The feature extraction methods are examined and one of these methods is selected and applied to the spectrograms. According to the chosen feature extraction method, six features, which are torso frequency, BW of the signal, offset of the signal, BW without micro Dopplers, standard

deviation of the signal strength, period of the arms or legs, are extracted from the spectrograms. These features are extracted from the human motions of walking, running, crawling and creeping to comprehend the possibility of discriminating these motions. Although each person has different feature values, in other words, distinctive signatures for each motion, these values can be grouped to obtain the general features of the motions. Each feature has different efficiency of classifying human motions. When the efficiency of features are ordered, the most discriminative feature is torso frequency, the offset value seems that it is the second efficient feature for classification, the bandwidth value can be considered at the third place, bandwidth width without micro Doppler has the fourth place of the list of classification performance of features, period is the feature at the fifth place, the least effective feature seems standard deviation.

- Neural network is constituted by using the extracted features from the different human motions. When neural network results are examined, it is seen that probability of successful classification for different motions and different walking azimuth angles are different. If these probabilities for different human motions are ordered, it is seen that running can be classified with the highest performance by using neural network. Secondly, successful classification probability of walking with 0° has the second place of the list of classification. Thirdly, probability of walking with 30° is sufficient enough. Fourthly, walking with 60° cannot be distinguished effectively because the angular effects decrease the clearness of the micro Dopplers. Lastly, crawling and creeping could not be discriminated from each other by using neural network. In brief, running, walking classes are discriminated from crawling and creeping classes by using neural network successfully; however, crawling and creeping results are hard to distinguish from extracted features of micro Doppler.

Future work may be considered as the collection of more experimental data to increase the efficiency of neural network classification. Each person has specific micro Doppler signatures for each motion; therefore, collecting experimental data from more human subjects will increase the efficiency of motion classification and may even lead to identification of physical attributes of the target. In addition, micro Doppler effects for azimuth angles of 0°, 30° and 60° are investigated; however, data for different azimuth angles such as 120°, 150° also should be collected to get the idea of changing the micro Doppler signatures for all angles. Moreover, extracting different features like stride length from the spectrograms will be beneficial, because these features can provide human characteristics like human length. Furthermore, acquiring data from women will be useful to expand the micro Doppler signatures database and increase the diversity of the features.

REFERENCES

[1] Chen V. C., The Micro Doppler Effect in Radar, Artech House, 2011.

[2] Cohen L., Time-Frequency Analysis, Prentice Hall, 1995.

[3] Chen V. C., Ling H., Time-Frequency Transforms For Radar Imaging and Signal Analysis, Artech House, 2002.

[4] Cai C., Liu W., Fu J.S., Lu Y., "Radar Micro-Doppler Signature Analysis with HHT," *IEEE,* pp. 929-938, 2010.

[5] Orovic I., Stankovic S., Amin M., "A new approach for classification of human gait based on time-frequency feature representation," *Signal Processing,* vol. 91, pp. 1448-1456, 2011.

[6] Setlur P., Amin M., Ahmad F., "Urban Target Classifications Using Time-Frequency Micro-Doppler Signatures," *ISSPA,* pp. 1-4, 2007.

[7] Youngwook K., Hao L., "Human Activity Classification Based on Micro-Doppler Signatures Using an Artificial Neural Network," *IEEE,* pp. 1-4, 2008.

[8] Kim Y., Ling H., "Human Activity Classification Based on Micro-Doppler Signatures Using a SVM," *IEEE,* vol. 47, pp. 1328-1337, 2009.

[9] Tahmoush D., Silvious J., "Radar Micro-Doppler for Long Range Front-View Gait Recognition," *IEEE,* pp. 1-6, 2009.

[10] Otero M., "Application of a continuous wave radar for human gait recognition," *SPIE,* vol. 5809, pp. 538-548, 2005.

[11] Ram S. S., Ling H., "Simulation of human microDopplers using computer animation data," *IEEE,* pp. 1-6, 2008.

[12] Tahmoush D., Silvius J., "Angle, elevation, PRF, and illumination in Radar MicroDoppler for Security Applications," 2009.

[13] Van Drop P., Groen F. C. A., "Feature-Based Human Motion Parameter Estimation with Radar," *IET,* vol. 2, pp. 135-145, 2008.

[14] Tahmoush D., Silvious J., “Modeled Gait Variations in Human Micro-Doppler,” *IRS*, pp. 1-4, 2010.

[15] Tahmoush D., Silvious J., «Radar MicroDoppler for Security Applications: Modeling Men versus Women,» 2009.

[16] Tan R., Bender R., “Analysis of Doppler measurements of people,” *SPIE*, vol. 6239, 2006.

[17] Lei J., “Pattern Recognition Based on Time-Frequency Distributions of Radar Micro-Doppler Dynamics,” *SNPD/SAWN*, pp. 14-18, 2005.

[18] Chen V. C., “Analysis of Radar Micro-Doppler Signature With Time-Frequency Transform,” *IEEE*, pp. 463-466, 2000.

[19] Vignaud L., Ghaleb A., Kernee J. L., “Radar high resolution range & micro-doppler analysis of human motions,” *International Radar Conference*, pp. 1-6, 2009.

[20] Gürbüz S. Z., Melvin W. L., Williams D. B., “Detection and Identification of Human Targets in Radar Data,” *SPIE*, vol. 6567, 2013.

[21] Yang Y., Lei J., Zhang W., Lu C., “Target Classification and Pattern Recognition Using Micro-Doppler Radar Signatures,” *SNPD*, pp. 213-217, 2006.

[22] Lei J., Lu C, “Target Classification Based on Micro-Doppler Signatures,” *IEEE*, pp. 179-183, 2005.

[23] Cai C., Liu W., Fu W. L., Lu L., “Empirical Mode Decomposition of Micro-Doppler Signature,” *IEEE*, pp. 895-899, 2005.

[24] Greneker G., Geishmer J., Asbell D., “Extraction of micro-Doppler from vehicle targets at X-band frequnecies,” *SPIE*, vol. 4374, pp. 1-9, 2001.

[25] Nanzer J. A., Rogers R. L., “Bayesian Classification of Humans and Vehicles Using Micro-Doppler Signals From a Scanning-Beam Radar,” *IEEE*, vol. 19, pp. 338-340, 2009.

[26] Li J., Phung S. L., Tivive F. H. C. and Bouzerdoum A., “Automatic Classification of Human Motions using Doppler Radar,” *IJCNN*, pp. 1-6, 2012.

[27] Smith G. E., Woodbridge K., Baker C. J., "Micro-Doppler Signature Classification," *CIE,* pp. 1-4, 2006.

[28] Smith G. E., Woodbridge K., Baker C. J., "Multiperspective Micro-Doppler Signature Classification," *IET,* pp. 1-5, 2007.

[29] Skolnik I. M., Introduction to Radar Systems, Mc Graw Hill, 2001.

[30] Richards M. A., Fundamentals of Radar Signal Processing, Mc Graw Hill, 2005.

[31] Stearns S. D., Digital Signal Processing with Examples in Matlab, CRC Press, 2003.

[32] Bishop C. M., Neural Networks for Pattern Recognition, Clarendon Press, 1995.

APPENDIX A

SPECTROGRAMS WITH DIFFERENT PULSE WIDTHS OF RADAR

A.1 Spectrograms of Human Walking with PW1

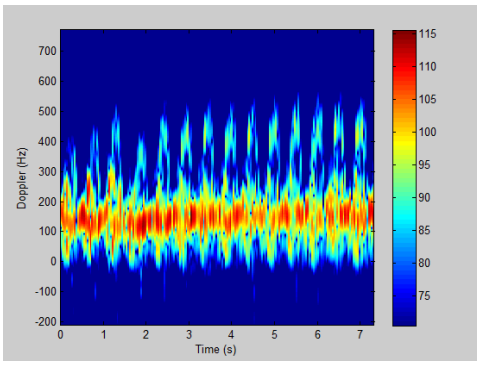

a) 1st Spectrogram of walking with PW1

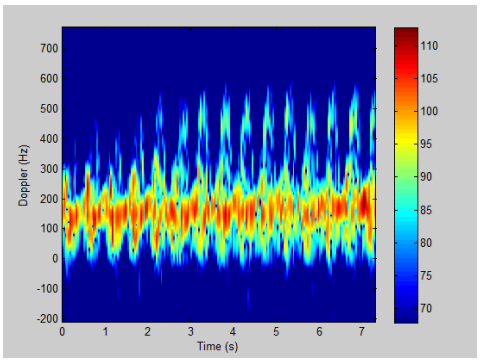

b) 2nd Spectrogram of walking with PW1

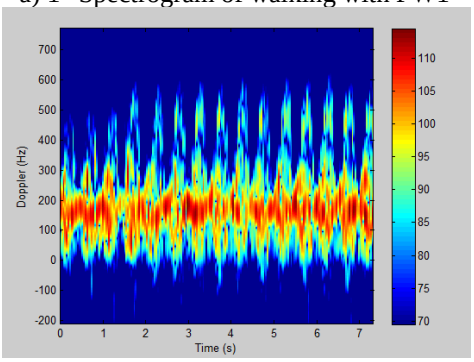

c) 3rd Spectrogram of walking with PW1

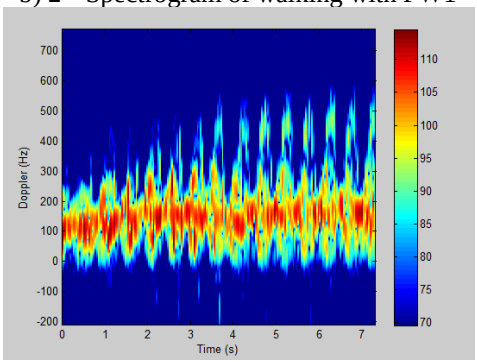

d) 4th Spectrogram of walking with PW1

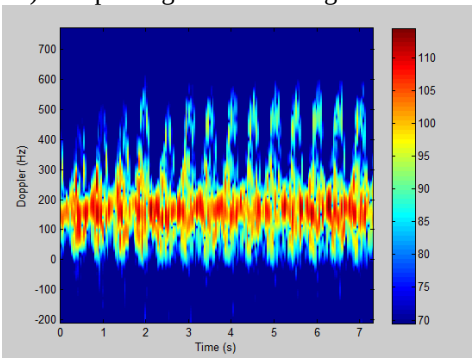

e) 5th Spectrogram of walking with PW1

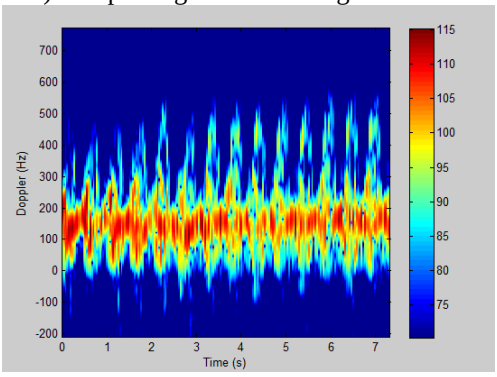

f) 6th Spectrogram of walking with PW1

Figure A.1 Spectrograms of human walking with PW1

A.2 Spectrograms of Human Walking with PW2

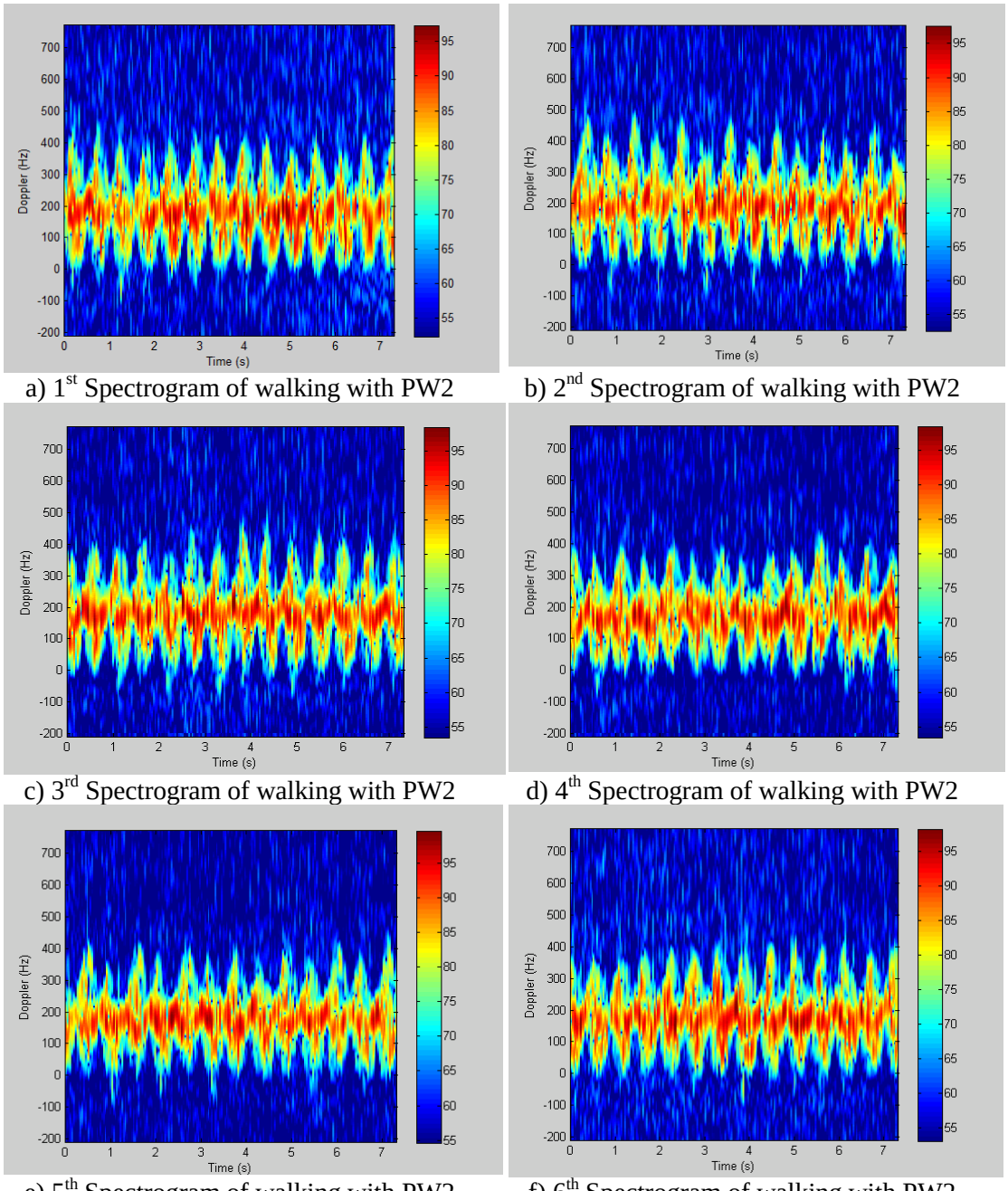

a) 1st Spectrogram of walking with PW2

b) 2nd Spectrogram of walking with PW2

c) 3rd Spectrogram of walking with PW2

d) 4th Spectrogram of walking with PW2

e) 5th Spectrogram of walking with PW2

f) 6th Spectrogram of walking with PW2

Figure A.2 Spectrograms of human walking with PW2

APPENDIX B

SPECTROGRAMS OF DIFFERENT TYPES OF HUMAN MOTIONS

B.1 Spectrograms of 1st Person's Walking with Azimuth Angle of 0°

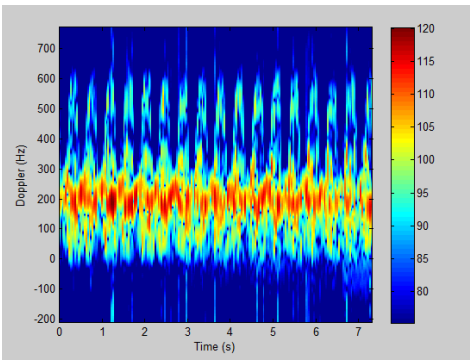

a) 1st spectrogram of 1st person walking with 0°

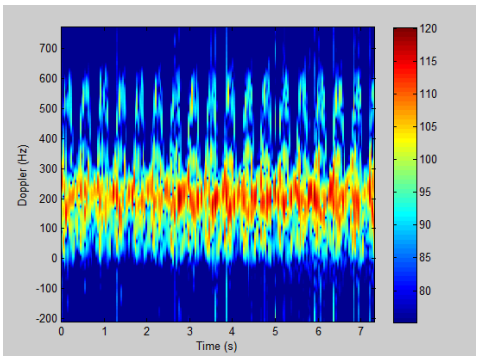

b) 2nd spectrogram of 1st person walking with 0°

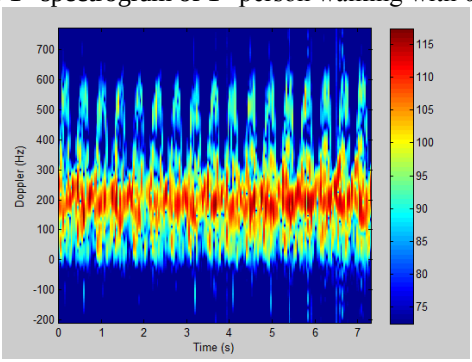

c) 3rd spectrogram of 1st person walking with 0°

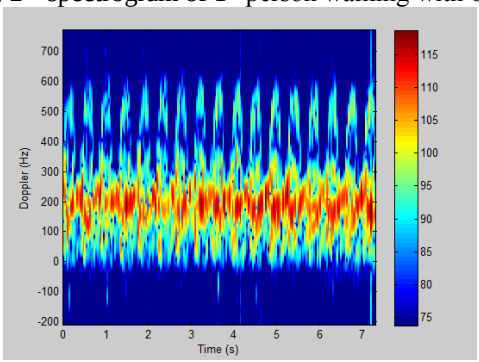

d) 4th spectrogram of 1st person walking with 0°

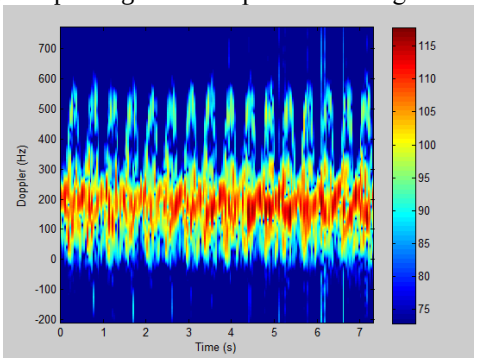

e) 5th spectrogram of 1st person walking with 0°

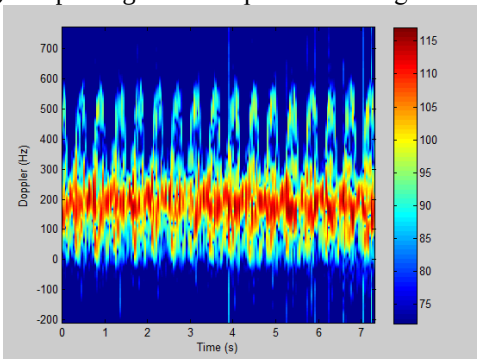

f) 6th spectrogram of 1st person walking with 0°

Figure B.1 Spectrograms of 1st person's human walking with azimuth angle of 0°

B.2 Spectrograms of 2nd Person's Walking with Azimuth Angle of 0°

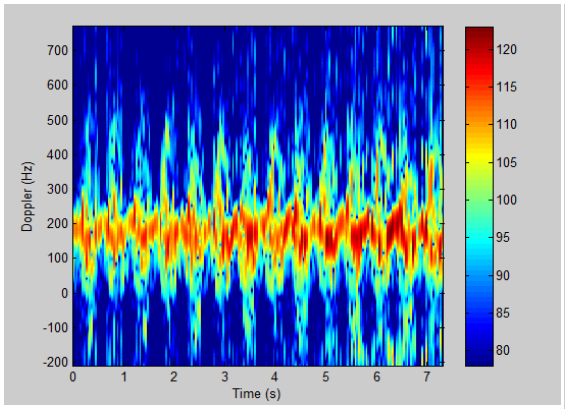

a) 1st spectrogram of 2nd person walking with 0°

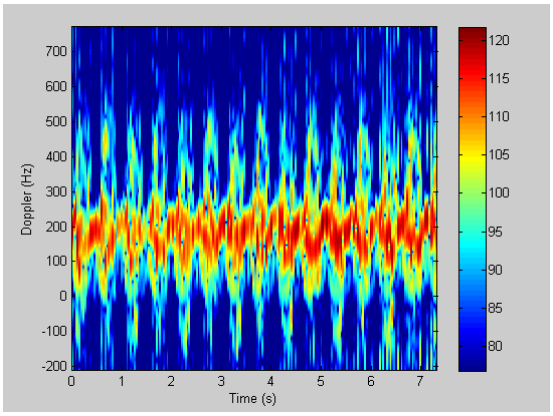

b)2nd spectrogram of 2nd person walking with 0°

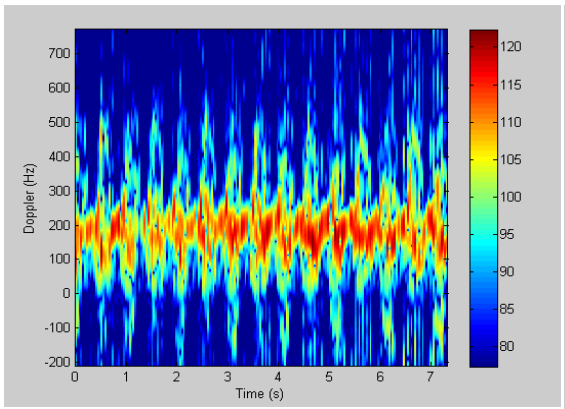

c) 3rd spectrogram of 2nd person walking with 0°

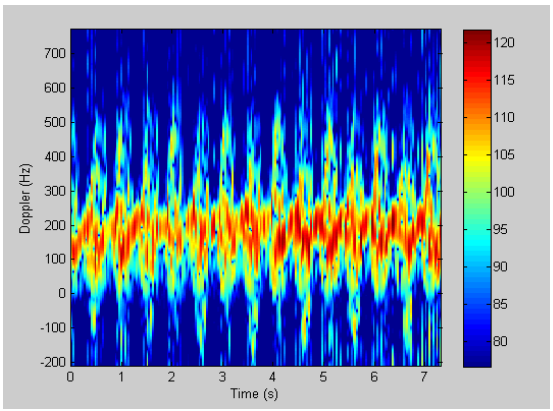

d)4th spectrogram of 2nd person walking with 0°

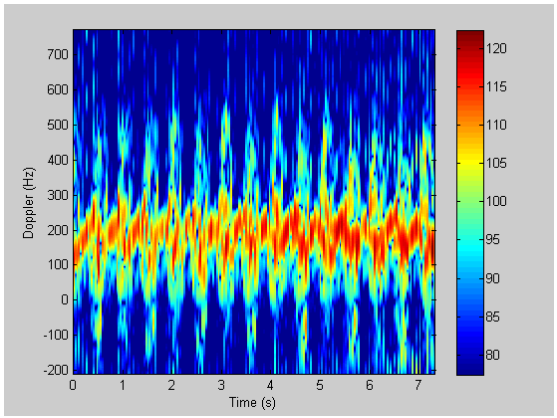

e) 5th spectrogram of 2nd person walking with 0°

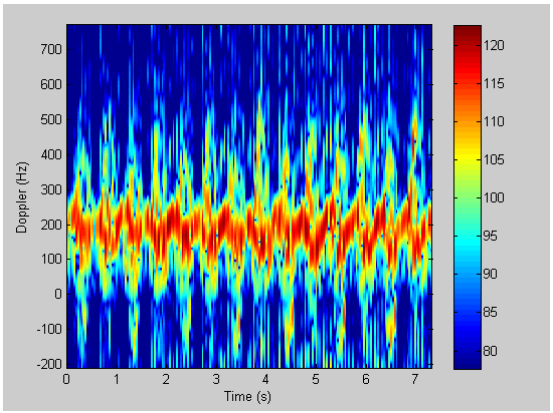

f)6th spectrogram of 2nd person walking with 0°

Figure B.2 Spectrograms of 2nd person's walking with azimuth angle of 0°

B.3 Spectrograms of 3rd Person's Walking with Azimuth Angle of 0°

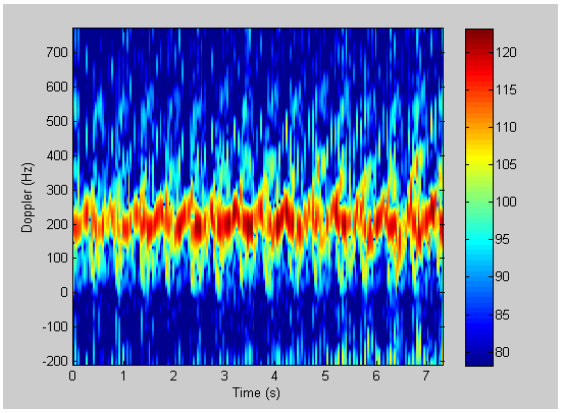

a) 1st spectrogram of 3rd person walking with 0°

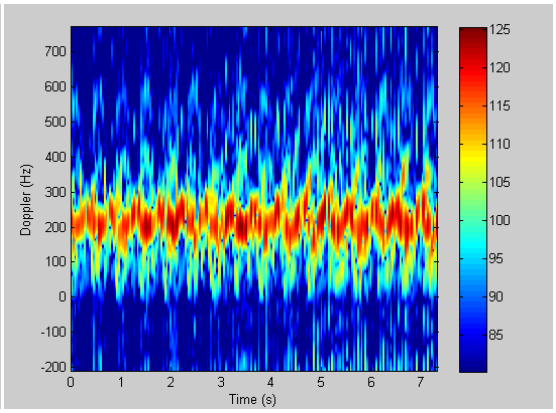

b)2nd spectrogram of 3rd person walking with 0°

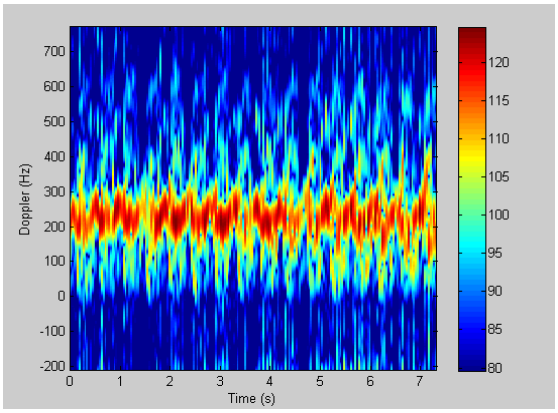

c) 3rd spectrogram of 3rd person walking with 0°

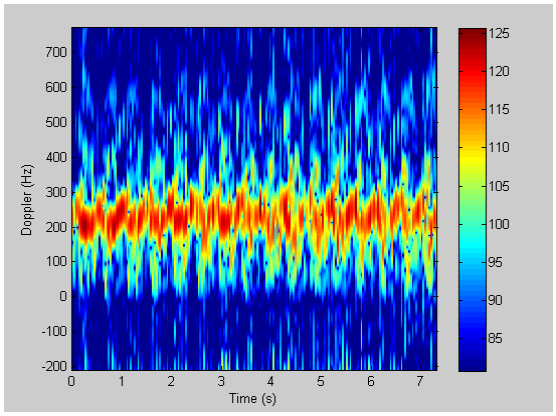

d)4th spectrogram of 3rd person walking with 0°

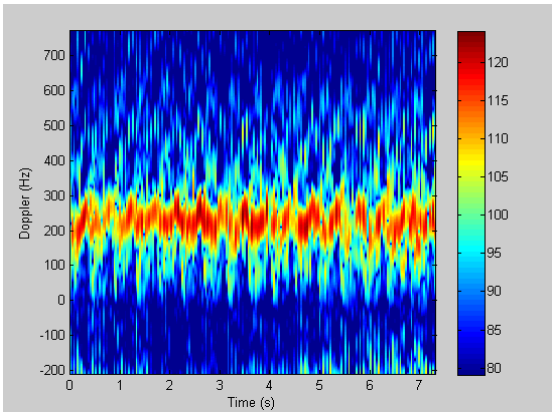

e) 5th spectrogram of 3rd person walking with 0°

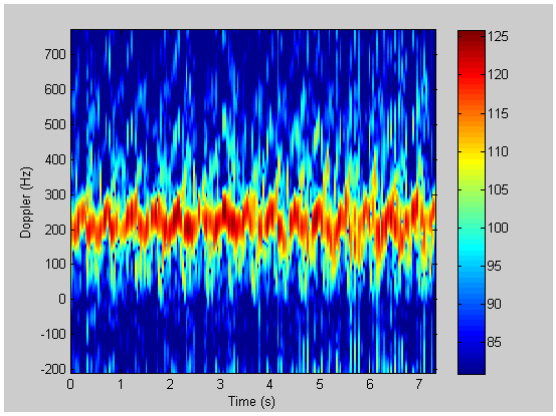

f) 6th spectrogram of 3rd person walking with 0°

Figure B.3 Spectrograms of 3rd person's walking with azimuth angle of 0°

B.4 Spectrograms of 1st Person's Walking with Azimuth Angle of 30°

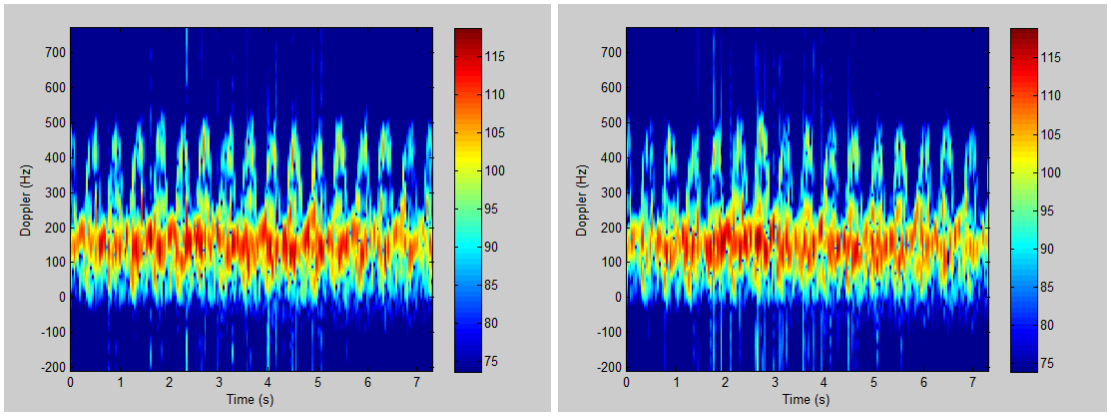

a)1st spectrogram of 1st person walking with 30° b)2nd spectrogram of 1st person walking with 30°

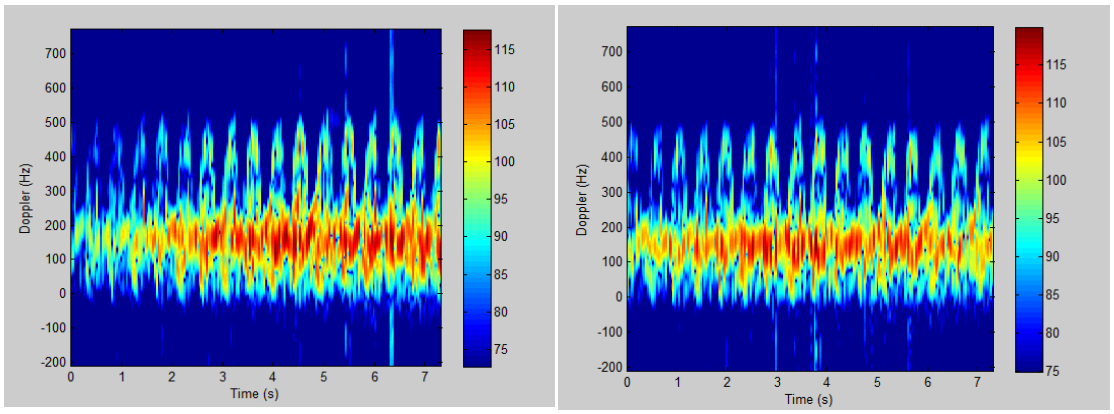

c)3rd spectrogram of 1st person walking with 30° d)4th spectrogram of 1st person walking with 30°

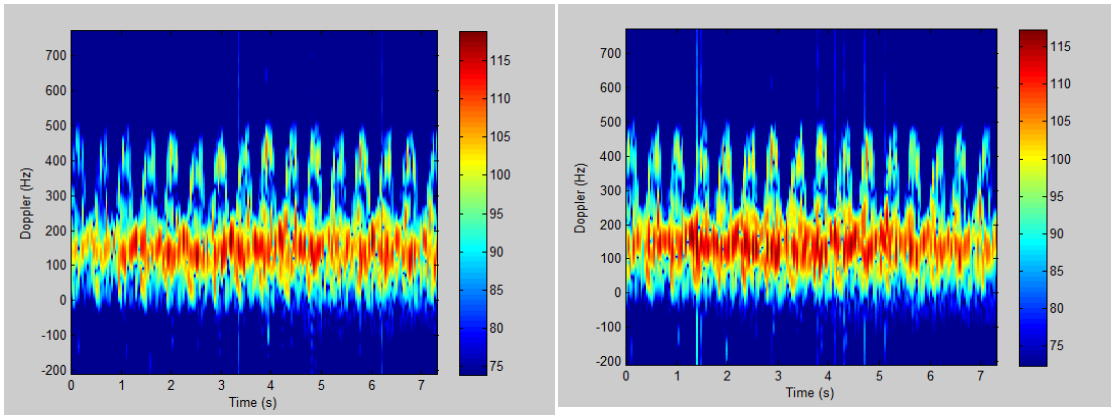

e)5th spectrogram of 1st person walking with 30° f) 6th spectrogram of 1st person walking with 30°

Figure B.4 Spectrograms of 1st person's walking with azimuth angle of 30°

B.5 Spectrograms of 2nd Person's Walking with Azimuth Angle of 30°

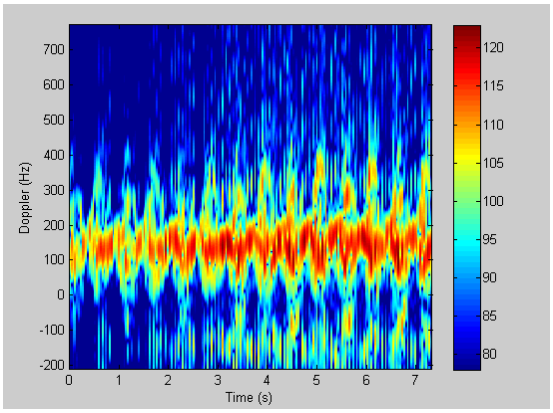

a)1st spectrogram of 2nd person walking with 30°

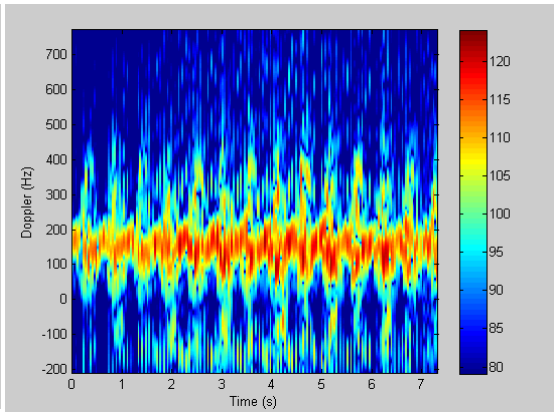

b)2nd spectrogram of 2nd person walking with 30°

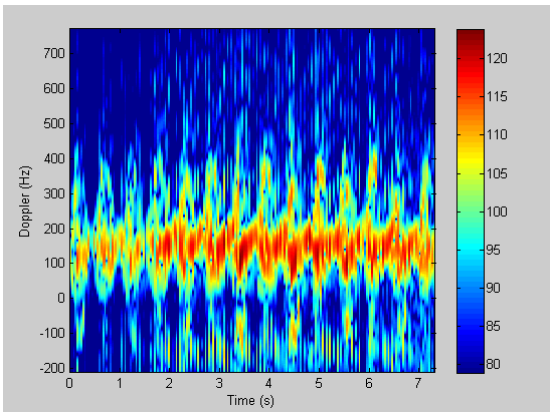

c)3rd spectrogram of 2nd person walking with 30°

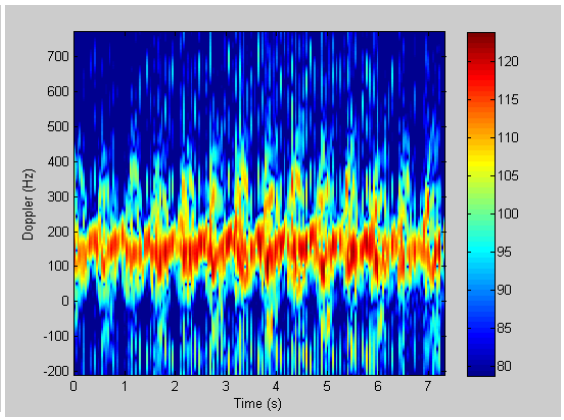

d)4th spectrogram of 2nd person walking with 30°

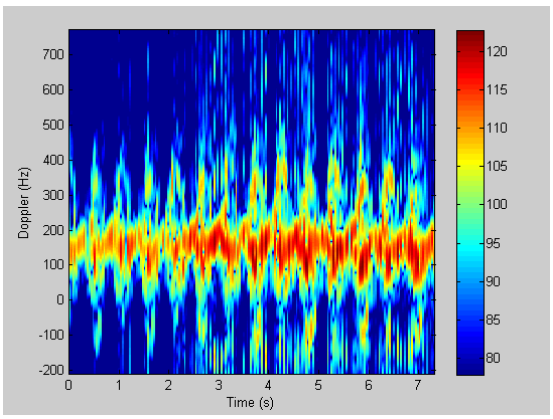

e)5th spectrogram of 2nd person walking with 30°

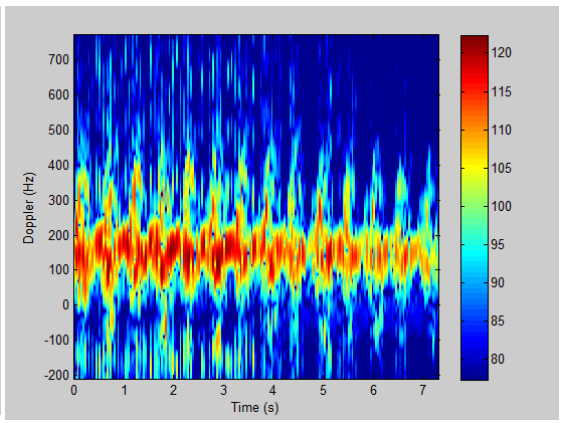

f) 6th spectrogram of 2nd person walking with 30°

Figure B.5 Spectrograms of 2nd person's walking with azimuth angle of 30°

B.6 Spectrograms of 3rd Person's Walking with Azimuth Angle of 30°

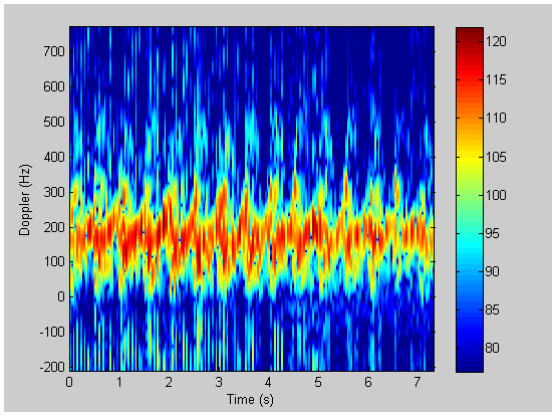

a)1st spectrogram of 3rd person walking with 30°

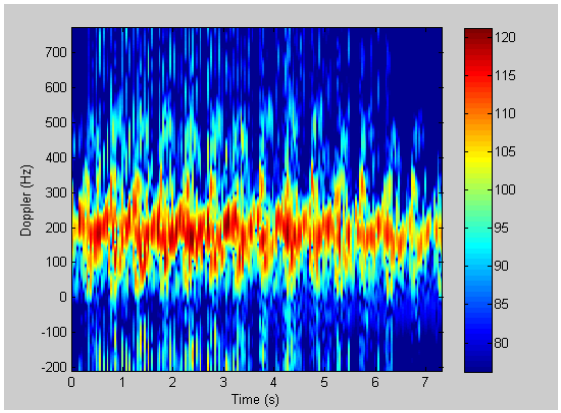

b)2nd spectrogram of 3rd person walking with 30°

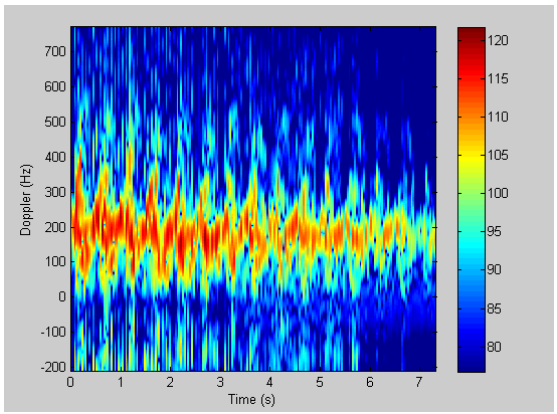

c)3rd spectrogram of 3rd person walking with 30°

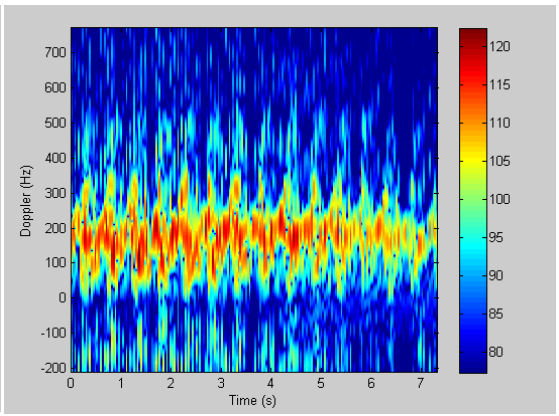

d)4th spectrogram of 3rd person walking with 30°

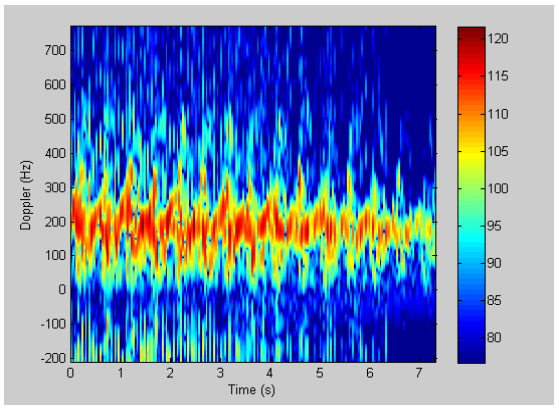

e)5th spectrogram of 3rd person walking with 30°

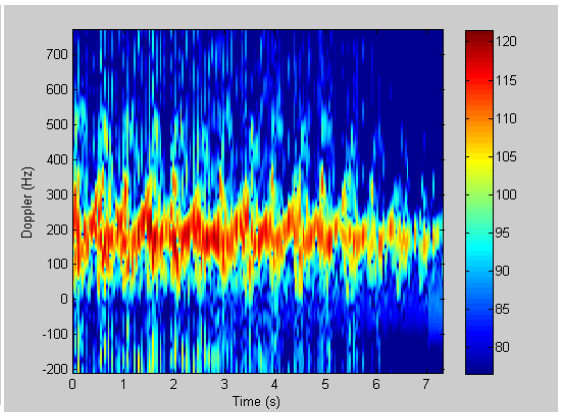

f)6th spectrogram of 3rd person walking with 30°

Figure B.6 Spectrograms of 3rd person's walking with azimuth angle of 30°

B.7 Spectrograms of 1st Person's Walking with Azimuth Angle of 60°

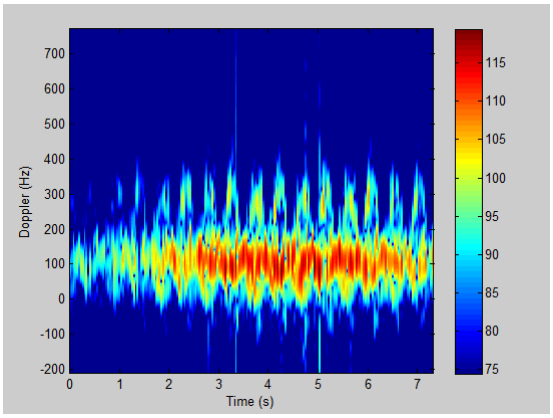

a) 1st spectrogram of 1st person walking with 60°

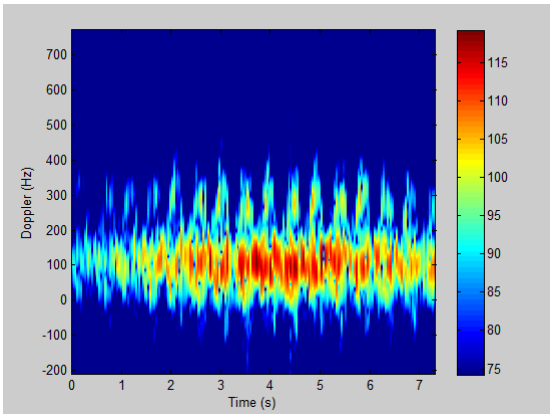

b) 2nd spectrogram of 1st person walking with 60°

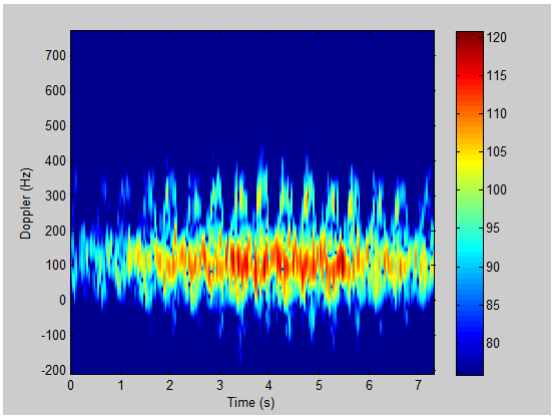

c) 3rd spectrogram of 1st person walking with 60°

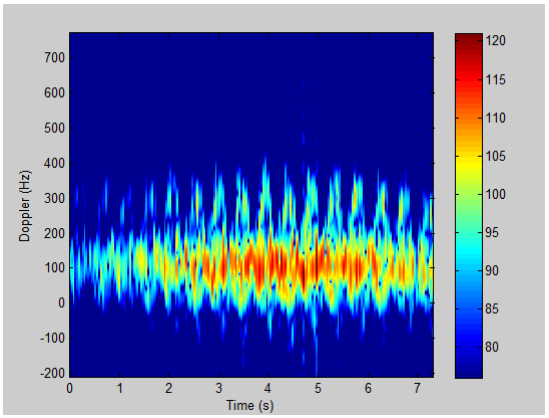

d) 4th spectrogram of 1st person walking with 60°

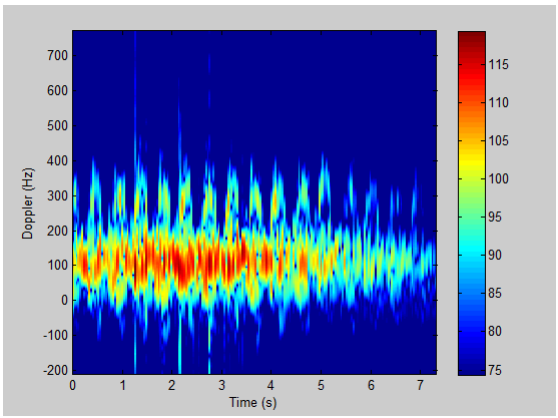

e) 5th spectrogram of 1st person walking with 60°

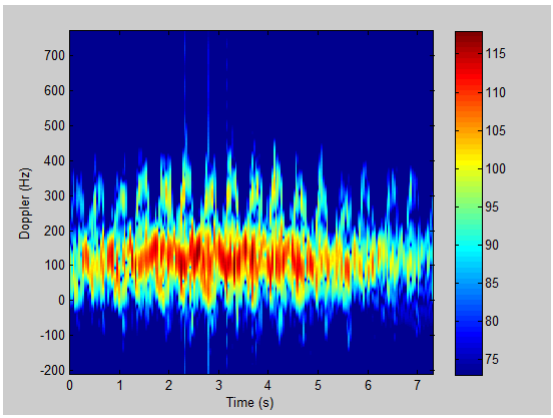

f) 6th spectrogram of 1st person walking with 60°

Figure B.7 Spectrograms of 1st person's walking with azimuth angle of 60°

B.8 Spectrograms of 2nd Person's Walking with Azimuth Angle of 60°

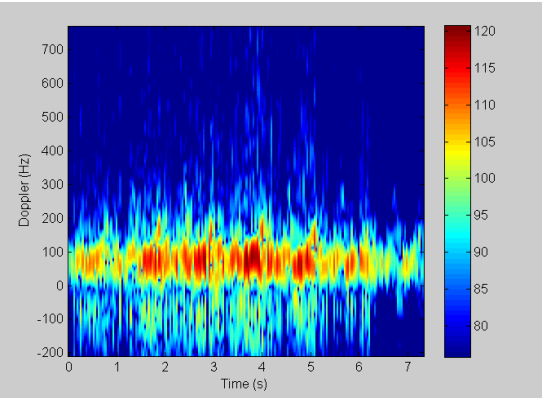

a)1st spectrogram of 2nd person walking with 60°

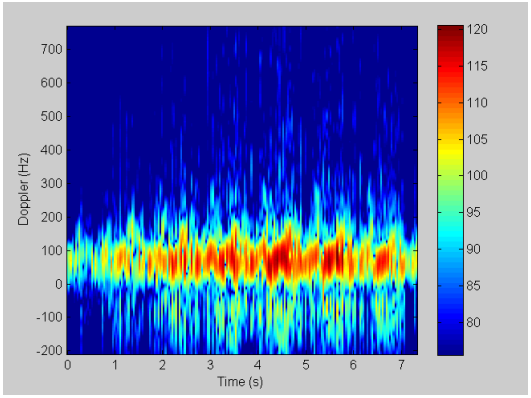

b)2nd spectrogram of 2nd person walking with 60°

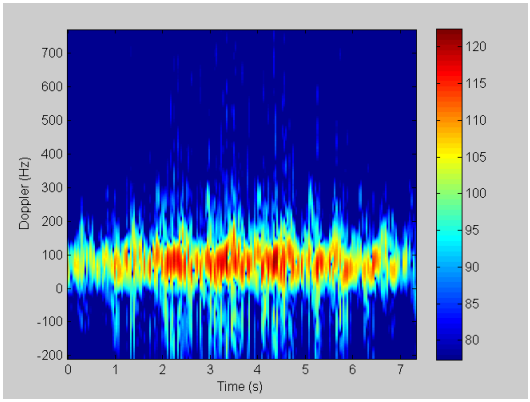

c)3rd spectrogram of 2nd person walking with 60°

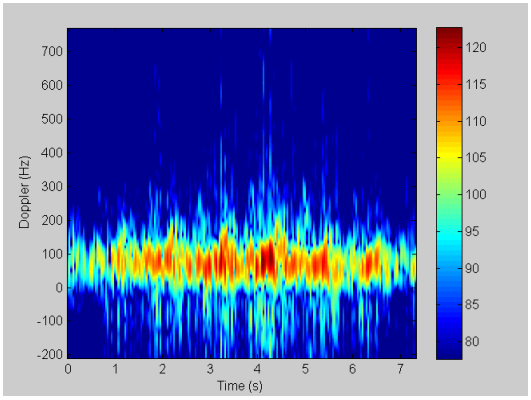

d)4th spectrogram of 2nd person walking with 60°

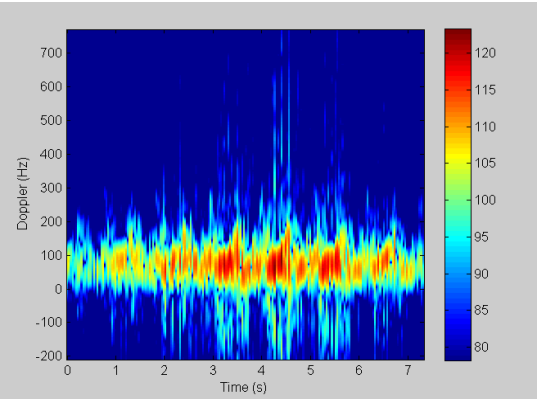

e)5th spectrogram of 2nd person walking with 60°

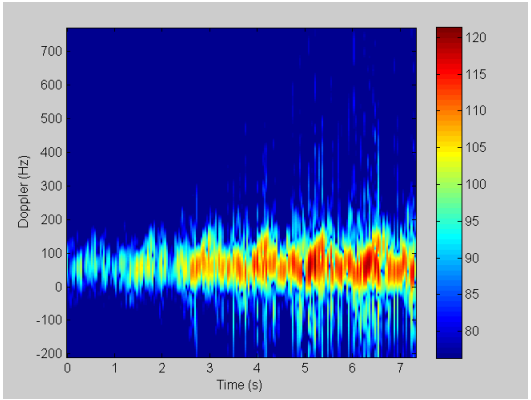

f)6th spectrogram of 2nd person walking with 60°

Figure B.8 Spectrograms of 2nd person's walking with azimuth angle of 60°

B.9 Spectrograms of 3rd Person's Walking with Azimuth Angle of 60°

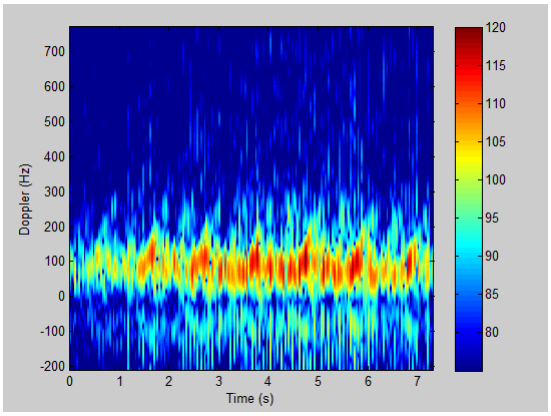

a)1st spectrogram of 3rd person walking with 60°

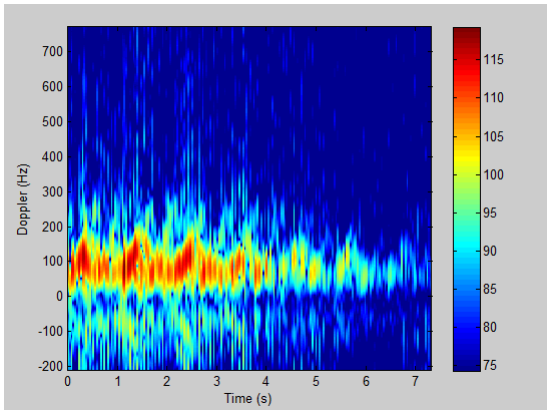

b)2nd spectrogram of 3rd person walking with 60°

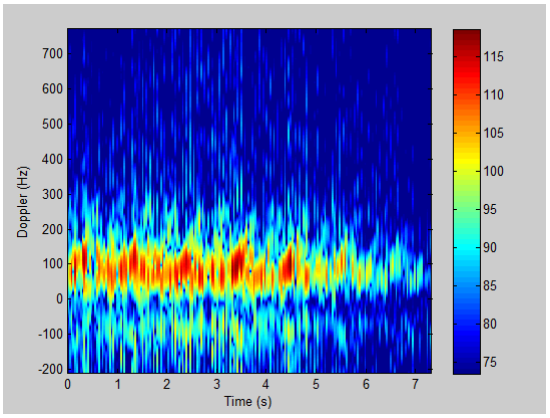

c)3rd spectrogram of 3rd person walking with 60°

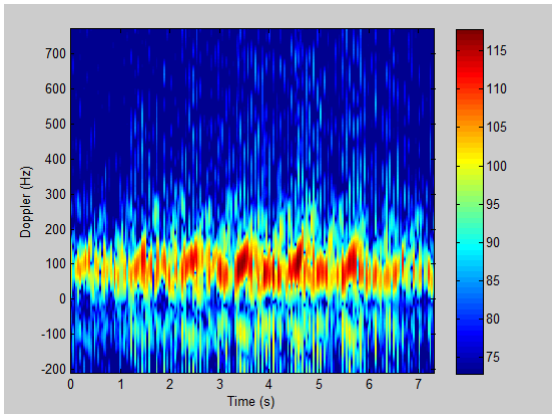

d)4th spectrogram of 3rd person walking with 60°

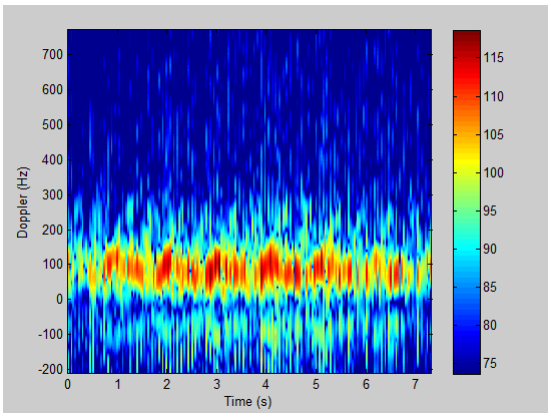

e)5th spectrogram of 3rd person walking with 60°

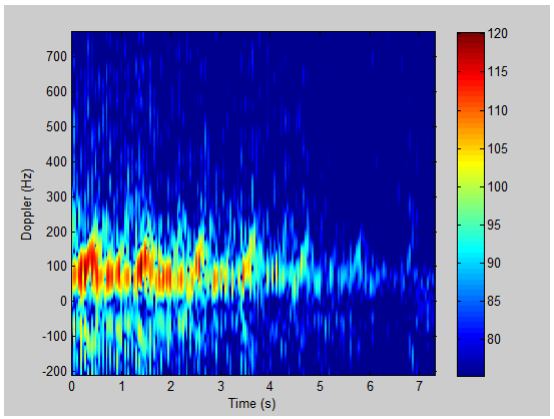

f) 6th spectrogram of 3rd person walking with 60°

Figure B.9 Spectrograms of 3rd person's walking with azimuth angle of 60°

B.10 Spectrograms of 1st Person's Running

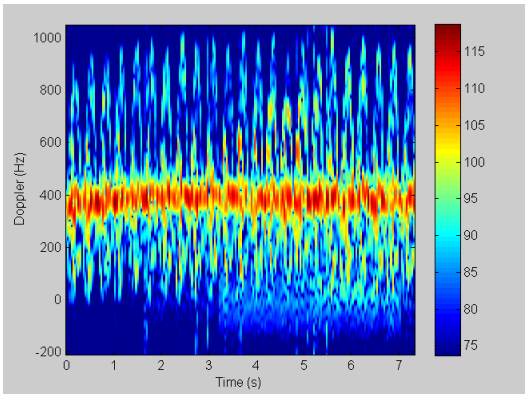

a) 1st spectrogram of 1st person's running

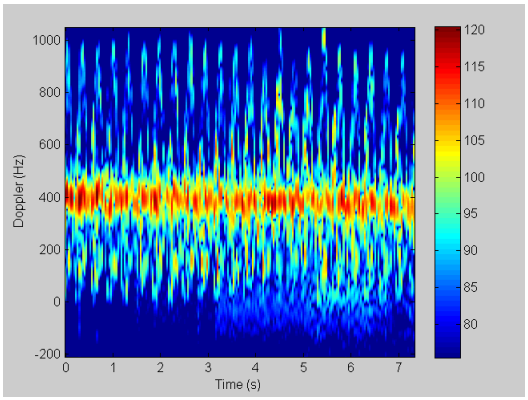

b) 2nd spectrogram of 1st person's running

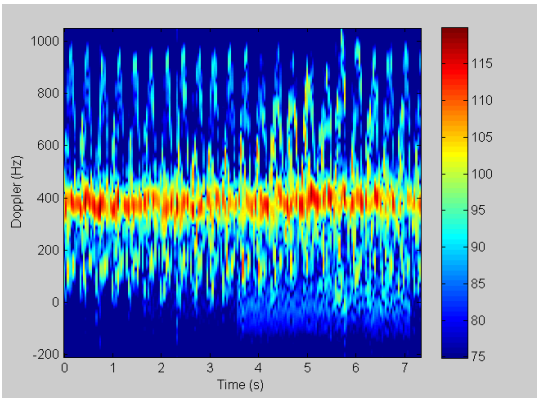

c) 3rd spectrogram of 1st person's running

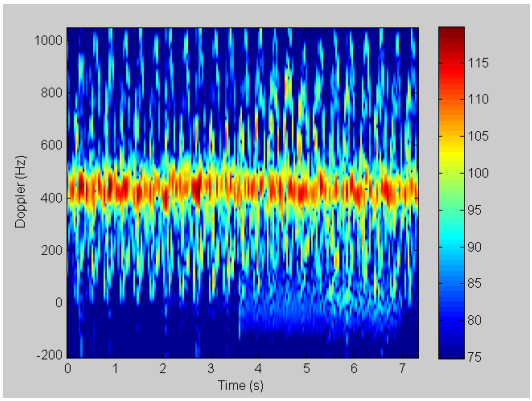

d) 4th spectrogram of 1st person's running

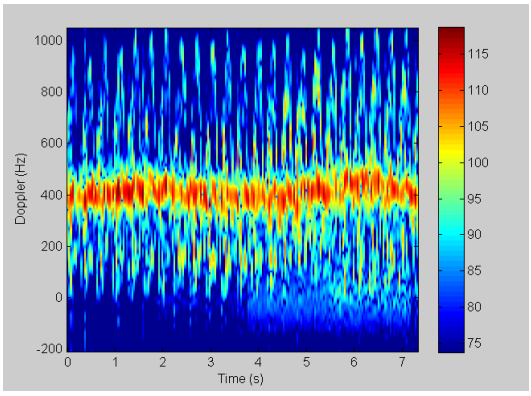

e) 5th spectrogram of 1st person's running

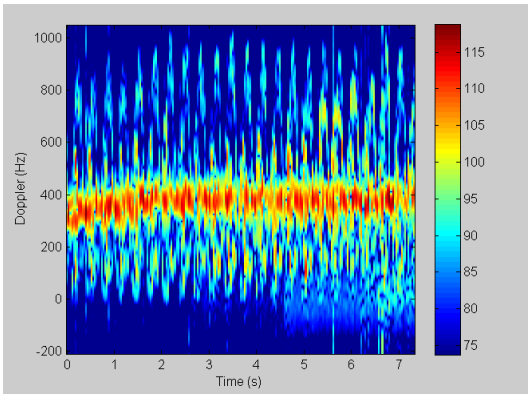

f) 6th spectrogram of 1st person's running

Figure B.10 Spectrograms of 1st person's running

B.11 Spectrograms of 2nd Person's Running

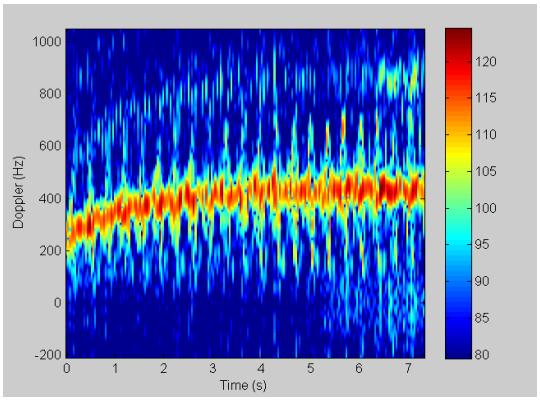

a) 1st spectrogram of 2nd person's running

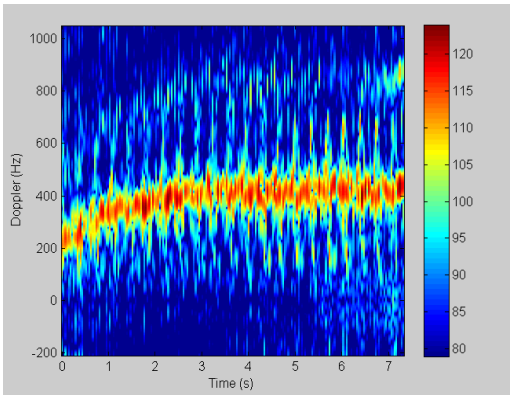

b) 2nd spectrogram of 2nd person's running

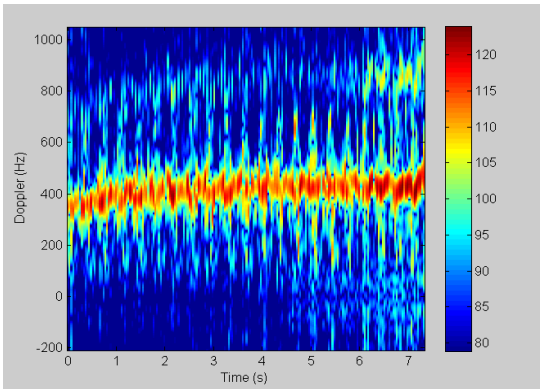

c) 3rd spectrogram of 2nd person's running

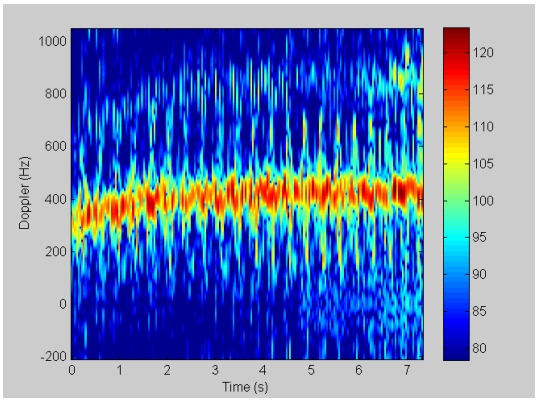

d) 4th spectrogram of 2nd person's running

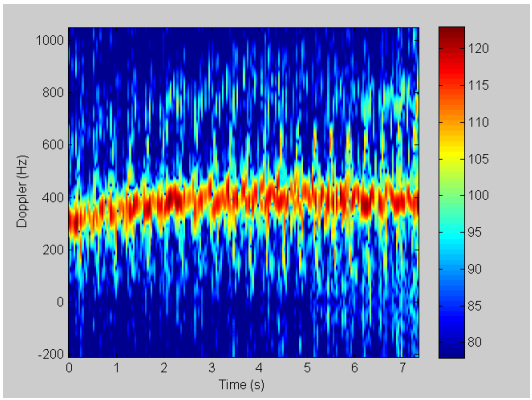

e) 5th spectrogram of 2nd person's running

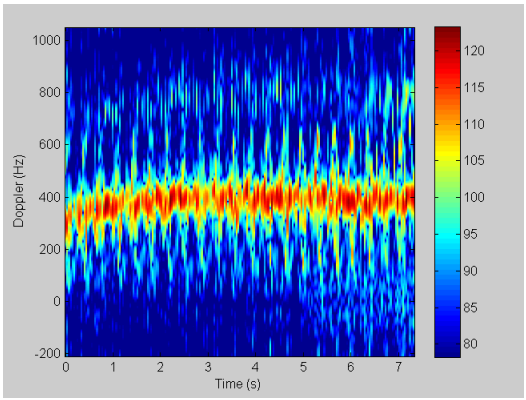

f) 6th spectrogram of 2nd person's running

Figure B.11 Spectrograms of 2nd person's running

B.12 Spectrograms of 3rd Person's Running

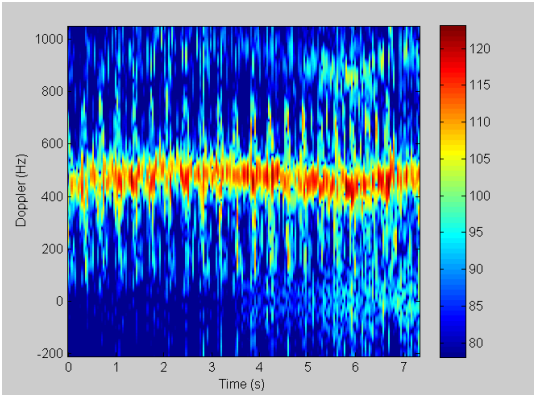

a) 1st spectrogram of 3rd person's running

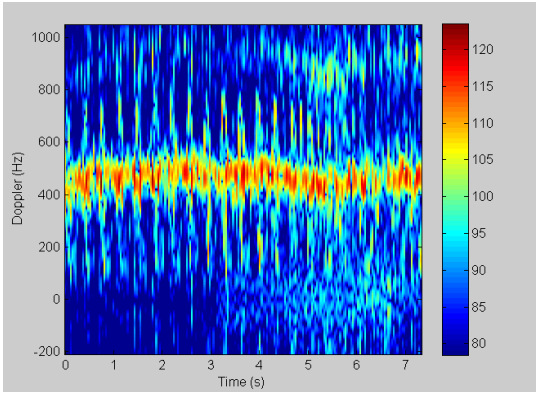

b) 2nd spectrogram of 3rd person's running

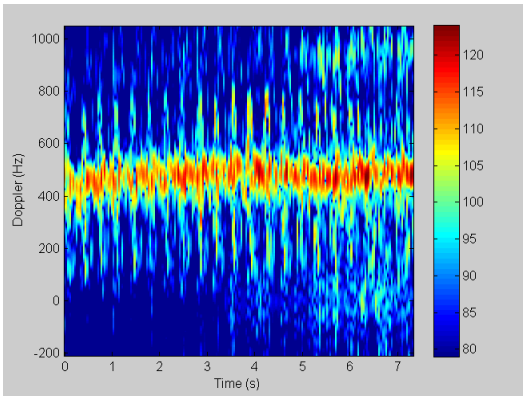

c) 3rd spectrogram of 3rd person's running

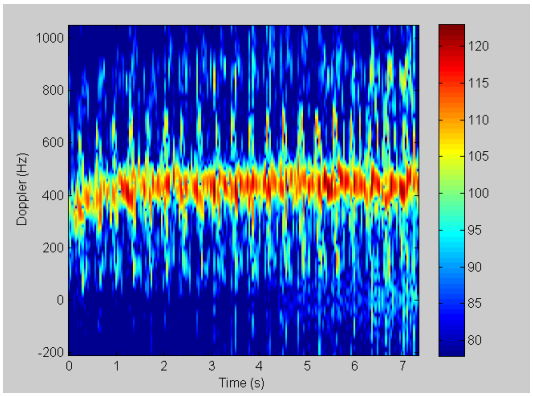

d) 4th spectrogram of 3rd person's running

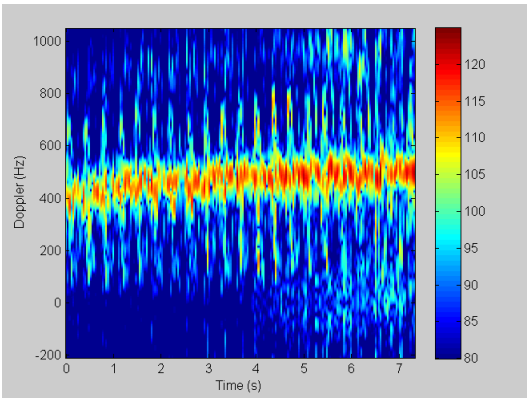

e) 5th spectrogram of 3rd person's running

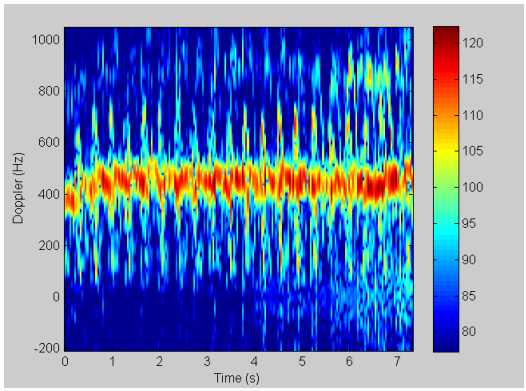

f) 6th spectrogram of 3rd person's running

Figure B.12 Spectrograms of 3rd person's running

B.13 Spectrograms of 1st Person's Crawling

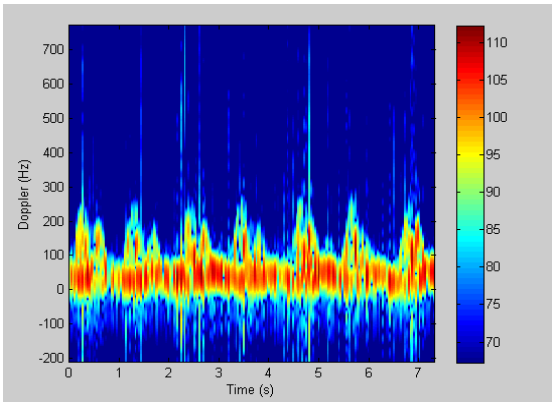

a) 1st spectrogram of 1st person's crawling

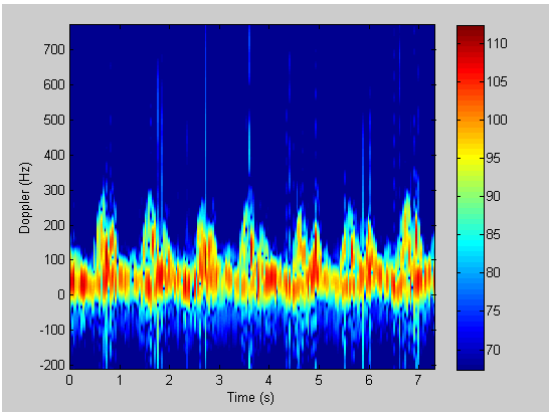

b) 2nd spectrogram of 1st person's crawling

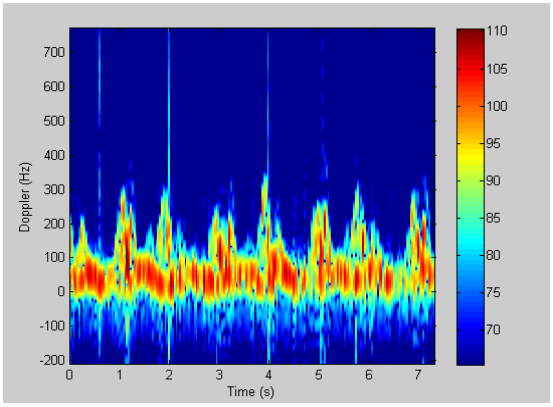

c) 3rd Spectrogram of 1st person's crawling

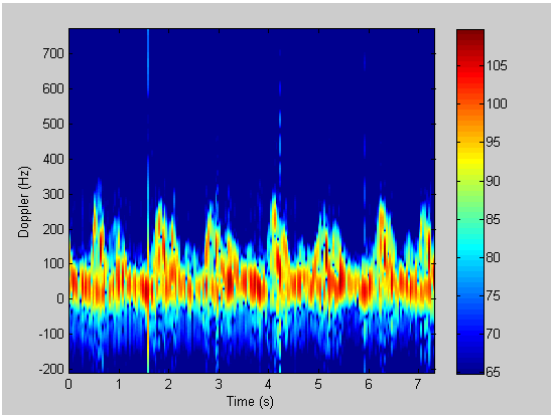

d) 4th Spectrogram of 1st person's crawling

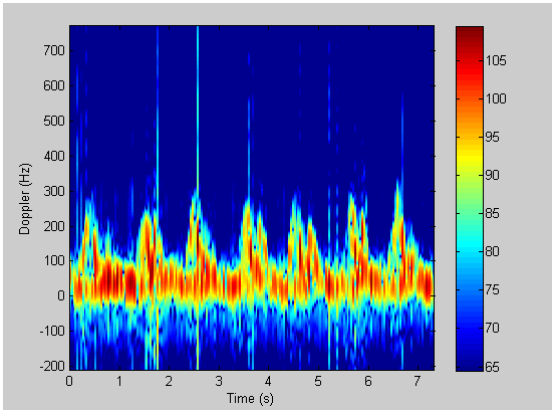

e) 5th Spectrogram of 1st person's crawling

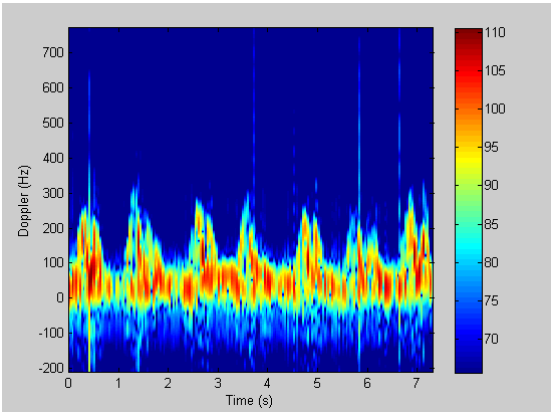

f) 6th Spectrogram of 1st person's crawling

Figure B.13 Spectrograms of 1st person's crawling

B.14 Spectrograms of 2nd Person's Crawling

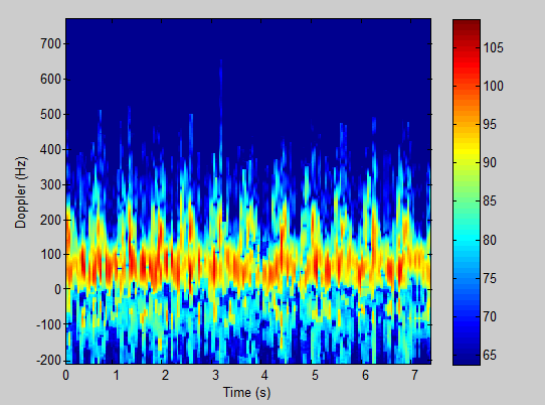

a) 1st spectrogram of 2nd person's crawling

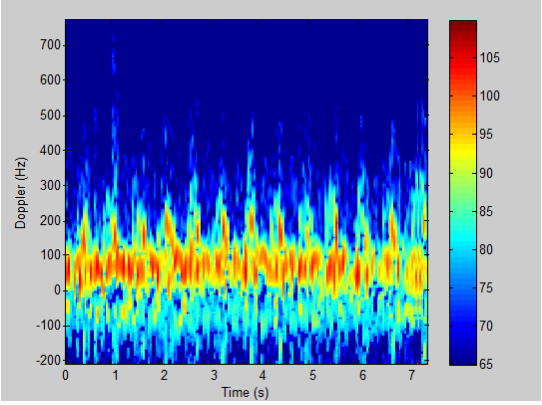

b) 2nd spectrogram of 2nd person's crawling

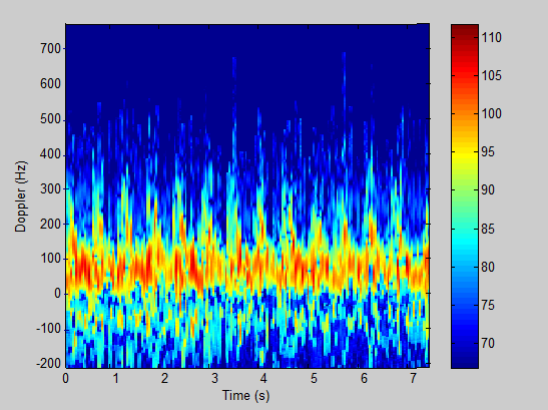

c) 3rd spectrogram of 2nd person's crawling

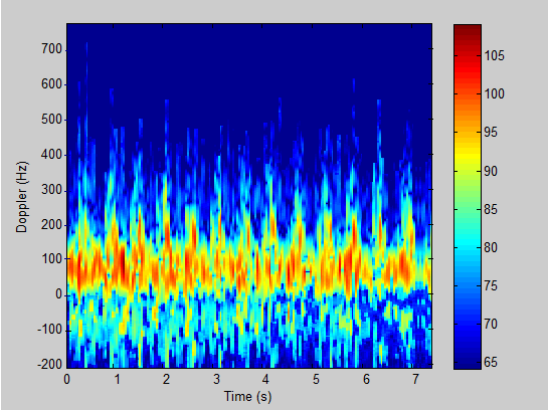

d) 4th spectrogram of 2nd person's crawling

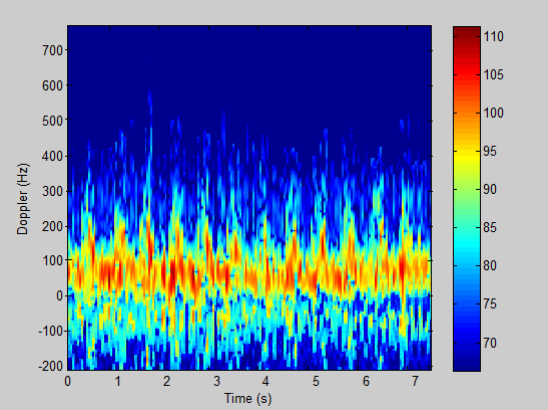

e) 5th spectrogram of 2nd person's crawling

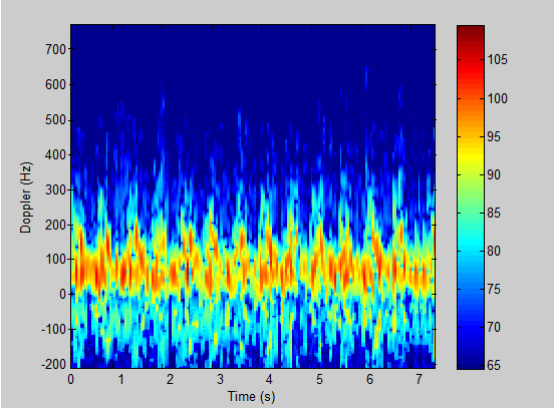

f) 6th spectrogram of 2nd person's crawling

Figure B.14 Spectrograms of 2nd person's crawling

B.15 Spectrograms of 3rd Person's Crawling

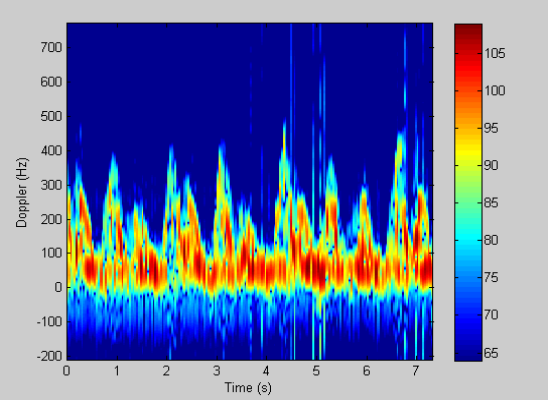

a) 1st spectrogram of 3rd person's crawling

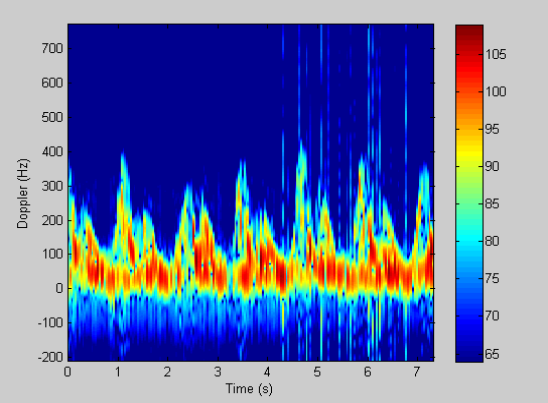

(b) 2nd spectrogram of 3rd person's crawling

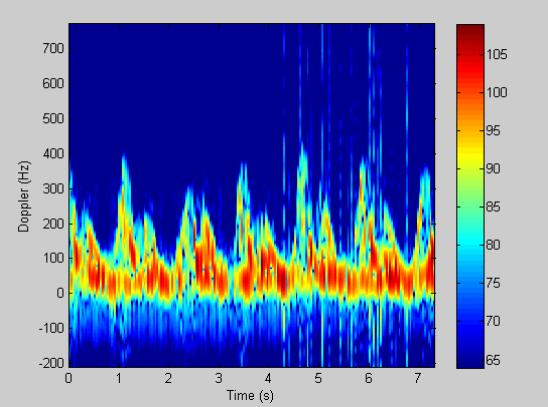

c) 3rd spectrogram of 3rd person's crawling

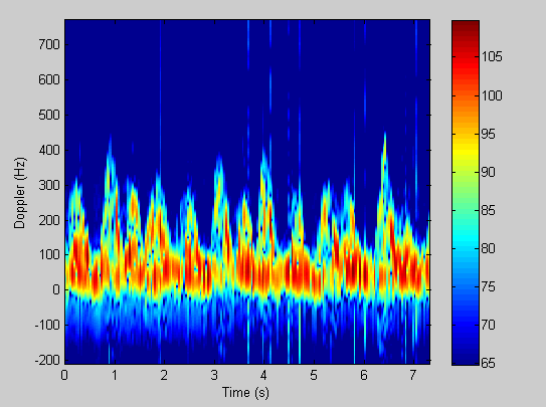

d) 4th spectrogram of 3rd person's crawling

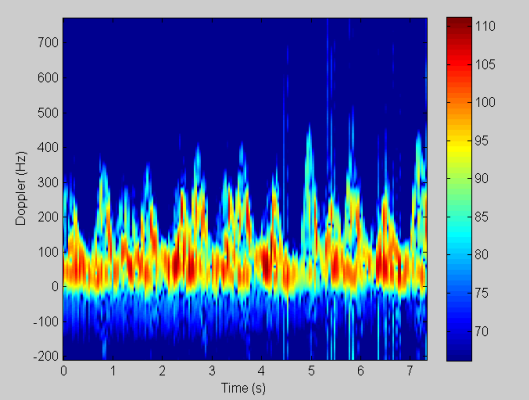

e) 5th spectrogram of 3rd person's crawling

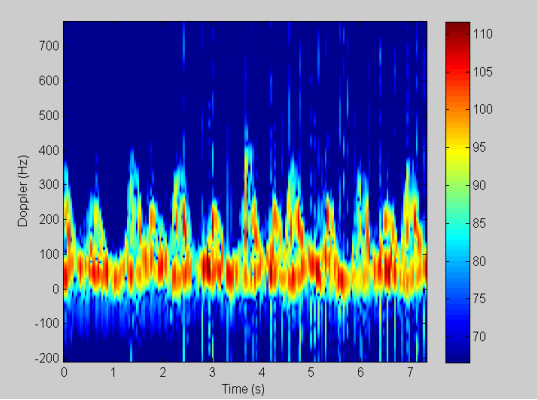

f) 6th spectrogram of 3rd person's crawling

Figure B.15 Spectrograms of 3rd person's crawling

B.16 Spectrograms of 1st Person's Creeping

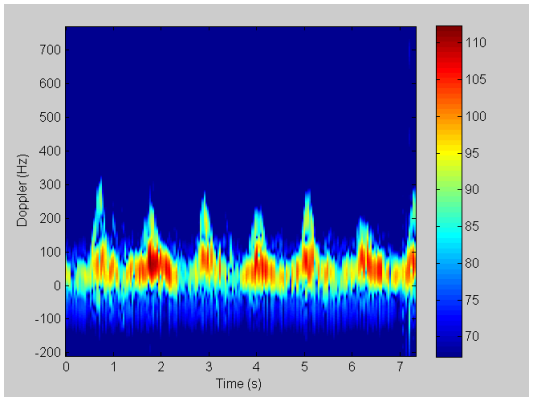

a) 1st spectrogram of 1st person's creeping

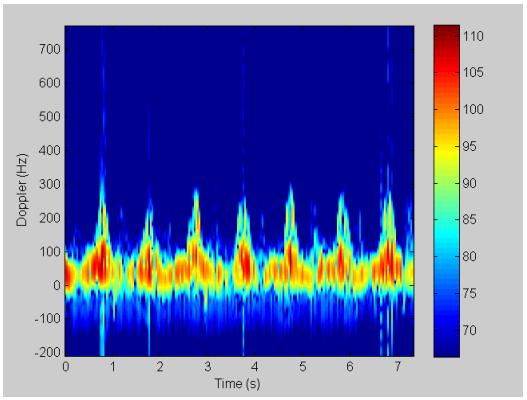

b) 2nd spectrogram of 1st person's creeping

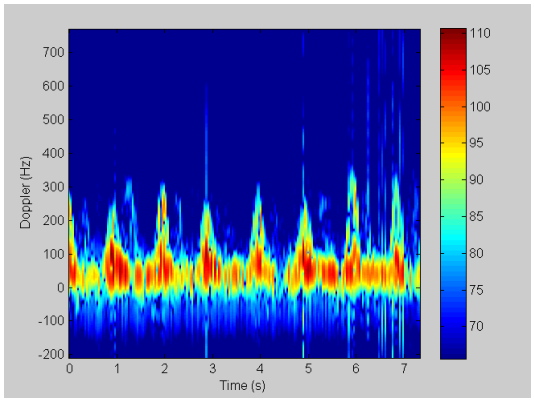

c) 3rd spectrogram of 1st person's creeping

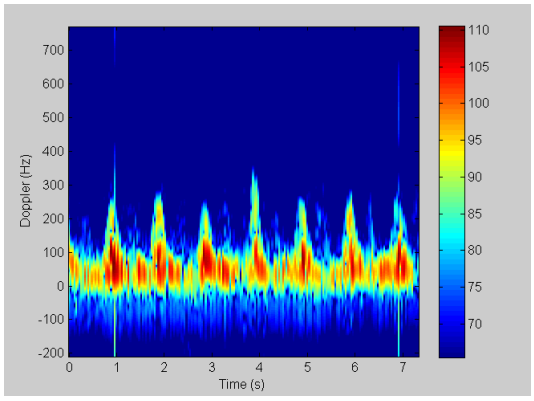

d) 4th spectrogram of 1st person's creeping

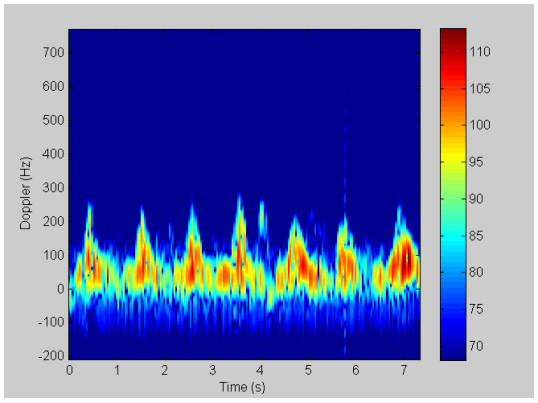

e) 5th spectrogram of 1st person's creeping

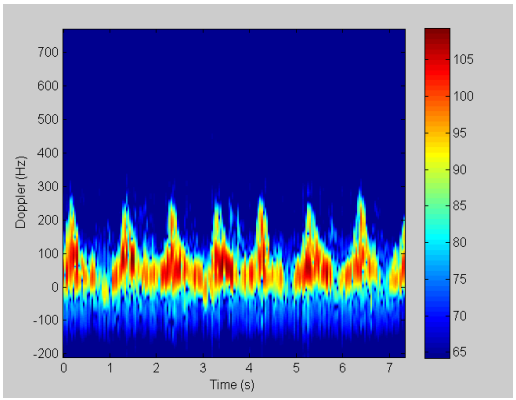

f) 6th spectrogram of 1st person's creeping

Figure B.16 Spectrograms of 1st person's creeping

B.17 Spectrograms of 2nd Person's Creeping

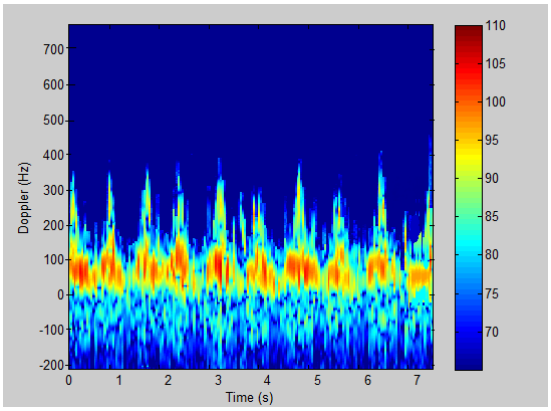

a) 1st spectrogram of 2nd person's creeping

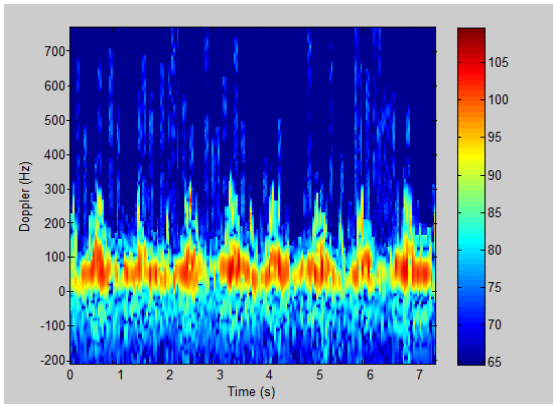

b) 2nd spectrogram of 2nd person's creeping

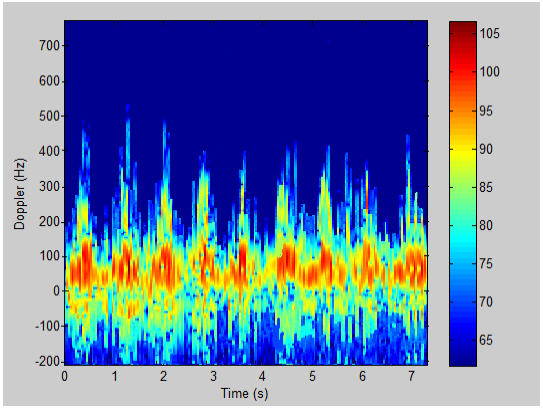

c) 3rd spectrogram of 2nd person's creeping

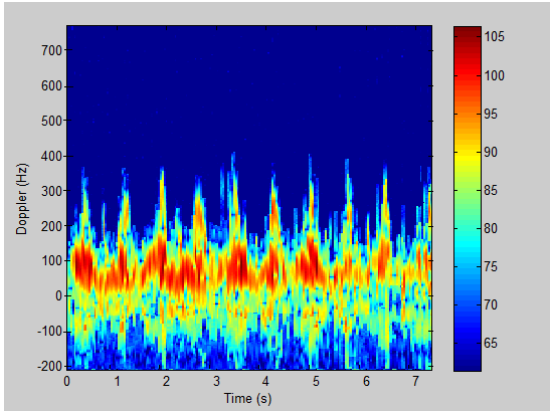

d) 4th spectrogram of 2nd person's creeping

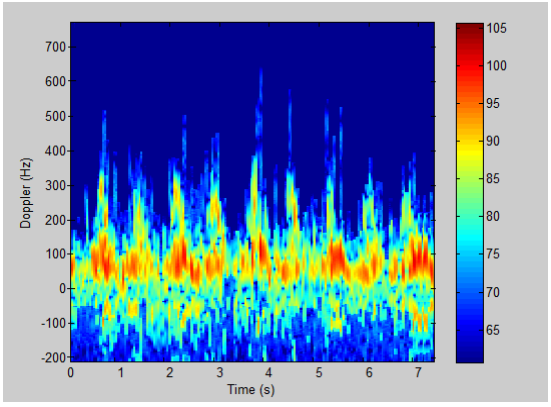

e) 5th spectrogram of 2nd person's creeping

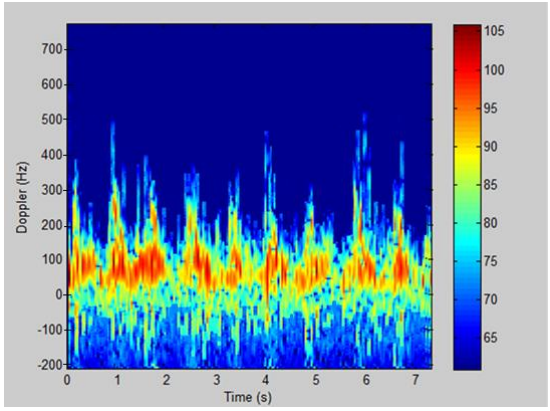

f) 6th spectrogram of 2nd person's creeping

Figure B.17 Spectrograms of 2nd person's creeping

B.18 Spectrograms of 3rd Person's Creeping

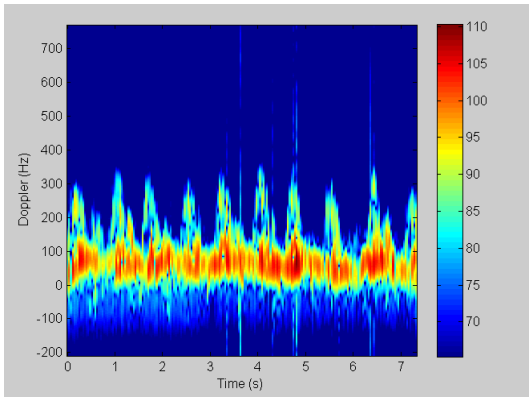

a) 1st spectrogram of 3rd person's creeping

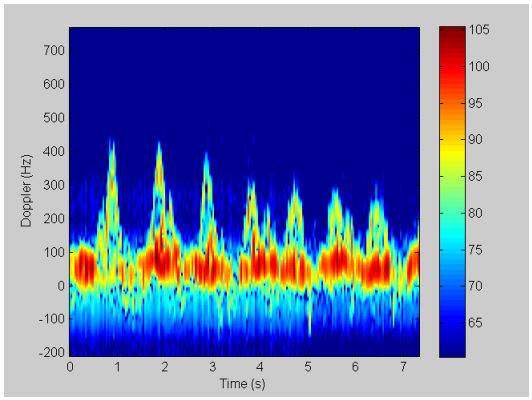

b) 2nd spectrogram of 3rd person's creeping

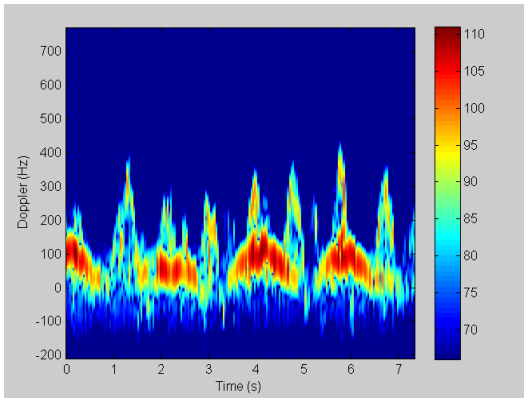

c) 3rd spectrogram of 3rd person's creeping

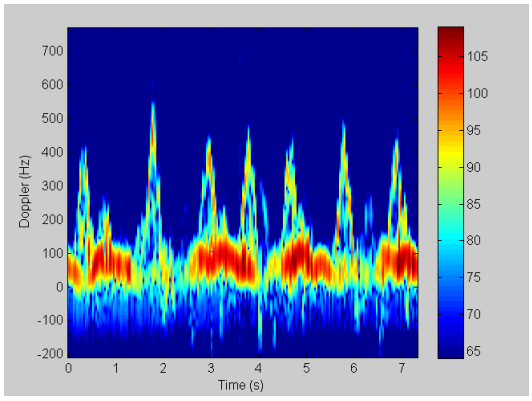

d) 4th spectrogram of 3rd person's creeping

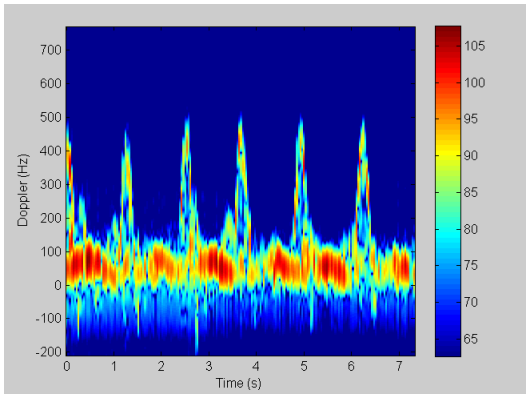

e) 5th spectrogram of 3rd person's creeping

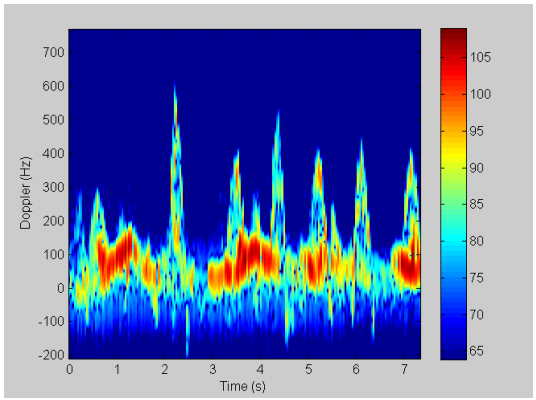

f) 6th spectrogram of 3rd person's creeping

Figure B.18 Spectrograms of 3rd person's creeping